In compliance with the
Canadian Privacy Legislation
some supporting forms
may have been removed from
this dissertation.

While these forms may be included
in the document page count,
their removal does not represent
any loss of content from the dissertation.

University of Alberta

Modes of Rock Slope Movement in the Colin Range, Jasper National Park

by

Karen D Hincks

A thesis submitted to the Faculty of Graduate Studies and Research in partial fulfillment of the

requirements for the degree of *Master of Science*

Department of *Earth and Atmospheric Sciences*

Edmonton, Alberta
Fall 2003

National Library
of Canada

Acquisitions and
Bibliographic Services

395 Wellington Street
Ottawa ON K1A 0N4
Canada

Bibliothèque nationale
du Canada

Acquisisitons et
services bibliographiques

395, rue Wellington
Ottawa ON K1A 0N4
Canada

Your file Votre référence
ISBN: 0-612-87781-7
Our file Notre référence
ISBN: 0-612-87781-7

The author has granted a non-exclusive licence allowing the National Library of Canada to reproduce, loan, distribute or sell copies of this thesis in microform, paper or electronic formats.

L'auteur a accordé une licence non exclusive permettant à la Bibliothèque nationale du Canada de reproduire, prêter, distribuer ou vendre des copies de cette thèse sous la forme de microfiche/film, de reproduction sur papier ou sur format électronique.

The author retains ownership of the copyright in this thesis. Neither the thesis nor substantial extracts from it may be printed or otherwise reproduced without the author's permission.

L'auteur conserve la propriété du droit d'auteur qui protège cette thèse. Ni la thèse ni des extraits substantiels de celle-ci ne doivent être imprimés ou aturement reproduits sans son autorisation.

Canada

University of Alberta

Library Release Form

Name of Author: *Karen Hincks*

Title of Thesis: *Modes of Rock Slope Movement in the Colin Range, Jsper National Park*

Degree: *Master of Science*

Year this Degree Granted: *2003*

Permission is hereby granted to the University of Alberta Library to reproduce single copies of this thesis and to lend or sell such copies for private, scholarly or scientific research purposes only.

The author reserves all other publication and other rights in association with the copyright in the thesis, and except as herein before provided, neither the thesis nor any substantial portion thereof may be printed or otherwise reproduced in any material form whatever without the author's prior written permission.

July 10, 2003

University of Alberta

Faculty of Graduate Studies and Research

The undersigned certify that they have read, and recommend to the Faculty of Graduate Studies and Research for acceptance, a thesis entitled **Modes of Rock Slope Movement in the Colin Range, Jasper National Park** submitted by **Karen Hincks** in partial fulfillment of the requirements for the degree of **Master of Science**.

10 July 2003

Dr. D.M. Cruden

Dr. J. Waldron

Dr. D. Tannant

Abstract

The Colin Range is located within the Front Ranges of the Rocky Mountains in the Canadian Cordillera. The bedrock geology within the Front Ranges is dominated by thrust sheets that dip steeply to the southwest. The terminology of Cruden and Hu (1996) is used to classify modes of slope movement according to the relationship of the slope to bedrock geology. Photographs from the Bridgland Repeat Photography Project are used to examine modes of slope movement in this study.

Models for sliding and toppling on orthoclinal slopes show that movement of blocks on these slopes is kinematically possible. Several examples of orthoclinal slope movements that occur in the Colin Range are documented, expanding the standard slope movement models to include orthoclinal slopes.

Toppling, exfoliation and sliding are modes of movement that occur on cataclinal slopes within the Colin Range of Jasper National Park. Exfoliation is the most active mode of movement on cataclinal slopes. A rock labyrinth was produced by a large relict slide.

A series of at least 3 debris flow deposits are present within the study area, along Debris Flow Creek, and support the interpretation of complex intermittent debris flows.

The hazard from slope movements is generally low along the west slope of the Colin Range, with the highest hazard being present along Debris Flow Creek and within the steep canyons in adverse weather conditions.

Acknowledgements

I am very grateful to NSERC for the financial support for this research. In addition, I would like to thank the Bridgland Repeat Photography Group, the staff of the Digital Imaging Facility and Jasper National Park for all of their support and help. I am grateful to Dr. Cruden, Dr. Shaw and Dr. Waldron for their help and guidance in the writing of this thesis.

I need to thank my parents for all of their support through the years of school. I would like to thank Trish, Jordana and Jackie for all of their help and love over the years. Thanks to Christine for keeping me sane over the writing of this thesis, Battle Axe Records and the Beastie Boys for providing the music that kept me working.

Table of Contents

Chapter				Page
1			**Introduction**	**1**
	1.1		General Overview	1
	1.2		Purpose and Scope	2
	1.3		Previous Work in the Canadian Rockies	5
2			**Site Description**	**7**
	2.1		Introduction	7
	2.2		Climate	9
	2.3		Surficial Geology	9
	2.4		Bedrock Geology	11
	2.5		Slope Types and Distribution	18
		2.5.1	Cataclinal Underdip Slopes, U	20
		2.5.2	Cataclinal Dip Slopes, D	23
		2.5.3	Cataclinal Overdip Slopes, Od	26
		2.5.4	Orthoclinal Slopes, O	26
		2.5.5.	Plagioclinal Slopes, P	29
		2.5.6	Anaclinal Slopes, A	30
	2.6		Conclusions	30
3			**Movements on Orthoclinal Slopes**	**33**
	3.1		Introduction	33
	3.2		Sliding on Orthoclinal Slopes	36
		3.2.1	Vertical Bedding Orientation	37
		3.2.2	Inclined Bedding Orientation	44
	3.3		Toppling on Orthoclinal Slopes	52
		3.3.1	Vertical Bedding Orientation	53
		3.3.2	Inclined Bedding Orientation	58
	3.4		Comparison of Sliding to Toppling	62
	3.5		Examples of Orthoclinal Movements in the Colin Range	66
		3.5.1	Morro Creek	66
		3.5.2	Garrone Creek	75
		3.5.3	Grand Trunk Pacific Railway Cut	77
		3.5.4	Northwest Slope of Morro Peak	77
	3.6		Conclusions	81
4			**Movements on Cataclinal Slopes**	**84**
	4.1		Introduction	84
	4.2		Toppling on Cataclinal Underdip Slopes	86
		4.2.1	Site 1	87
		4.2.2	Site 2	89

		4.2.3	Site 3	93
		4.2.4	Site 4	95
		4.2.5	Site 5	95
		4.2.6	Overview of Toppling on Cataclinal Slopes	99
	4.3		Exfoliation of Cataclinal Underdip Slopes	101
	4.4		The Rock and Boulder Gardens	112
		4.4.1	Introduction	112
		4.4.2	Scarp Area Observations	118
		4.4.3	Labyrinth Observations	122
		4.4.4	Down Slope Colluvium Observations	131
	4.5		Interpretations of the Rock and Boulder Gardens	131
	4.6		Conclusions	138
5			**Debris Flow Creek**	**140**
	5.1		Introduction	140
	5.2		Bedrock Geology	143
	5.3		Terrain Analysis	148
	5.4		Historic Sediments	158
	5.5		Current Movement in Debris Flow Creek	174
	5.6		Conclusions	175
6			**The Use of Repeat Photography in the Analysis of Landslide Hazards**	**178**
	6.1		Introduction	178
	6.2		Recent Slope Movements and the Photos	179
		6.2.1	Toppling	179
		6.2.2	Exfoliation	184
		6.2.3	Debris Flows	187
	6.3		History	187
	6.4		Photographic Information	190
	6.5		Conclusions	193
7			**Conclusions**	**195**
	7.1		Introduction	195
	7.2		Results	196
	7.3		Land Use Implications	201
	7.4		Further Work Recommendations	203
			References	**204**

List of Tables

Table		Page
3.1	Range of s/b ratios as calculated with Equation 3.4, and corresponding predicted slope angles, β, as calculated with Equation 3.5, for a range of rock unit weights, γ_r.	43
3.2	Range of s/b ratios as calculated from Equation 3.9, and corresponding slope angles, β, as calculated using Equation 3.10, for a range of possible rock unit weights.	51
3.3	Range of s/b ratios as calculated with Equation 3.14, and the corresponding slope angle, β, as calculated with Equation 3.5.	57
3.4	Range of possible s/b ratios as calculated with Equation 3.17, and corresponding slope angles, β, as calculated using Equation 3.10.	61
3.5	Range of possible slope angles of orthoclinal slopes, comparing the predicted slope angles as controlled by toppling motion as opposed to sliding motion. Dolomite has a unit weight of 27.5–28.4 kN/m^3, calcite has a unit weight of 26.5 kN/m^3, and clay minerals have a unit weight in the range of 25.5-27.5 kN/m^3, as an indication of the range of unit weights of some of the rocks found within the study area.	63
3.6	Range of possible orthoclinal slope angles, given a range of possible friction angles. Cruden and Hu (1988) indicate that carbonates can have a friction angle that ranges from 21.5° up to 41.3°.	64
3.7	Range of predicted slope angles for orthoclinal slopes in inclined strata. Cruden and Hu (1988) found that carbonates have a range in friction angles from 21.5° up to 41.3°.	65
3.8	Factor of safety calculations for toppling and sliding on the cut slope within the study area. ϕ=21° is used as a lower limit of friction angle, and ϕ=41° is used as an upper limit for the friction angle of the material.	80

3.9	Factor of safety calculations for the northwest slope of Morro Peak for several blocks that were measured in the field, and noted to show motion in the orthoclinal direction.	82
6.1	List of the principal photographic surveys in Canada in chronological order up to 1923, as included in Bridgland (1924). Interior – TSC is the Topographical Survey of Canada, Department of the Interior; Mines – GSC is the Geological Survey, Department of Mines; Interior – IBS is the International Boundary Surveys and the Geodetic Survey, Department of the Interior.	191-192

List of Figures

Figure		
1.1	deFreitas and Watters' (1975) concept of toppling and how toppling was considered to occur only on anaclinal slopes. The axis of rotation is into the page in the direction of strike of the beds, and the slope direction and the dip direction of bedding are taken into account.	3
2.1	Topographic map showing the Colin Range and the area of the geological map in Figure 2.3. The figure is derived from the 1:200 000 topographic map of Jasper National Park by the Surveys and Mapping Branch, Energy, Mines and Resources Canada (1985).	8
2.2	Natural scale geological cross section of the 1:50 000 geological map in Figure 2.3, from A to B. Formation colours correspond to those in Figure 2.4.	13
2.3	Geological map of the area outlined on Figure 2.1. Scale was originally 1:50 000. Legend is Figure 2.4. Data taken from Mountjoy (1959, 1978) and Mountjoy and Price (1976, 1985)	14
2.4	Legend and stratigraphic column to accompany Figures 2.2 and 2.3. The section is 1680m thick. A yellow environment indicates deposition in a marine environment, and the colour of the rock is indicated in the colour column of the diagram. The width of the lithology and map colour column indicates the competence of the rock to resist erosion.	15
2.5	Idealized sections through rock slopes, with bedding dipping at 45° shown by thin lines and slope surfaces are shown by thick lines.	19
2.6	A lower hemisphere equal angle stereonet with the pole to one bedding plane, P, plotted. The bedding plane dips in the direction 220°. The stereogram shows the classification of slopes if poles to the planes were to be plotted. It a pole to a slopes was plotted on this stereonet, the slope would be classified by the labels, based on the difference in dip direction of the bedding and the direction of the slope. Examples of cataclinal overdip	21

(Od) and underdip (U) slopes, and anaclinal normal escarpment (N), subdued escarpment (S) and steepened escarpment (E) plotted on the diagram.

2.7 Aerial photograph of the study area showing the classification of the slopes. Arrows indicate the direction of slope for each of the classified slopes. Air photo # A23015-138, Government of Canada – Ministry of Energy, Mines and Resources, originally at a scale of 1:60 000. U indicates an underdip slope, O indicates and orthoclinal slope, A indicates an anaclinal slope (undifferentiated) and Od indicates an overdip slope. The locations of 2.8-2.12 are indicated on the photograph. 22

2.8 Photograph of a ridge to the east of Morro Peak, taken from Morro Peak, showing a cataclinal underdip slope composed of alternating dip slopes, D, and underdip slopes, U. This is a relatively steep cataclinal underdip slope that is formed in steeply dipping beds. The location of the slope is indicated on Figure 2.7. 24

2.9 Photograph of the Mount Colin – Hawk Mountain col, taken from the Mount Colin Centennial Hut looking north. The photograph shows the area of dip slopes on the face of Mount Colin, and to a lesser extent on Hawk Mountain. The slopes follow the bedding at this location, which dips at an angle of 60°. 25

2.10 Photograph of a cataclinal overdip slope, showing the daylighting of the toe of two bedding planes. The slope is marked on Figure 2.7 as Od, and occurs within the watershed of Debris Flow Creek. 27

2.11 North slope of Morro Peak, an orthoclinal slope. Photo is taken from River Rock, where the Yellowhead River bridge crosses over the Athabasca River, looking south-southeast. The trace of bedding and the true dip of the bedding are shown on the slope. 28

2.12 Oblique photograph of an apparent plagioclinal slopes, which is composed of orthoclinal slopes, O, and cataclinal underdip slopes, U. Photograph number 485 from the Bridgland Repeat Photography, taken by M.P. Bridgland in 1915. The bedding is striking from the left to the right in 31

the photograph, and dipping out of the page. The photograph was taken to the northeast.

3.1 Simple model of the plan view of an orthoclinal slope in inclined bedded strata, showing the intersections of bedding with a strike joint set numbered 1 through 6. The perpendicular lines represent the dip joint set. Numbering and lettering correspond to Figure 3.2. 34

3.2 Cross-section AB on Figure 3.1, showing the true dip of the bedding, ψ_b, as seen in an orthoclinal slope. Bedding spacing=h, strike joint spacing=s and the height of water in the dip joint is z_w. 35

3.3 Diagram of blocks that are bounded by bedding planes and kathetal joints. Upper block represents the situation where bedding is vertical, and the view is looking at the bedding plane. The lower block represents the situation where bedding is inclined, and the three dimensional view as well as the view along the strike of the bedding are shown. 39

3.4 Diagram of a block bounded by a bedding plane and a kathetal joint set showing the pressures acting on the block to drive and resist sliding. The bedding in this situation is vertical, with s=strike joint separation and b=dip joint separation. 40

3.5 Diagram showing the generalized slope angle, β, as controlled by the block dimensions b, the dip joint spacing, and s, the strike joint spacing, for the situation where bedding is vertical. 42

3.6 Boulders and debris infilling a crack that has been created by the rotation of a block, opening the dip joints and allowing for the infilling of the open space. Photograph is taken at the Morro Creek orthoclinal block as shown in in Figure 3.13. 45

3.7 Geometry of an orthoclinal wedge after Hoek and Bray (1973). 47

3.8 Cross-section of a simple example of an orthoclinal wedge, showing ψ_b=45° and s=h. 49

3.9	Diagram of the generalized slope angle, β, based on the rock geometry.	50
3.10	Geometry of a block in a vertically bedded orthoclinal slope that is subject to toppling, looking at the bedding plane, showing s (the strike joint separation), b (the dip joint separation) and θ.	54
3.11	Diagram of a block in a vertically bedded orthoclinal slope looking at the bedding surface, showing the centre of gravity. O_g, the centre of rotation, O_r, and the pressures on the block, V and W.	55
3.12	Diagram of 3-dimensional block geometry.	59
3.13	Map showing the areas where orthoclinal slope movements are documented within the study area. Map taken from the 1:50 000 topographic maps of the area.	67
3.14	View of the canyon of Morro Creek taken from the Snaring River Bridge on the secondary road. The bedding is dipping to the southwest at 70°, and the canyon is cut at a right angle to the bedding.	68
3.15	View from the east into the canyon of Garrone Creek (Figure 3.13). The canyon is 3m wide at the base at this location, and the canyon walls slope at angles up to 90°.	69
3.16	Photograph of the cut slope adjacent to the Athabasca River (Figure 3.13). Photo is taken on a bearing of 130°.	70
3.17	Block of Gog Quartzite on the right side of the photograph that is preventing a block of Turner Valley Formation rock from rotating into Morro Creek.	72
3.18	Photograph of the top of the block that is in the process of toppling into Morro Creek.	73
3.19	Toppling block showing rotational type movement of the block to the right of the photograph, into Morro Creek. The photograph is taken looking at the bedding surface from the direction of dip.	74

3.20	Several blocks in Garrone Creek that look to have fallen recently. The blocks are angular, not rounded, and the block on the right is balanced on a thinner side. The long dimension of the block is parallel to the bedding, and the bedding spacing is 18cm.	76
3.21	A block on the cut face along the Yellowhead Highway, that has moved out from the slope in the direction of strike, to the northwest.	78
3.22	View along the cut slope, looking northeast, showing the slope and several blocks at the base of the slope that have come off of the slope.	79
4.1	Part of the process diagram from Cruden and Hu (1996, Figure 3), showing the locations of movements that are discussed in this chapter. The plots labeled as L1-L6 refer to the locations of toppling, with L2' and L3' plotted with the localized slope angle. Ex indicates where exfoliation plots on the diagram, and RBG indicates roughly where the Rock and Boulder Gardens plot on the diagram. Ψ is the dip of the bedding and β is the slope angle.	85
4.2	Oblique photograph showing Morro Peak from the southwest, showing the cataclinal slopes of Morro Peak. The locations of sites 1-3 are shown on the photograph, with the formations that they occur in. Photograph number 470, M.P. Bridgland, 1915.	88
4.3	Toppling block located at location 1, at the north end of the slope.	90
4.4	Downslope at Location 2, showing the blocky talus deposits, the sparse vegetation and the use of the slope by Big Horn Sheep. The slope ends on the Athabasca Flood Plain, and blocks of rock can be seen resting on the flood plain.	91
4.5	Outcrop of Pekisko Formation along the Overlander Trail at Site 2. The in place bedding is shown, as well as the bedding that is showing some rotation.	92
4.6	Rotated bedding at Location 3, within the shales of the Banff Formation. The toppled tree is 1.5m high.	94

4.7	Oblique photograph showing locations 4 and 5 and the bedrock geology. Bridgland Repeat Photography collection, photo B474, showing Mount Hawk, and Mount Colin on the right side of the photograph.	96
4.8	Rotated block within the Turner Valley Formation at Location 4. The space that has been opened up by rotation has been subsequently infilled with debris, soils and vegetation.	97
4.9	Rotated blocks within the Banff Formation shales at Location 5.	98
4.10	Rotated bedding at Location 5 within the crinoidal limestone of the Banff Formation.	100
4.11	Aerial photograph showing the location of Sites 1 and 2. Aerial photograph #A23015-138, originally at a scale of 1:60 000.	102
4.12	Upper exfoliation at Site 1, showing the dip slope bedding planes, strike joints and dip joints, with the underdip slope visible in the foreground.	103
4.13	Lower exfoliation at Site 1, taken from the bottom of the feature looking up along the dip of the bedding, showing the bedding planes that daylight in the feature, and the strike and dip joints.	104
4.14	View along the strike of bedding of the area of exfoliation at Site 1. The location of Figures 4.12 and 4.13 are shown, along with the daylighting bedding planes and the location of Morro Creek and Morro Creek Canyon.	105
4.15	Recent tree damage at the base of the slope of Site 1, below the areas of exfoliation. Talus blocks can be seen where there is a build up of talus up slope of the tree trunk.	107
4.16	An example of exfoliation at Site 2, on the dip slope face of Mount Colin. The depression of the exfoliation is 3.5m deep.	108

4.17	Another example of exfoliation at Site 2, to the south of Figure 4.15. An avalanche chute extends downslope from the narrow base of the exfoliation.	109
4.18	Idealized cross-section across an exfoliation. The solid lines indicate the bedding planes, and the dashed lines indicate joint set 2, the strike joints, and the triangles indicate talus. Small black arrows show the movement of water along the bedding planes, down to the water table, and a possible mode of movement of the blocks out of the slope.	111
4.19	Topographic map enlarged from 1:50 000 scale, showing the location of the Rock and Boulder Gardens study area.	113
4.20	Aerial photograph at a scale of 1:20 000, showing the bedrock geology in the vicinity, the scarp area, the labyrinth area and the colluvial area of the Rock and Boulder Gardens. Photograph courtesy of the Jasper National Park Wardens Office.	114
4.21	Lower hemisphere equal angle stereographic projection of the poles to the measured joints within the Rock and Boulder Gardens, showing the strike joint set and the dip joint set.	115
4.22	Detailed map of the surficial geology in the vicinity of the Rock and Boulder Gardens (Mountjoy, 1974), showing the location of the Athabasca Glacier Moraine in green and the Maligne Glacier Lateral Moraine in purple.	116
4.23	View from the south scarp toward the north scarp, showing the tree cover in the bowl area. The area with no tree cover is a dip slope. The north scarp of the feature can be seen in the middle ground.	117
4.24	Area from Figure 4.1 enlarged to show the location of figures, the location of a depression through the scarp area, and heights of the south scarp of the Rock Gardens.	119
4.25	Joint control of the south scarp in the Rock Gardens area. Where the dip joint controls the slope, the slope is an	120

orthoclinal slope, and where the strike joints control the slope, the slope is an anaclinal slope.

4.26 Tree damage and rock fall debris at the base of the south scarp. The damaged tree has a diameter of 10cm. 121

4.27 Randomly oriented boulders within the graben at the base of the south scarp. 123

4.28 Large, randomly oriented blocks within the transitional area between the scarp and the labyrinth. Backpack is included for scale. 124

4.29 Map of the labyrinth and some orientations of other boulders down slope, at a scale of 1:500. 125

4.30 A street within the labyrinth proper. The street narrows to the south, the direction of view of the photograph. 127

4.31 A street infilled with debris (fallen rock, pine needles and branches), with a backpack for scale. 128

4.32 Boulders dipping at 26° resting on top of a rock blocks, indicating that the friction angle of this material is greater than 26°. 129

4.33 Dolomitic mottling of the Palliser Formation limestone, with a notebook for scale. 130

4.34 Karren on the vertical surface of a boulder within the downslope colluvial area of the Rock and Boulder Gardens, with a notebook for scale. 132

4.35 Stereographic projection of measured bedding orientations within the downslope colluvial area of the Rock and Boulder Gardens. Projection of poles to the planes on an equal-angle, lower hemisphere stereogram. The star is a plot of the pole to the average bedding orientation, and the gray poles are plots of poles to two of the regional slopes. 133

4.36 Colluvial material in the Maligne River at the toe of the colluvial area of the Rock and Boulder Gardens. The large boulder is 2m high. 134

4.37	Diagram showing the general trend of the slope break, and the resulting kinematically free blocks.	136
5.1	Topographic map showing Debris Flow Creek and the informally named tributary creeks that feed into the canyon. UTM co-ordinates are given in the northwest corner of the map. Map is at a scale of 1:50 000.	141
5.2	Outline of Debris Flow Creek on airphoto A23015-139, showing the division of the area into the upper valley, the canyon and the fan.	142
5.3	Portion of Figure 2.3 enlarged to show the area of Debris Flow Creek. The outline of the bowl shaped feature on the north side of the creek is shown with some bedding orientations. The locations of Figures 5.10-5.12 are shown on the map.	144
5.4	Equal angle, lower hemisphere stereogram of the poles to bedding in the vicinity of the syncline, and the fold axis. The fold axis has an orientation of 169°/12°. The approximate orientation of the north wall of the canyon is shown to demonstrate that blocks are kinematically free to slide along the fold axis on this slope.	146
5.5	Photograph of the bedrock at the top of the canyon. Note that the beds are gently dipping, with open joints.	147
5.6	Terrain analysis of Debris Flow Creek on airphoto A23015-139. Terminology follows that of Cruden and Thompson (1987) with triangles indicating talus slopes.	149
5.7	Till deposits within the upper canyon, at the location where the large U-shaped valley meets with the main creek, near the top of the canyon.	150
5.8	Oblique photograph showing the location of the syncline adjacent to Debris Flow Creek. Photograph number 460 by M.P. Bridgland. The locations of Figures 5.9, 5.15 and 5.16 are shown, along with the different terrain units to the north of the creek.	151

5.9	Photograph of an area of large displaced boulders. Location of this photograph is on the east side of the syncline at the base of the cataclinal overdip slope (Figure 2.8). Karren are present on the surface of the boulders, and can be seen on the boulder in the foreground. Pack is used for scale.	152
5.10	Jointed bedrock of the Palliser Formation within the canyon of Debris Flow Creek. The trace of bedding and the trace of joint 1 are shown on the photograph. The line in the photograph is the boundary between the colluvial material and the in place bedrock.	154
5.11	Photograph of the north wall of the canyon, showing the colluvium the composes this wall. Notice the angular nature of the material, as well as the distribution of grain sizes. View is from the creek bed looking NE. The goat is for scale.	155
5.12	The north slope of the canyon showing the difference in vegetation between the active and the inactive colluvium. Photograph is taken from the creek bed looking west, near the axis of the syncline.	156
5.13	Enlargement of air photograph A23015-139, showing the location of the cirques within the watershed of Debris Flow Creek, and the corresponding direction of ice flow. The headwall of the cirques is an orthoclinal slope.	157
5.14	Diagram showing one possible source of the colluvial material present to the north of the canyon. The colluvial material is produced after glacial retreat by the sliding of rock along bedding planes on oversteepened slopes. Only one cataclinal overdip slope remains in this area.	159
5.15	Photograph of striations on a boulder of Palliser Formation limestone within the canyon of Debris Flow Creek. The arrows point out some of the striations, and indicate the direction of flow.	160

5.16 Photograph of the sediments in the upper valley, taken from the location of Figure 6.15, at the top of the canyon, where the upper valley starts. Notice the rounding, and the well sorted nature of the sediments. Photograph is taken from the narrow top of the canyon, looking upstream to the east. 162

5.17 Photograph of the fan of Debris Flow Creek. Vegetation Zone 1 is dominated by coniferous trees, Zone 2 is mixed coniferous and deciduous trees and Zone 3 is mostly unvegetated, with Poplar tress making up the majority of the vegetation. The location where the creek changes flow direction around the till is shown with a white dot. 163

5.18 Location of the spring system on the alluvial fan, showing the spring and the regularly flowing stream at the base of the till in white. The intermittent stream location is shown in black where the two creeks meet. The inset is a photograph of one of the springs. 164

5.19 A poplar tree showing roots that are exposed above the surface of the ground. The location of the photograph is in the fan area. Downstream from the glacial till deposits. 166

5.20 Several of the trees that have recently been knocked over, and the accumulation of debris on the upstream side of a tree trunk on the alluvial fan. The presence of needles on the fallen tree indicate that this event is no older than 2-3 years. 167

5.21 The current creek flowing underneath the edge of the till, a few metres upstream from the 90° turn of the creek. The creek has cut roughly 1 m into the unit. 168

5.22 Cracks in the till above where the creek is undercutting the till. 170

5.23 Dead trees in from of a large boulder at the downstream extent of the deposit. The boulder on the left side of the photograph is 1.75 m long. Photograph is taken in a direction perpendicular to the inferred flow direction. 171

5.24 Photograph of the large boulder at the head of the deposit. The boulder is oriented with its long axis in the 172

downstream direction, with the upper surface of the boulder dipping in the downstream direction.

5.25 Photograph of vegetation adjacent to the deposit. The thick black line shows the boundary of the deposit. Vegetation is likely 10-15 years old. The tape measure in the photograph is 12 mm wide. 173

6.1 The west slope of the Colin Range, Jasper National Park, showing areas of exfoliation, E; orthoclinal toppling, O; cataclinal toppling, C; anaclinal toppling, A and debris flow deposits, DF, overlain on part of aerial photograph A23025-138, Natural Resources Canada. Scale 1:60 000. 180

6.2 View of the Colin Range from the Palisades repeat photography set from the Bridgland collection. The upper set of photos is the repeat set, photos 470 and 471, and the bottom photograph is that of Bridgland, 1915, photo numbers 470 and 471. 181

6.3 Original and repeat photographs number 336 showing the enlarged area shown at the bottom, with Rhemtulla and Higgs photograph in front of Bridgland's photograph. The dotted line corresponds to the slope profile of the 1999 photograph, and the solid line corresponds to the slope profile in the 1915 photograph. The areas where the slope profile differs are shown in the figure. In addition, there is more talus in the 1999 photograph than in the 1915 photograph. 183

6.4 View of exfoliation below a cataclinal underdip slope, showing no sign of the exfoliation from above, limiting the ability of exfoliation to be observed on aerial photographs. 185

6.5 Area of exfoliation on the face of Morro Peak, enlarged from Bridgland photo 470 on the top, and enlargement from photo 467 on the bottom. The photographs have been enlarged 200% and an additional 200% to make the exfoliations visible. The individual bedding planes create the flat surfaces above the depressions. 186

6.6 Set of repeat photographs, photos #460, with the top photo from Higgs and Rhemtulla, and the bottom photograph by Bridgland. The photograph shows the area 188

of Debris Flow Creek.

6.7 Enlarged 200% repeat set of photograph number 460, with the original photo on the left and the repeat photograph (Higgs and Rhemtulla) on the right side. Vegetation changes are easy to see on the alluvial fan, and the changes in the moraine include the removal of the hoodoos over the 85 year time span between the photographs. The moraine is roughly 40m high at this location. 189

List of Symbols

Φ = friction angle of material

Ψ = dip angle of the bedding plane

β = angle of slope

γ_w = unit weight of water

γ_r = unit weight of rock

W = weight of a block

U = hydrostatic force on the base of a block

V = hydrostatic force in a dip joint

c = cohesion of a block along a bedding plane

A = area of the base of a block

FS = factor of safety (limit equilibrium analysis)

1 Introduction

1.1 General Overview

Jasper National Park is located in the Rocky Mountains, in the Canadian Cordillera. The geology of Jasper National Park is dominated by Cambrian to Tertiary sedimentary rocks (Yorath and Gadd, 1995). These rocks have been folded and thrust to create the mountain chains of the Rocky Mountains. Since the uplift of the Rocky Mountains, both ice and water have been working to erode the mountain chains (Baird, 1972). The oversteepening of slopes due to glacial erosion during the last ice age and the constant erosion of running water lead to the instability of slopes.

Jasper National Park is an active recreational area in both the summer and the winter. As there are many people who enjoy the beauty of the park, it is important to know the stability of the slopes that create the majesty of the park. As the last ice age ended roughly 10,000 years ago (Clague, 1989), the slopes in Jasper National Park are geologically young.

This study focuses on the Colin Range, an area of active limestone karst (Thompson, 1976), within Jasper National Park. The bedrock is dominated by the thickly bedded, uniform limestone of the Palliser Formation (Mountjoy, 1959; Mountjoy, 1964; Mountjoy and Price, 1976; Mountjoy and Price, 1985). This is a recreational area that is located near to the townsite of Jasper, and there are at least 4 backcountry campsites located in the vicinity of the Colin Range. In addition, the recreational area of Maligne Canyon is included within the Colin Range. It is an area that is well used by recreational users, including the area of the Rock and Boulder Gardens, a common rock climbing area, and the Mount Colin Centennial Hut, also a common area for rock climbers. This study classifies the slopes of the mountains within the Colin Range and characterizes the stability of the shapes and forms of the mountains, in order to assess the potential for

slope stability problems that could affect the recreational users of the Colin Range within Jasper National Park.

This study also utilizes photos from the Bridgland Repeat Photography project (http://bridgland.sunsite.ualberta.ca/, 2001). The repeat photos are helpful to check predictions of rockfall hazards within the Colin Range, as well as to study any accumulation of rockfall debris that has collected over the 85 years between the sets of photos. The photographs are used for reconnaissance of the study area to highlight any areas of interest to focus on.

In the past, toppling and sliding on slopes were considered to be the main modes of slope movement in hard rock. Hoek and Bray (1974), for instance, analyzed slope instability by sliding, for both planar movements as well as the movement of wedges of rock. Hoek and Bray's work was restricted to slopes where the dip direction of the penetrative discontinuities was within 20° of the dip direction of the slope under analysis, or limited to the study of cataclinal slopes (Norrish and Wyllie, 1996), where a cataclinal slope has a slope direction within 20° of the dip direction of bedding (Cruden and Hu, 1996). deFreitas and Watters (1973) worked on toppling found to occur in nature; Hoek and Bray (1974) looked at a kinematic analysis of toppling in rock. Hoek and Bray (1974) analyzed the simplest mode of toppling, "a model of a block resting on an inclined plane" (p. 28). This model required the weight vector to fall outside the base of the block in order for toppling to occur (Hoek and Bray, 1974). In order for the weight vector to fall outside the base of the block, the block should sit on an inclined plane that is dipping in the direction of the slope. A block was assumed to rotate about an axis parallel to the strike of the inclined plane and not in any other direction, indicating that toppling could only occur on anaclinal slopes, where the dip direction of the bedding is 180° (+/- 20°) from the direction of the slope (Figure 1.1). Cruden (1989) has shown that toppling of beds in a much wider range of orientations is possible.

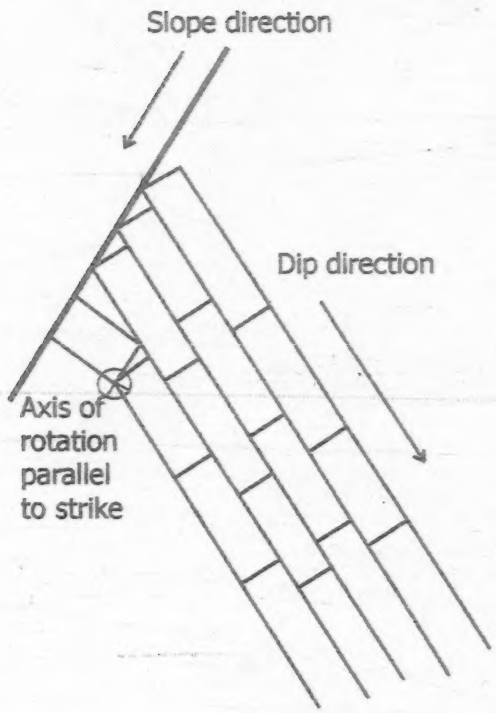

Figure 1.1 – deFreitas and Watters' (1975) concept of toppling and how toppling was considered to occur only on anaclinal slopes. The axis of rotation is into the page in the direction of strike of the beds, and the slope direction and the dip direction of the bedding are taken into account.

1.2 Purpose and Scope

This research extends the modes of rock slope movements to those movements that occur on orthoclinal slopes, and documents movements on orthoclinal slopes within the Colin Range of Jasper National Park. Additional modes of rock slope movement within the Colin Range are documented in the field as well. In addition, the usefulness of the Bridgland Repeat Photography Project with respect to rock slope movement analysis is examined. The findings are presented in the following chapters.

The climate, bedrock geology and the geomorphology of the area of the study, within the Colin Range of Jasper National Park, is described in Chapter 2. In addition, the slopes within the study area are divided on an aerial photograph following the terminology of Cruden and Hu (1996). The study area is dominated by orthoclinal and cataclinal slopes.

A basic model for sliding and toppling on orthoclinal slopes driven by water pressure is derived in chapter 3. Several examples of toppling and sliding on orthoclinal slopes in the Colin Range are also discussed, and the feasibility of the model is discussed in relation to the field examples.

Chapter 4 discusses modes of slope movement on cataclinal slopes within the Colin Range. Toppling on cataclinal underdip slopes is documented, exfoliation is discussed and documented on cataclinal underdip to dip slopes, and a translational slide on a former cataclinal overdip slope is documented and discussed. All of the slope movements that are discussed and documented are plotted on a process diagram (Cruden and Hu, 1996) in order to extend the knowledge of slope processes on cataclinal slopes in nature.

Evidence for a complex intermittent debris flow is presented in Chapter 5. The bedrock geology and the geomorphology are discussed in detail, as they exhibit control on the debris flows, snow avalanches and slush avalanches that occur at this location.

The usefulness of repeat photography projects in relation to the analysis of landslide hazards is presented in Chapter 6. The Bridgland Repeat Photography is used in the evaluation of landslide hazards for the slope movements that are discussed in Chapters 3-5, and in relation to other uses of photography from the Canadian Dominion Surveys.

A summary and recommendations are presented in Chapter 7.

1.3 Previous Work in the Canadian Rockies

E. Mountjoy and R. Price of the Geological Survey of Canada undertook detailed mapping of Banff, Yoho, Kootenay and Jasper National Parks in 1965 and 1966 (Yorath and Gadd, 1995). Geological maps produced by Mountjoy and Price (1976, 1985) at a scale of 1:50 000 were published for Medicine Lake (NTS 83C/13) and for the Jasper Townsite (NTS 83D/16). The Geology of Mount Robson map was published at a scale of 1:126 720 (Mountjoy, 1964), and the Miette map sheet was published in 1959 at a scale of 1 inch to 1 mile (Mountjoy, 1959). Charlesworth, of the University of Alberta, led the mapping of the Pre-Cambrian geology of the Jasper National Park area (Charlesworth et. al., 1966). D.M. Baird (1972) published a book on the geology of Jasper National Park for the Geological Survey of Canada. Yorath and Gadd, with the help of the Geological Survey of Canada, published an overview of the accumulated geological data of this region in 1995, including a geological map of the park. Gadd (1995) also presented an overview of the geological history of the area. Mountjoy and Price (1970) wrote on the geological structures of the central Rocky Mountains. The Geological Survey of Canada "A" Series Map 1611A at a scale of 1:50,000 covers NTS area 83D/16 (Mountjoy and Price, 1986). NTS area 83C/13 is covered by Mountjoy and Price (1976). Alberta Environment and the Alberta Research Council (1980) published maps of the surficial geology of the Rocky Mountains, yet only the NTS sheet 83D/overlaps the study area. The

Quaternary geology of the Canadian Cordillera was compiled by John Clague (1989).

Studies conducted on rock-slope movements in the Canadian Rocky Mountains include movement on both natural slopes and engineered slopes. Simmons and Cruden (1980) explored a rock labyrinth within the Front Ranges of the Rocky Mountains. Cruden (1985) discussed rock slope movements in the Canadian Cordillera, which includes the Canadian Rocky Mountains. McAffee and Cruden (1996) examined landslides that occurred in Highwood Pass, Alberta. Cruden and Hu (1996) discussed hazardous modes of rock slope movements in the Canadian Rockies. Cruden et. al. (1993) looked at topples occurring west of Clairvaux Creek in Jasper National Park along a road cut.

Hazard assessment is becoming common practice in the field of environmental earth science. As an example, Eaton (1986) completed a thesis on the rock slide hazards that exist within Kananaskis Country, Alberta. This provided guidance for the recreational development in the area.

2 Site Description

2.1 Introduction

The study area is located in the Colin Range of Jasper National Park, in the Front Ranges of the Rocky Mountains, within the Canadian Cordillera. The southwest facing slopes of the Colin Range, where the Athabasca River cuts the Colin Range, are the focus for this study (Figure 2.1). The region is bounded to the northwest and the west by the Athabasca River, to the south by the Maligne River and to the east by the summits of Morro Peak, Hawk Mountain, Mount Colin and Roche Bonhomme. All of the individual sites were accessed by the Overlander Trail in Jasper National Park.

The area is at the corners of 4 NTS map sheets, 83E/1, 83F/4, 83D/16 and 83C13, northeast of the Jasper townsite. The climate of the region affects slope movements, and so is discussed in Chapter 2.2. The surficial geology also can affect slope movements, and is considered in Chapter 2.3. The bedrock geology at this location is composed of 2 thrust sheets, the Chetamon Thrust Sheet and the Colin Thrust Sheet, and is discussed in Chapter 2.4. For the sake of discussion, slopes are separated into different types based on the relationship of the dip direction of the bedding and the direction of slope in Chapter 2.5. The slopes are divided into cataclinal slopes, orthoclinal slopes (Chapter 2.5.4), plagioclinal slopes (Chapter 2.5.5) and anaclinal slopes (Chapter 2.5.6). Cataclinal slopes are further separated based on the relationship between the angle of slope and the angle of bedding, into cataclinal underdip slopes (Chapter 2.5.1), dip slopes (Chapter 2.5.2) and overdip slopes (Chapter 2.5.3).

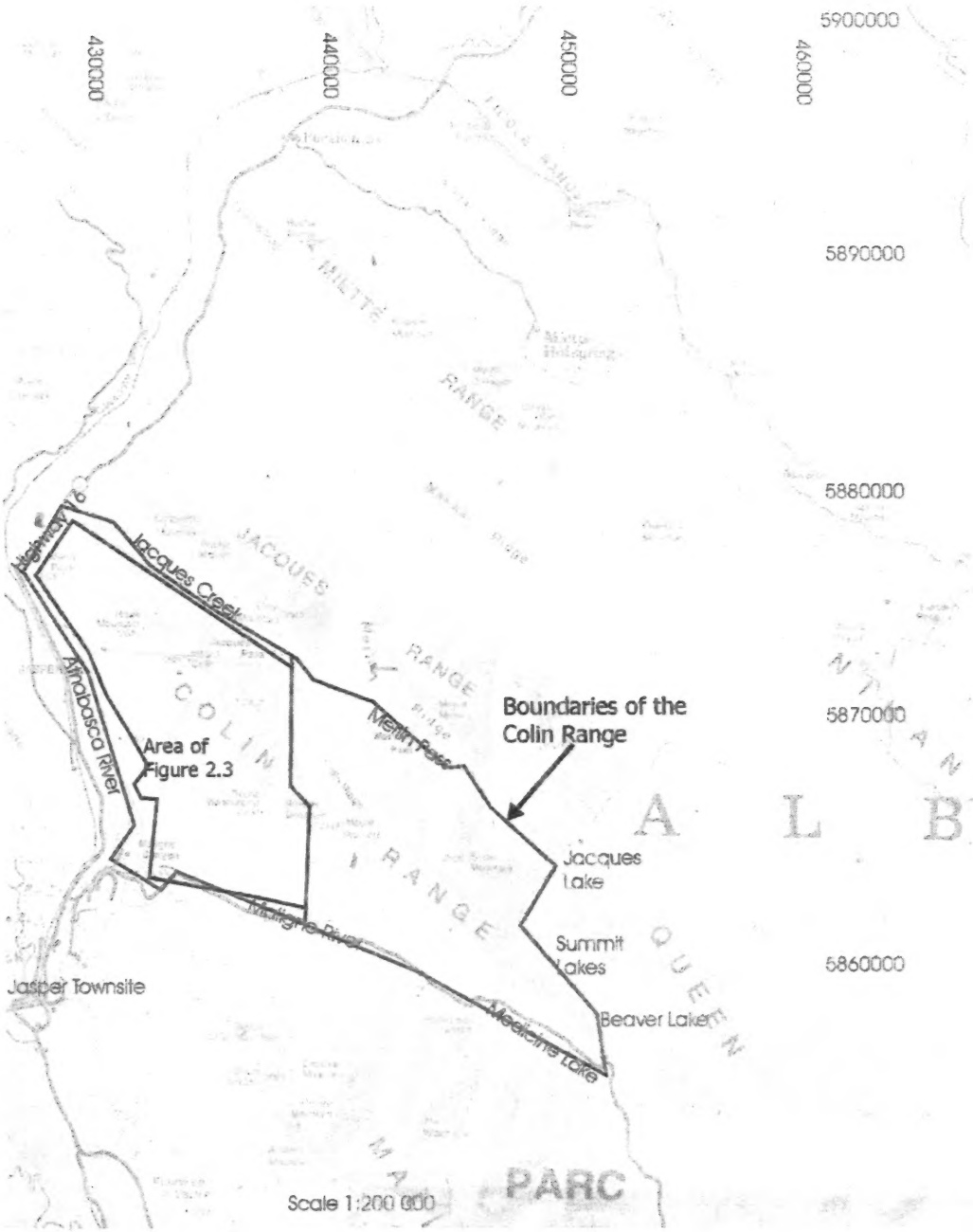

Figure 2.1 – Topographic map showing the Colin Range and the area of the geological map in Figure 2.3. The figure is derived from the 1:200 000 topographic map of Jasper National Park by the Surveys and Mapping Branch, Energy, Mines and Resources Canada (1985).

2.2 Climate

Environment Canada maintains a weather station in Jasper, at latitude 52°53'N, longitude 118°04'W, at an elevation of 1062.2m (Environment Canada, 2000). The weather station is 2.9km north of the townsite of Jasper, on the west side of the Athabasca River. Based on observations over the period 1971 to 2000, the daily mean temperature for the area is 3.3°C. Average annual precipitation for Jasper is 398.8mm, with 296.7mm of rainfall and 138.0cm of snow. The majority of the rainfall occurs in the months June, July and August, with the majority of snow falling in November, December and January.

Elevations within the study area range from 1020m to 2700m; conditions at higher elevations are not necessarily reflected in the climate data provided. With the low average annual temperature, and 5 of the 12 months measuring average temperatures below zero degrees (Environment Canada, 2000), freeze and thaw conditions are likely to occur throughout the study area. In addition, during the field study that ran from June 2002 to August 2002, snow fall occurred on two separate occasions, indicating freeze and thaw conditions at higher elevations during the summer months.

2.3 Surficial Geology

The surficial geology of the area was shaped by glaciation during the Late Pleistocene to the Early Holocene (Luckman and Osborn, 1979; Luckman, 1986). The Little Ice Age led to the readvance of glaciers within Jasper National Park between 0.6 ka and 0.1 ka (Ryder, 1989). The Athabasca River Valley was shaped by several individual glacial advances and retreats (Mountjoy, 1974). Apart from glacial shaping of the landscape, periglacial, fluvial and mass wasting processes shaped the landscape in the Quaternary, and continue to shape the landscape (Clague, 1989). Glacial flow generally followed the trend of the pre-

existing river valleys within the Rocky Mountains, leading to the removal of most pre-glacial sediments (Clague, 1989).

Fluvial erosion took place during the uplift of the Rocky Mountains, and by the end of the mountain building, drainage patterns that crossed the mountain chain were established (Mountjoy, 1974). The Athabasca River, which cuts across the strike of the mountain range, is fed by several river valleys that follow the regional strike of the area, including the Maligne River and Jacques Creek. These tributary strike drainages are believed to have been forming valleys by the end of the mountain building episode (Mountjoy, 1974). Preglacial valleys were important during glaciation in the Rocky Mountains, as the glaciers generally followed the paths of the pre-existing river valleys, with a few exceptions, where drainage was disrupted by glaciation and subsequent glacial deposits (Mountjoy, 1974).

Evidence for the glaciation of the Athabasca Valley, and the Colin Range adjacent to the Athabasca River, is widespread throughout the study area. The Athabasca River Valley is a broad U-shaped valley with hanging tributary valleys (Mountjoy, 1974). Cirques are present in the Colin Range, and cirque development led to the formation of arêtes and horns (Mountjoy, 1974). Erratics, especially of the Gog Group, are widespread, and are found near the top of Hawk Mountain and Mount Colin, indicating an ice level of at least 2000m (Kane, 1999). Mountjoy (1974) mentioned that the presence of Gog quartzite erratics indicates that the ice reached at least 8000 feet (2438 m) in altitude in the area, resulting in the glaciation of all but the highest peaks in the Colin Range.

The surficial deposits that were left behind by the glaciers in the area include moraines, kame terraces and hummocky moraine, with kettle lakes (Mountjoy, 1974). Lateral moraines, likely left by the Athabasca Glacier, are present along the southwest slope of the Colin Range, and have been dissected post-glacially by creeks that follow the dip direction of the slope. Several authors (McEvoy, 1901; Kindle, 1929; MacKay, 1929 and Taylor, 1960) proposed that a

proglacial lake existed at one time. That view is no longer held; what were formerly thought to be lake terraces are modified kame terraces (Mountjoy, 1974). Post-glacial loess deposits are also present within the Athabasca Valley (Mountjoy, 1974). Dunes still present in the Athabasca River Valley are active in the winter, when Jasper Lake contains little to no water and the silts can be transported by wind.

Post-glacially, rivers have downcut through the glacial deposits, and deposited alluvial fans in the Athabasca Valley, like the alluvial fan of Debris Flow Creek, discussed in Chapter 5. Slope movement has shaped the landscape post-glacially, leading to an abundance of colluvial deposits, including deposits in the area of Debris Flow Creek (Chapter 5). Creeks that were formed in hanging valleys have also cut into bedrock post-glacially, producing the steep-walled canyons of Morro Creek, Garrone Creek and Maligne River (Mountjoy, 1974b). The canyons of Morro Creek and Garrone Creek are discussed further in Chapter 3.

Unfortunately, Geological Survey of Canada surficial geology maps have not been published to cover any of Jasper National Park, so surficial geology maps are not available for the study area. Bayrock and Reimchen (1976) undertook a terrain analysis of Jasper National Park, and produced a surficial geology map of parts of the park, including the area of the NTS map sheet 83D/16. The surficial geology map of the Alberta Foothills and the Rocky Mountains (Alberta Environment, 1980) does not cover and of the area of Jasper National Park.

2.4 Bedrock Geology

The Colin Range is located within the Canadian Cordillera, a structurally controlled northwest-southeast trending mountain chain composed of the deformed western edge of the North American Plate (Clague, 1989). The Rocky Mountains is the easternmost belt within the Canadian Cordillera, and borders on

the Great Plains region. The trend of the geological structure within the Rocky Mountains controls the topography within the region; both the geology and the topography trend northwest-southeast.

The Colin Range is bounded to the southwest by the Maligne River and the Maligne River Valley, a former glacial valley (Mountjoy, 1974a), to the east by a creek that runs from Jacques Lake into the east end of Medicine Lake, to the northwest by Jacques Creek, and to the west by the Athabasca River and the Athabasca River Valley (Figure 2.1). The Colin Range is composed of two major southwest-dipping thrust sheets, the Chetamon Thrust Sheet and the Colin Thrust Sheet (Figure 2.2). The strata within the thrust sheets are composed of formations and groups of sedimentary rocks that range in age from Paleozoic to Mesozoic (Mountjoy and Price, 1976; Mountjoy and Price, 1985). There are several small thrust faults within the range as well. For the most part, the structure appears homoclinal at the surface, with the Devonian Palliser Formation creating the crest of the range (Mountjoy and Price, 1976; Mountjoy and Price, 1985). A synclinal structure occurs at the south end of the study area, forming Roche Bonhomme. A detailed geological map has been compiled from the data in Mountjoy (1959, 1964, 1978), Mountjoy and Price (1976, 1985) and my observations and interpretations, at the junction of 4 NTS map sheets (Figure 2.3).

The Pyramid Thrust Fault (Figure 2.3) is the boundary between the Main Ranges of the Rocky Mountains and the Front Ranges of the Rocky Mountains. The Main Ranges are characterized by gently dipping strata that range in age from Proterozoic to Middle Cambrian. The rocks of the Main Ranges are, for the most part, composed of clastics of Proterozoic to Early Cambrian age. In the Early Cambrian carbonate rocks start to appear in the stratigraphic sequence. The Front Ranges, located on the northeast side of the Pyramid Thrust, are composed mainly of carbonates, with interbedded calcareous shales, and minor clastics (Mountjoy and Price, 1976; Mountjoy, 1978; Mountjoy and Price, 1985). In the vicinity of the study area, the Pyramid

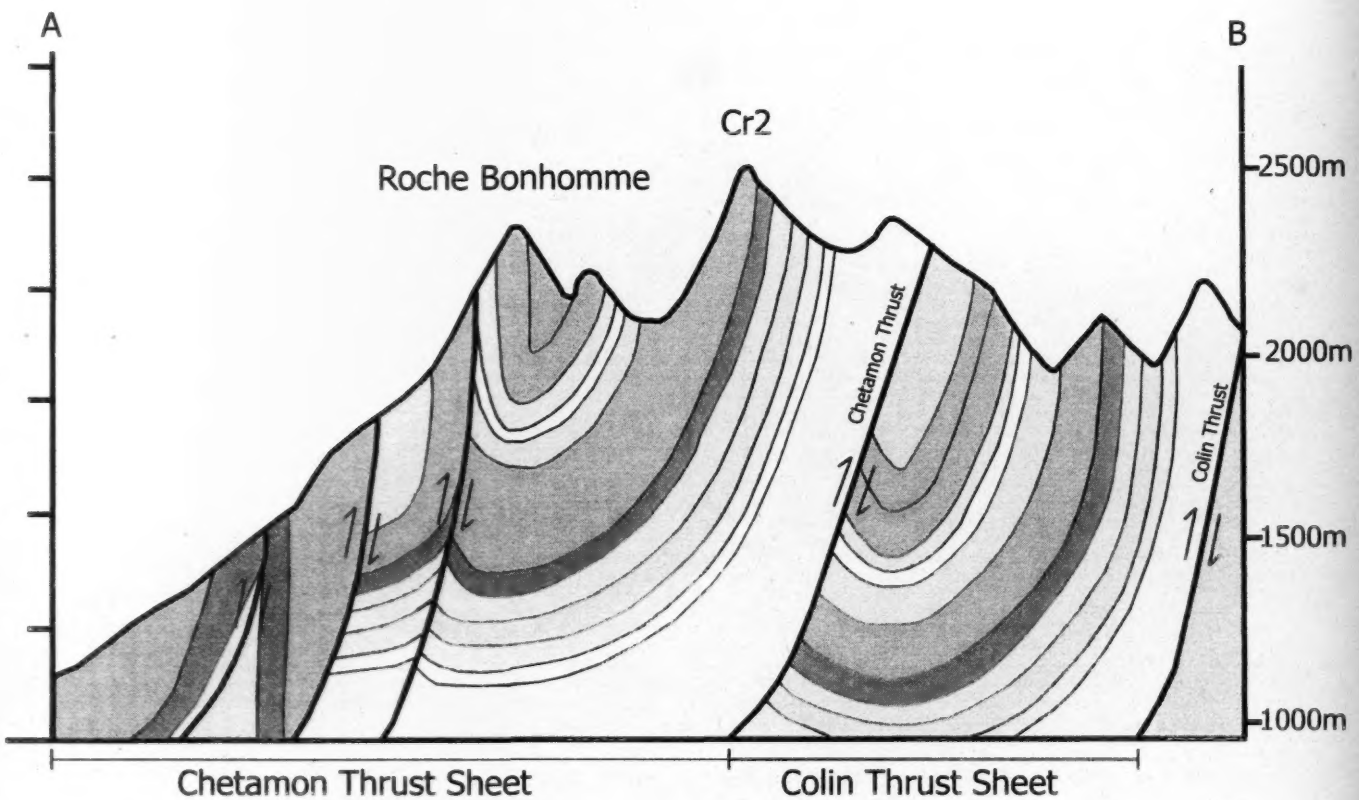

Figure 2.2 – Natural scale geological cross section of the 1:50 000 geological map in Figure 2.3, from A to B. Formation colours correspond to those in Figure 2.4.

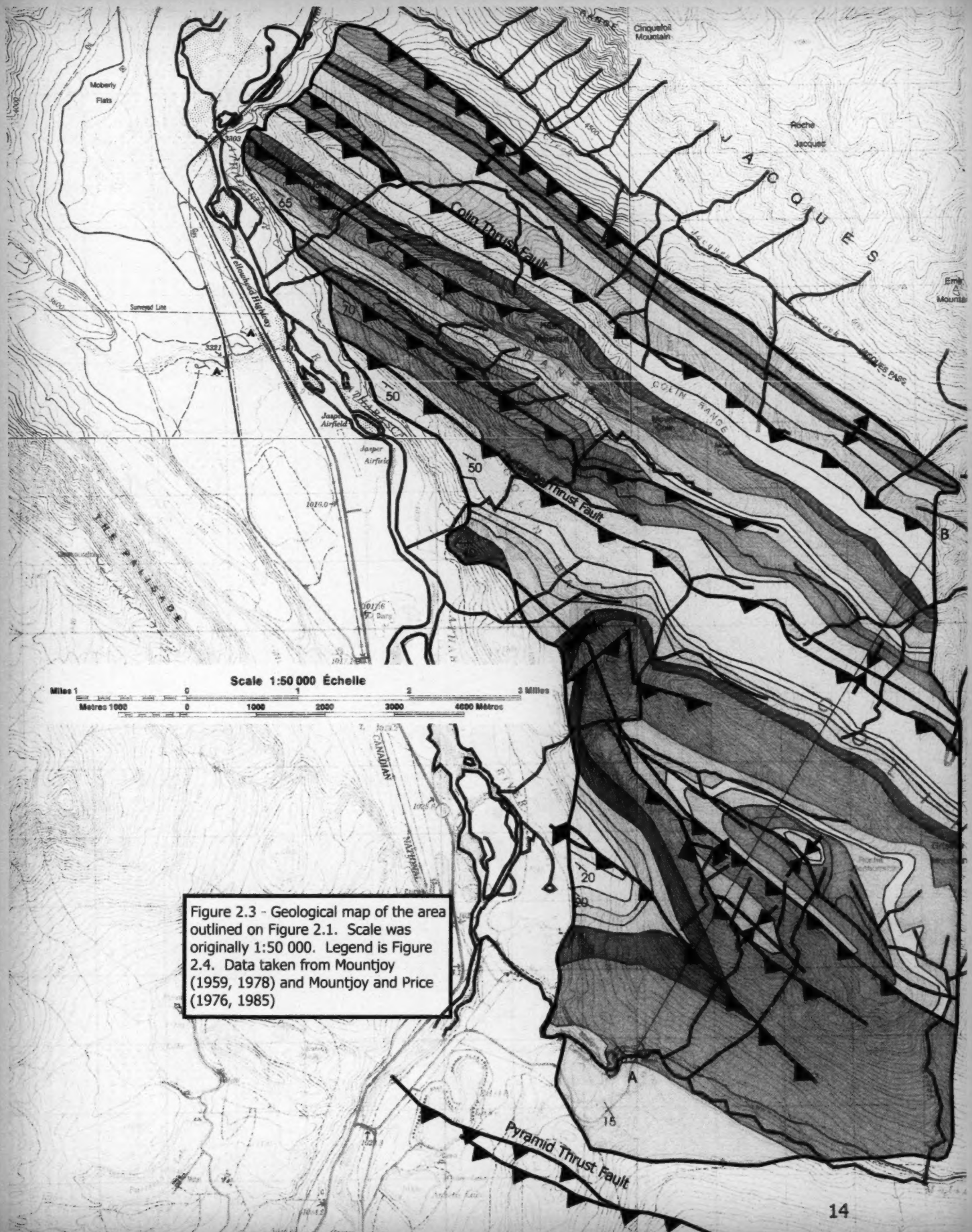

Figure 2.3 - Geological map of the area outlined on Figure 2.1. Scale was originally 1:50 000. Legend is Figure 2.4. Data taken from Mountjoy (1959, 1978) and Mountjoy and Price (1976, 1985)

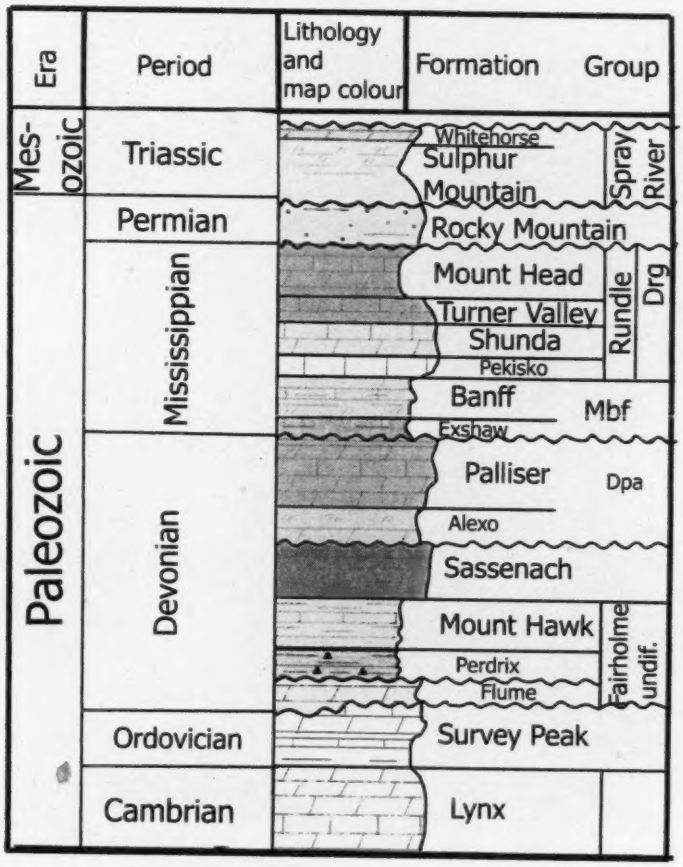

Figure 2.4 – Legend and stratigraphic column to accompany Figures 2.2 and 2.3. The section is 1680m thick. A yellow environment indicates deposition in a marine environment, and the colour of the rock is indicated in the colour column of the diagram. The width of the Lithology and map colour column indicate the competence of the rock to resist erosion.

Thrust follows the Maligne River Valley on the southwest side of the Maligne River (Mountjoy and Price 1976; Mountjoy and Price, 1985), placing the study area within the Front Ranges of the Rocky Mountains.

The Cambrian Lynx Formation is the oldest formation in the study area and outcrops above the Chetamon Thrust and the Colin Thrust (Figure 2.3). The Cambrian Lynx Formation consists of dolostone, siltstone and limestone (Mountjoy, 1978). This formation is thick bedded to massively bedded (Mountjoy and Price, 1976; Mountjoy and Price, 1985). Based on outcrop formation and topography, including ridges and mountain peaks, the Lynx Formation is resistant to erosion (Figure 2.3).

The formation stratigraphically above the Lynx Formation is the Cambrian/Ordovician Survey Peak Formation, composed of calcareous shale, limestone and limestone conglomerate (Mountjoy, 1978). This formation is found within valleys, along with the overlying Fairholme Group and the Sassenach Formation (Figure 2.3). The shales at the base of this formation are recessive (Figure 2.4).

Above the Survey Peak Formation lies the Fairholme Group, containing the Flume, Perdrix and the Mount Hawk Formations (Figure 2.4). The Flume Formation is fine-grained to micritic cherty limestone (Mountjoy and Price, 1976; Mountjoy and Price, 1985), the Perdrix Formation is pyritic calcareous shale, with interbedded thin layers of limestone (Mountjoy and Price, 1976; Mountjoy and Price, 1985) and the Mount Hawk Formation is thinly-bedded calcareous mudstone, which is recessive (Mountjoy and Price, 1976; Mountjoy and Price, 1985). The Fairholme Group rocks are found in valley bottoms (Figure 2.3), with creeks flowing along strikes of the bedding.

Overlying the Fairholme Group is the Devonian Sassenach Formation. The Sassenach Formation is composed of fine-grained sandstone, siltstone, silty limestone and silty calcareous shale (Mountjoy and Price, 1976; Mountjoy, 1978; Mountjoy and Price, 1985). The Sassenach Formation outcrops directly below the Palliser Formation, and so is found on the east side of the crest of the range.

Above the Sassenach Formation is the Devonian Palliser Formation. The Palliser Formation forms the crest of the Colin Range, and creates the summits of Morro Peak, Mount Colin, Hawk Mountain and CR2 (Figure 2.3). The Palliser Formation has been thickened in the south portion of the Colin Range by folding and minor thrust faulting. The Palliser Formation is a dolomitic limestone (Mountjoy, 1978), thickly-bedded, resistant to erosion and forming steep dip slopes (Figure 2.3). The thickness of the Palliser Formation at Hawk Mountain is 865 feet (264m) (deWit and McLaren, 1950).

While the geologic maps that are published for this location do not include the Exshaw Formation at this location, deWit and McLaren (1950) indicate that it is present yet covered on the west slope of Hawk Mountain. The Exshaw Formation is a black, thinly bedded or laminated shale (deWit and McLaren, 1950) that commonly overlies the Palliser elsewhere in the front ranges. While the Exshaw Formation was not observed in the field, it may underlie the talus slopes that occur at the base of slopes at the top of the Palliser Formation throughout the study area. The Exshaw Formation is included with the Banff Formation by Mountjoy and Price (1976).

The Banff Formation is composed of argillaceous limestone and calcareous shale (Mountjoy, 1978). Within the Banff Formation there are several beds of crinoidal limestone (Mountjoy and Price, 1985). The Banff Formation outcrops on the west slopes of the Colin Range and in the syncline on Roche Bonhomme. The Banff Formation a recessive unit, and has been considered to be the filling portion of the "late Paleozoic sandwich" (Gadd, 1999, p.15).

Overlying the Banff Formation is the Rundle Group, which is composed of the Pekisko, Shunda, Turner Valley and Mount Head Formations. The Pekisko Formation is easily identified by the abundance of crinoidal fragments within the unit. Mountjoy and Price (1976) described the Pekisko as a thick-bedded unit, while Mountjoy and Price (1985) described the Pekisko as a thinly bedded unit. The Shunda Formation is micritic limestone containing some breccia (Mountjoy and Price, 1978; Mountjoy and Price, 1985), and is recessive. Above the Shunda

Formation lies the Turner Valley Formation, which is porous, coarse-grained brown dolomite (Mountjoy, 1961), and is easily separated from the Shunda Formation. The Mount Head Formation is cherty dolomite, and is identified by chert nodules that are more resistant to erosion and stick out from the surface of outcrops. The Rundle Group rocks outcrop on the west slope of Hawk Mountain, where the Turner Valley and Mount Head formations are repeated due to a thrust fault (Mountjoy and Price, 1985).

Overlying the Rundle Group is the Triassic Sulphur Mountain Formation. This formation is composed of siltstone, mudstone, sandstone and shale (Mountjoy and Price, 1976; Mountjoy and Price, 1985), and is thinly bedded and recessive. Three different creeks within the study area head within the Sulphur Mountain Formation (Figure 2.3).

The uppermost formation within the study area is the Triassic Whitehorse Formation, which consists of white limestone, sandy dolostone and red mudstone (Mountjoy, 1978). The Whitehorse Formation outcrops on a ridge to the northeast of the crest of the Colin Range, indicating that it is a resistant unit (Figure 2.3 and 2.4). The Whitehorse Formation also outcrops in a few isolated areas below the Chetamon Thrust.

The homoclinal nature of the geology within the Colin Range makes this a suitable area for studying slope movements in orthoclinal and cataclinal slopes. In addition, the Devonian and Mississippian sections are relatively complete within the study area, making the study of types of slope movements within different rock units accessible.

2.5 Slope Types and Distribution

Cruden and Hu (1996) expanded the work of Powell (1875) to define slope geometry with the use of the terms anaclinal and cataclinal slopes (Figure 2.5). Cataclinal slopes are defined as slopes where "the penetrative discontinuity dips in the same direction as the slope" and anaclinal slopes are defined as

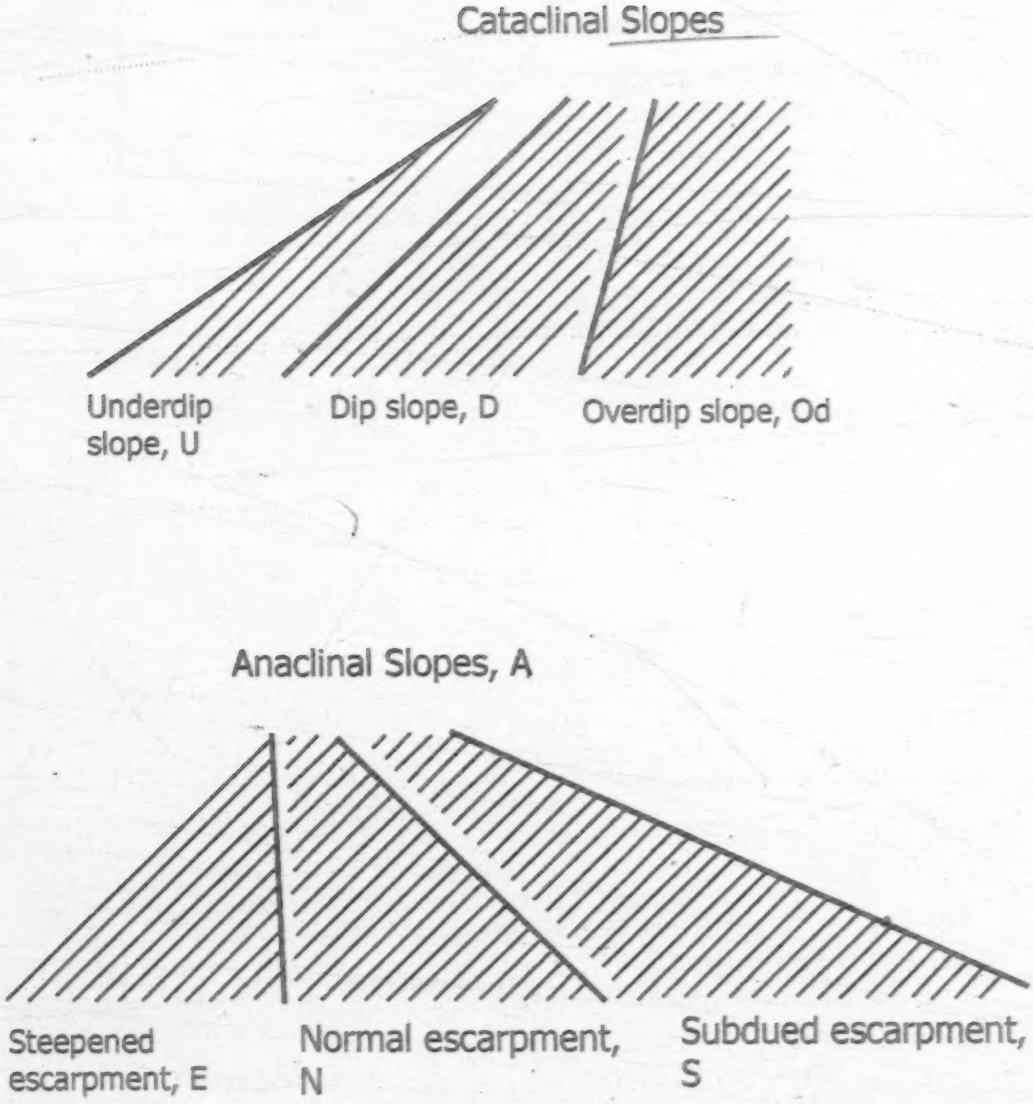

Figure 2.5 – Idealized sections through rock slopes, with bedding dipping at 45° shown by thin lines and slope surfaces are shown by thick lines.

slopes where "the penetrative discontinuity dips in the direction opposite to the slope" (Cruden and Hu, 1996, p. 507). Dip directions are limited to be within 20° of the slope direction for these definitions (Cruden and Hu, 1996). In consideration of this, only 80° of a possible 360°, or 22% of all possible slope orientations are included in these two types of slopes (Figure 2.6). The other 78% of possible slopes are defined as either plagioclinal or orthoclinal slopes. Plagioclinal slopes are taken to be those slopes where the direction of dip of bedding was 20-70° away from the bearing of the slope, and make up 56% of all possible slope orientations. The last type of slope, orthoclinal slopes, comprise 22% of possible slopes and are defined to be slopes that are orthogonal to the dip direction of the penetrative discontinuities, within a range of 20° in either direction from the direction of strike (Cruden and Hu, 1996). While cataclinal and anaclinal slopes can only exist in 1 sector (Figure 2.6) for any given bedding orientation, there are 2 possible sectors for orthoclinal slopes and 4 possible sectors for plagioclinal slopes to occur for a given orientation of bedding.

An aerial photograph with the slope types and directions overlain has been compiled on Figure 2.7. The overlay was created using information from the geological maps of the area (and Figure 2.3), the topographic maps, aerial photographs and from data collected in the field. This overlay is a useful tool, as it divides the territory into slope types, and each individual slope can be explored for types of slope movements, as discussed further in Chapters 3 and 4, as well as by Cruden and Hu (1996).

2.5.1 Cataclinal Underdip Slopes, U

A cataclinal underdip slope has an angle of the slope, β, less than the dip of the bedding, ψ, with a dip direction within 20° of the direction of slope (Figure 2.5) (Cruden and Hu, 1996). The Colin Range is dominated by a homoclinal structure dipping to the west, leading to the formation of cataclinal slopes on the

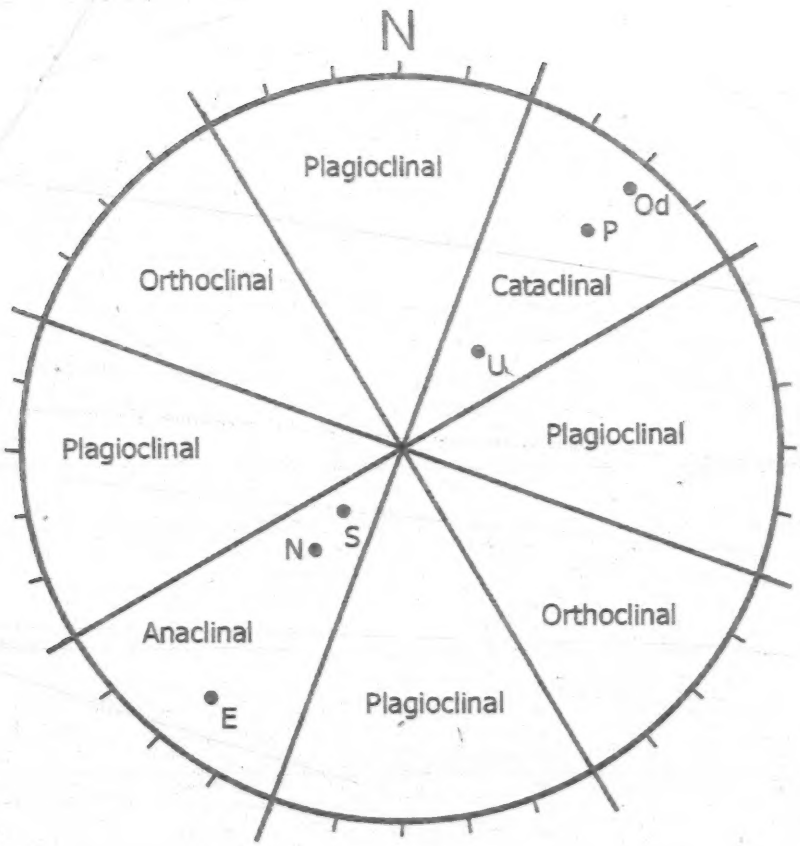

Figure 2.6 – A lower hemisphere equal angle stereonet with the pole to one bedding plane, P, plotted. The bedding plane dips in the direction 220°. The stereogram shows the classification of slopes if poles to the slope planes were to be plotted. If a pole to a slope were plotted on this stereonet, the slope would be classified by the labels, based on the difference in dip direction of the bedding and the slope. Examples of cataclinal overdip (Od) and underdip (U) slopes, and anaclinal normal escarpment (N), subdued escarpment (S) and steepened escarpment (E) plotted on the diagram.

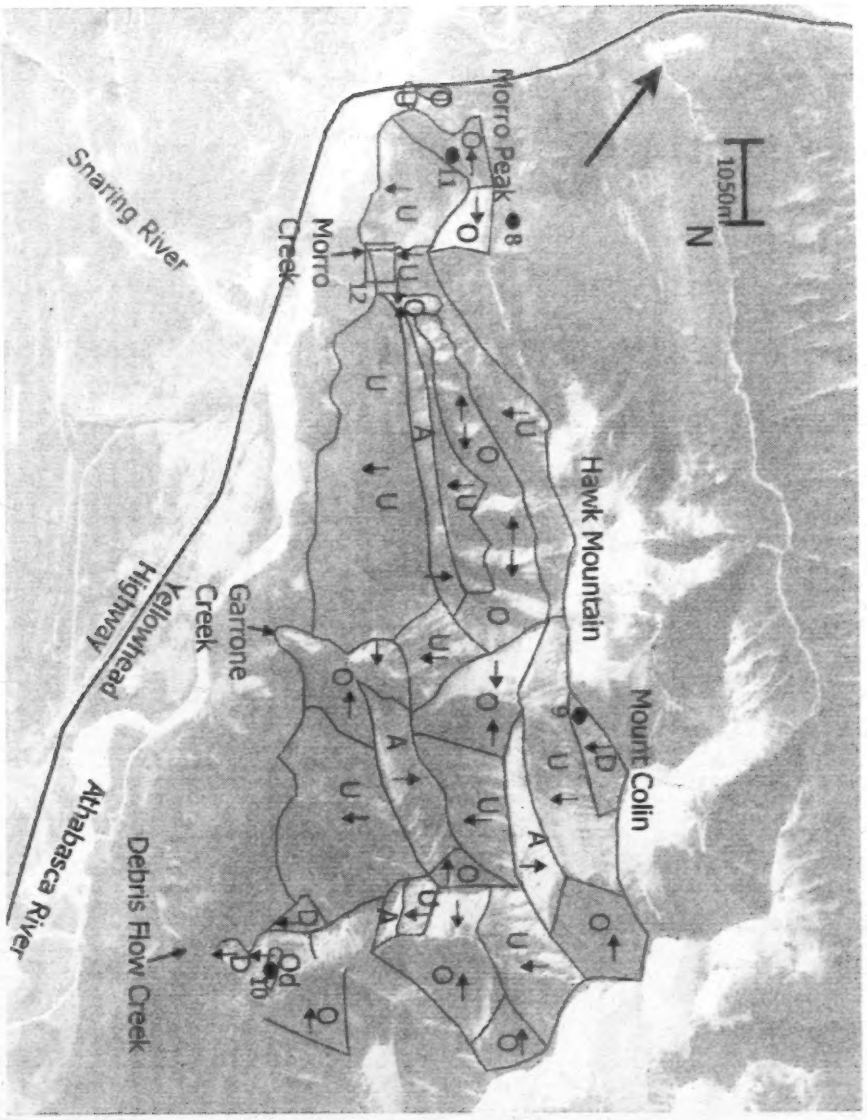

Figure 2.7 – Aerial photograph of the study area showing the classification of the slopes. Arrows indicate the direction of slope for each of the classified slopes. Air photo # A23015-138, Government of Canada – Ministry of Energy, Mines and Resources, originally at a scale of 1:60 000. U indicates an underdip slope, O indicates an orthoclinal slope, A indicates an anaclinal slope (undifferentiated) and Od indicates an overdip slope. The locations of Figures 2.8-2.12 are indicated on the photograph.

west side of the Colin Range. The distribution of cataclinal underdip slopes can be seen on Figure 2.7.

The orientation of cataclinal underdip slopes varies within the study area; slope angles range from a minimum of 17° (toward 222°) to a maximum of 61° (toward 225°). Minimum slope angles occur within the Banff Formation and the Rundle Group rocks, on the lower west slope of the Colin Range. Maximum slope angles occur within the Palliser Formation rocks, on the upper west slopes of the range. The cataclinal underdip slopes are composed of alternating dip faces and gently sloping steps (Figure 2.8). The shallow steps are covered by thin veneers of till and colluvium.

2.5.2 Cataclinal Dip Slopes, D

A cataclinal dip slope (Figure 2.5) has an angle of slope, β, the same as the angle of bedding dip, ψ, and the slope direction is within 20° of the dip direction of the bedding (Cruden and Hu, 1996). Dip slopes are generally formed as a response to oversteepening of the slope at the toe by glaciation, and the subsequent sliding along bedding planes (Cruden and Hu, 1996).

Large dip slopes are not common, as the process of buckling often reduces slopes (Cruden and Hu, 1996). On a much smaller scale, dip slopes were observed to exist within cataclinal underdip slopes (Figure 2.8). The distribution of dip slopes is shown in Figure 2.9. One mode of movement on cataclinal dip slopes will be further discussed in Chapter 4.3.

Dip slopes are considered in Chapter 4 in conjunction with cataclinal underdip slopes, as they make up significant portions of underdip slopes within the study area (Figure 2.7). Dip slopes have slope angles between 40° and 65° within the study area.

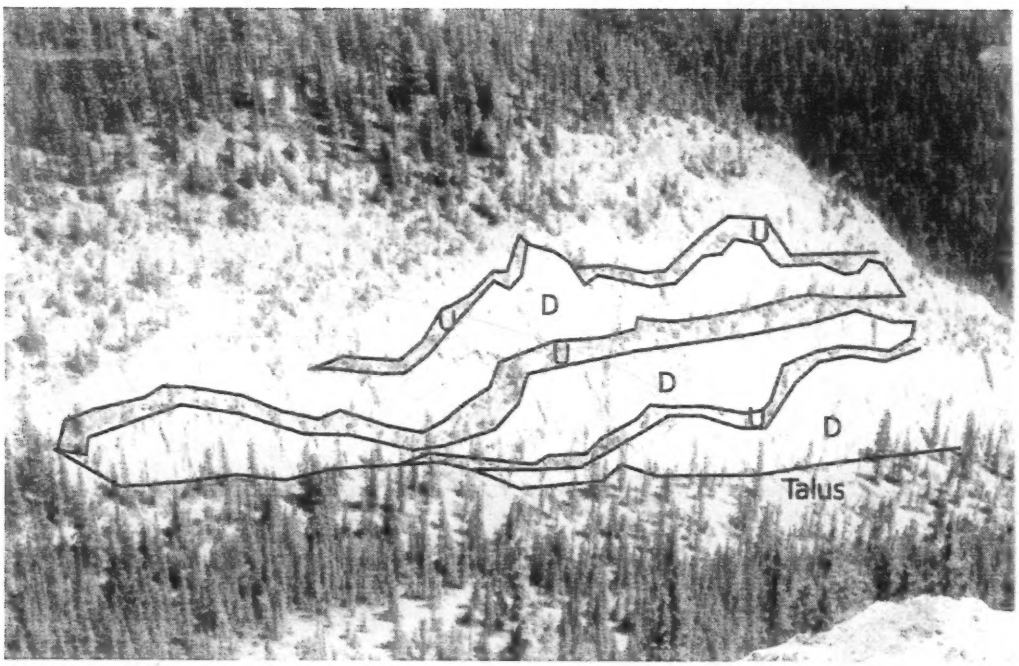

Figure 2.8 – Photograph of a ridge to the east of Morro Peak, taken from Morro Peak, showing a cataclinal underdip slope composed of alternating dip slopes, D, and underdip slopes, U. This is a relatively steep cataclinal underdip slope that is formed in steeply dipping beds. The location of this slope is indicated on Figure 2.7.

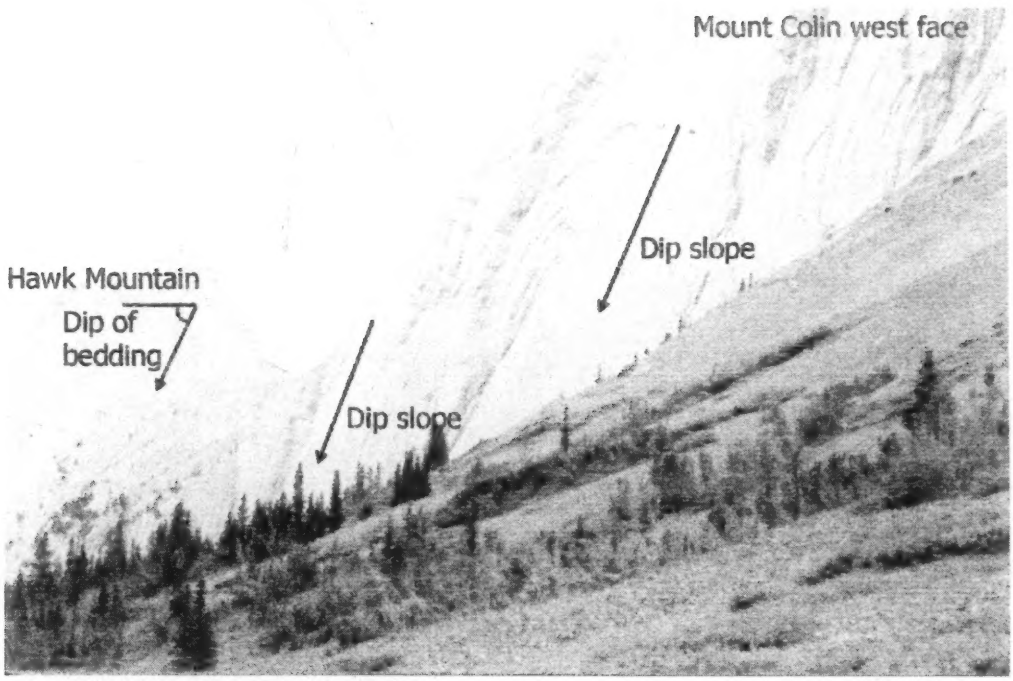

Figure 2.9 – Photograph of the Mount Colin – Hawk Mountain col, taken from the Mount Colin Centennial Hut looking north. The photograph shows the areas of dip slopes on the face of Mount Colin, and to a lesser extent on Hawk Mountain. The slopes follow the bedding at this location, which dips at an angle of 60°.

2.5.3 Cataclinal Overdip Slopes, Od

A cataclinal overdip slope (Figure 2.5) has a slope angle, β, which exceeds the dip of the penetrative discontinuity, ψ, and the direction of slope is within 20° of the dip direction of the penetrative discontinuity (Cruden and Hu, 1996).

The only observed overdip slope (Figure 2.7) is identified by the daylighting of bedding planes on the slope (Figure 2.10). Steep cataclinal overdip slopes are subject to sliding on bedding planes, as there is nothing restricting the toes of bedding planes from sliding (Cruden and Hu, 1996). The cataclinal overdip slope shows signs of active sliding, including an accumulation of young talus at the base of the slope. The talus is interpreted to be recent because there is no vegetation at the base of the slope, the surface of the talus is dark gray (the hydrocarbons within the rock had not yet oxidized), with no lichen present on the surface of the rocks. The Rock and Boulder Gardens, discussed in Chapter 4.4 and 4.5, were formed by the rock sliding on bedding planes on a cataclinal overdip slope that was formed by the Athabasca Glacier and the formation of the south scarp.

The overdip slope has a slope angle of 40° toward 220°, and the bedding dips 35° toward 212°, making it a cataclinal overdip slope.

2.5.4 Orthoclinal Slopes, O

An orthoclinal slope has a slope at 90° ±20° (Figure 2.6) to the direction of the dip of the penetrative discontinuity (Cruden and Hu, 1996). Orthoclinal slopes are found in the Colin Range where creeks cut through the regional structure, where rock was blasted to make way for the Grand Trunk railway through the Athabasca River Valley in 1915 (Parks Canada, 2000) and where the Athabasca Glacier cut across the regional structure. Orthoclinal slopes show the approximate true dip of the bedding on the face of the slope (Figure 2.11).

Figure 2.10 – Photograph of a cataclinal overdip slope, showing the daylighting of the toe of two beds within the Devonian Palliser Formation. This slope is marked on Figure 2.7 as Od, and occurs within the watershed of Debris Flow Creek.

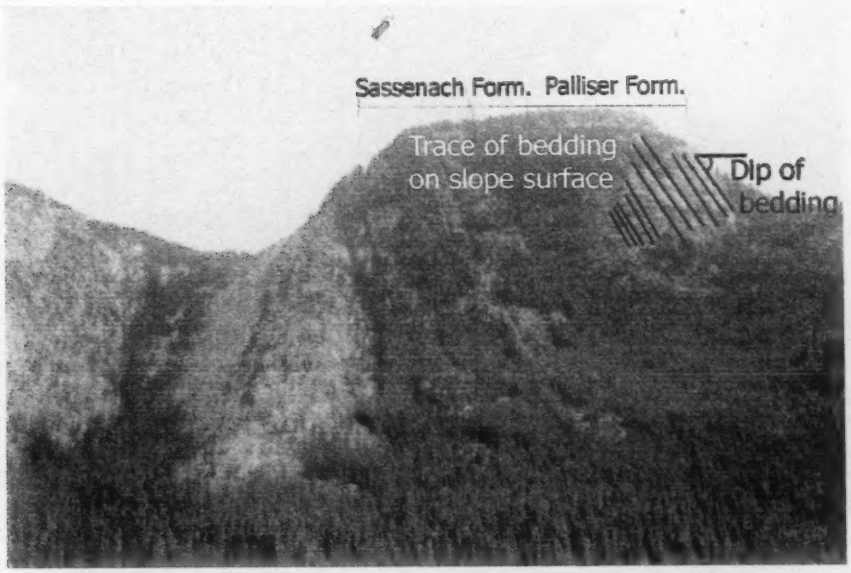

Figure 2.11 –North slope of Morro Peak, an orthoclinal slope. Photo is taken from River Rock, where the Yellowhead River bridge crosses over the Athabasca River, looking south-southeast. The trace of the bedding and the true dip of the bedding are shown on the slope.

Orthoclinal slopes within the study area were found to occur at angles of 22° toward 300° on glaciated slopes along the Yellowhead Highway, up to 90° in post-glacial creek valleys like Garrone Creek and Morro Creek.

Movements on orthoclinal rock slopes are not included in the toppling modes of deFreitas and Watters (1973) or the sliding modes of Hoek and Bray (1975). Chapter 3 discusses different possible modes of movement on orthoclinal slopes.

2.5.5 Plagioclinal Slopes, P

Plagioclinal slopes make up 56% of possible slope orientations (Figure 2.6). A plagioclinal slope is not within 20° of the strike or the dip direction of the penetrative discontinuities. Plagioclinal slopes were not included in the standard modes of sliding (Hoek and Bray, 1975) and toppling (deFreitas and Watters, 1973). The slopes that appeared to be plagioclinal on air and oblique photos are actually cataclinal and orthoclinal slopes that alternate to create the appearance of plagioclinal slopes (Figure 2.12). On aerial photographs, the truncation of the apparently plagioclinal slopes is noticeably orthogonal in nature, and examination of these slopes in the field reveal that these slopes are indeed composed of orthoclinal and cataclinal slopes, and the orthogonal nature of these slopes can also be seen in Figure 2.7. It is likely that these slopes were left after glaciation as roches moutonnees, with quarrying of down-ice ends of outcrops of the Rundle Group rocks (Benn and Evans, 1998). These slopes are not examined further in this study, as plagioclinal slopes were not found within the study area.

2.5.6 Anaclinal Slopes, A

An anaclinal slope has the same strike as that of the penetrative discontinuity, within 20°, yet slopes in a direction opposite to the dip of the penetrative discontinuity. Anaclinal slopes can be broken into three categories, steepened escarpments, normal escarpments and subdued escarpments (Figure 2.5).

Anaclinal slopes are not divided into different types in this study; the slopes examined include both subdued escarpments and normal escarpments. All of the anaclinal slopes are shown on Figure 2.7 as A for the purpose of simplification.

2.6 Conclusions

Aerial photographs and terrestrial photographs (Figure 2.12) are valuable tools for the mapping of slope types and the further analysis of hazards. Aerial photographs, with the use of other geological information, can be used to successfully divide slopes into anaclinal, cataclinal, orthoclinal and plagioclinal slope types. This is useful for landslide hazard analysis, as it focuses the study, as some slope movements occur on specific slope types. For instance, large rapid rock slides typically occur on overdip cataclinal slopes (Cruden, 1976; Cruden, 1982).

Slopes that appear to be plagioclinal on oblique photographs and topographic maps of the Colin Range are composed of cataclinal slopes and orthoclinal slopes that alternate to create the appearance of plagioclinal slopes. Apparently plagioclinal slopes may have been created by the action of ice on the intact rock. The quarrying at the down ice end of the roches moutonnees was likely controlled by the bedding and joint orientation, leading to the formation of

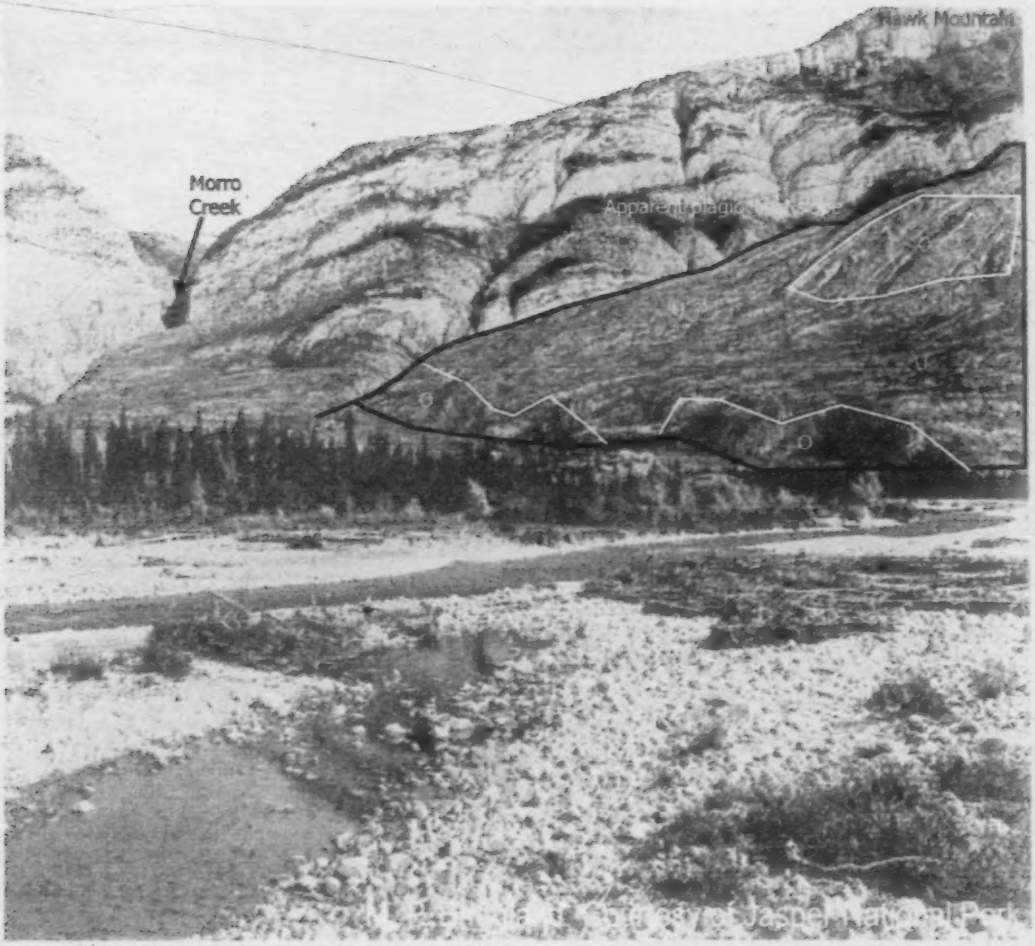

Figure 2.12 – Oblique photograph of an apparent plagioclinal slope, which is composed of orthoclinal slopes, O and cataclinal underdip slopes, U. Photograph number 485 from the Bridgland Repeat Photography, taken by M.P. Bridgland in 1915 (Higgs, 2001). The bedding is striking from the left to the right in the photograph, and dipping out of the page. The photograph was taken to the northeast.

cataclinal and orthoclinal slopes. Different slope geometries may result where ice flow was not parallel to the strike of the beds.

Only one cataclinal overdip slope occurs within the region of the study, indicating that other overdip slopes that were left by the retreat of glaciers in the area have since been exhausted by slope movement processes. The remaining cataclinal overdip slope is an area of active slope movement, in the process of exhausting itself by the sliding of blocks on bedding planes.

3 Movements on orthoclinal slopes

3.1 Introduction

Orthoclinal slopes are those slopes where penetrative discontinuities dip perpendicular to the slope (Figure 3.1). The penetrative discontinuities referred to in this chapter are bedding surfaces. As well, there are assumed to be two sets of orthogonal joints, a set of strike joints, that have the same strike as the bedding, and a set of dip joints, which strike in the direction of dip of the bedding plane, which are observable in the field. Such a joint is a kathetal joint, defined as "a joint surface normal to a bedding surface where the orientation of the joint is a function of the orientation of the bedding" by Hancock (1964, p. 175). In a cross section, AB, along an orthoclinal slope, the true dip, ψ, of the penetrative discontinuities is seen in the slope (Figure 3.2).

The purpose of this chapter is to consider simple modes of movement that may be expected to occur on orthoclinal slopes in sedimentary rocks that contain kathetal joints. The potential for sliding to take place on an orthoclinal slope is examined in Chapter 3.2. A model for sliding in vertically bedded rocks on orthoclinal slopes is derived in Chapter 3.2.1, and a model for sliding in inclined bedded rock on orthoclinal slopes is derived in Chapter 3.2.2. The kinematics of toppling on orthoclinal slopes is explored in Chapter 3.3. A model for toppling on an orthoclinal slope in vertically bedded rock is derived in Chapter 3.3.1, while the case of toppling in inclined bedding on an orthoclinal slope is considered in Chapter 3.3.2. The models for sliding and toppling are compared in Chapter 3.4. This information is then compared to data and observations from the Colin Range, Jasper National Park in Chapter 3.5. An overview and conclusions are presented in Chapter 3.6.

In orthoclinal slopes, there is no apparent dip of the bedding in the direction of the slope, leading to an analysis that is dependent on external

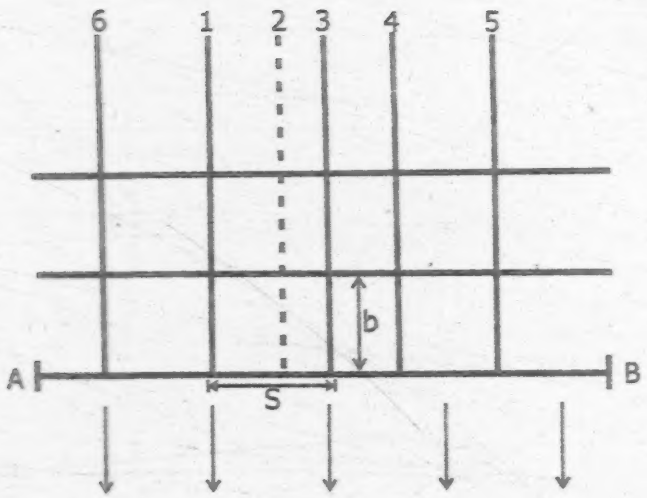

Figure 3.1 – Simple model of the plan view of an orthoclinal slope in inclined bedded strata, showing the intersections of bedding with a strike joint set numbered 1 through 6. The perpendicular lines represent the dip joint set. Numbering and lettering correspond to Figure 3.2.

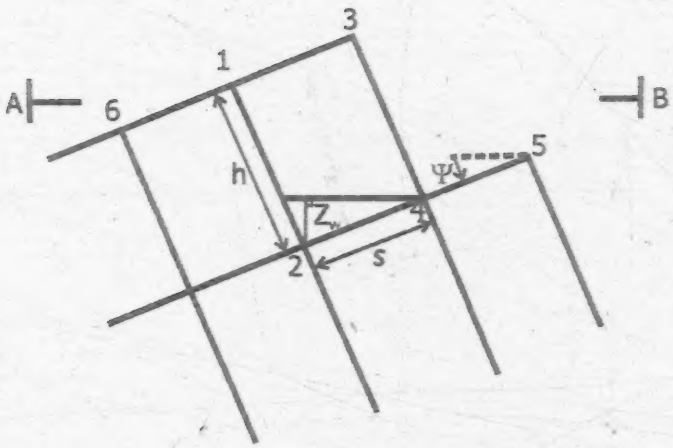

Figure 3.2 – Cross-section AB on Figure 3.1, showing the true dip of the bedding, ψ_b, as seen in an orthoclinal slope. Bedding spacing=h, strike joint spacing=s and the height of water in the dip joint is z_w.

forces, like water pressure, for movement to occur, as gravity adds to the normal force, and resists movement. The analysis in this chapter considers only the effect of water pressures on the movement of blocks on orthoclinal slopes. Other external processes that may have an effect on movement on orthoclinal slopes are frost shattering, freeze and thaw, water freezing in joints, growth of trees and other vegetation in joints, the action of animals in the area and the creep of overlying material (Selby, 1993).

3.2 Sliding on Orthoclinal slopes

Norrish and Wyllie (1996, section 2) divided slope movements into 4 categories. These four categories were:

- Planar failures
- Wedge failures
- Toppling failures
- Circular failures (for soils)

Planar failures were defined as "those in which movement occurs by sliding on a single discrete surface that approximates a plane" (Norrish and Wyllie, 1996, p. 395). According to Norrish and Wyllie (1996, p. 395), in order for planar failure to occur, the following kinematic conditions were to be satisfied:

1 The dip direction of the failure plane must be within 20 degrees of the direction of the slope
2 The dip of the failure plane must be less than the angle of slope
3 The dip of the failure plane must be greater than the angle of friction of the surface.

By definition, an orthoclinal slope does not satisfy the first condition. For the case of an orthoclinal slope, the apparent dip in the direction of the slope is used for analysis. This geometry does not satisfy the third condition mentioned above, as the apparent dip in the direction of slope is 0°, yet Norrish and Wyllie (1996) mention that "the presence of significant pore-water pressures along the

failure surfaces can in some cases alter the kinematic possibility of failure" (p. 396). The water pressure on individual blocks bounded by bedding and kathetal joints is considered to be the main driving force, and dynamic analyses are undertaken to determine if sliding is a possible mode of slope movement on orthoclinal slopes.

3.2.1 Vertical bedding orientation

The vertical bedding orientation is the simplest case to consider, as there are no frictional forces on the block margins in the 2 dimensional analysis, and therefore it is assumed that there are no normal forces acting on these faces. This assumption is used to expand the existing kinematics of planar sliding failure on a slope within 20° of the dip direction of the bedding to that of an orthoclinal slope. According to Norrish and Wyllie (1996, Eq. 15.2), the factor of safety, FS, for a planar failure could be calculated by:

$$FS = \frac{cA + [W(\cos\psi_p - a\sin\psi_p) - U - V\sin\psi_p + T\cos\theta]\tan\phi}{W(\sin\psi_p + a\cos\psi_p) + V\cos\psi_p} \qquad \text{(Eq. 3.1)}$$

where:
a=acceleration due to earthquakes, T=tension on a rock bolt, θ=angle of the rock bolt. Other symbols are included in the List of Symbols (p. xxii).

Considering natural slopes, there are no rockbolts present, and the terms involving the tension of rockbolts, T, can be dropped from the equation. In addition, acceleration due to earthquakes, a, is not considered in this analysis. Simplifying

$$FS = \frac{cA + [W\cos\psi_p - U - V\sin\psi_p]\tan\phi}{W\sin\psi_p + V\cos\psi_p}$$

Assuming that there is no cohesion, c, along the discontinuities, the equation can be further simplified to

$$FS = \frac{[W\cos\psi_p - U - V\sin\psi_p]\tan\phi}{W\sin\psi_p + V\cos\psi_p}$$

In the case of orthoclinal slopes, the apparent dip of the discontinuities in the direction of the slope, ψ_p, is 0 degrees. Substituting this value, the equation further simplifies to

$$FS = \frac{(W - U)\tan\phi}{V} \qquad \text{(Eq. 3.2)}$$

The parameters that are left in the equation, the weight of the block, W; friction resisting sliding, tan ϕ; uplift, U; and the outward force of water, V, are used as resisting and driving forces for sliding in this analysis (Figures 3.3 and 3.4). The parameters W, U and V can be calculated per unit width by: $W=bs\gamma_r$, $U=0.5\gamma_w z_w b$, $V=0.5\gamma_w z_w^2$ where: s= the height of the block under consideration, or the strike joint separation, b= the width of the block under consideration, which is the dip joint separation, γ_r= the unit weight of the rock, γ_w= the unit weight of the water, z_w= the height of the water in the open crack and the block extends unchanged perpendicular to the plane of Figure 3.4.
Assuming that the joint at the back of the block (the dip joint) is filled with water, s can be substituted for z_w. W and U are now defined as $U=0.5\gamma_w bs$ and $V=0.5\gamma_w s^2$.

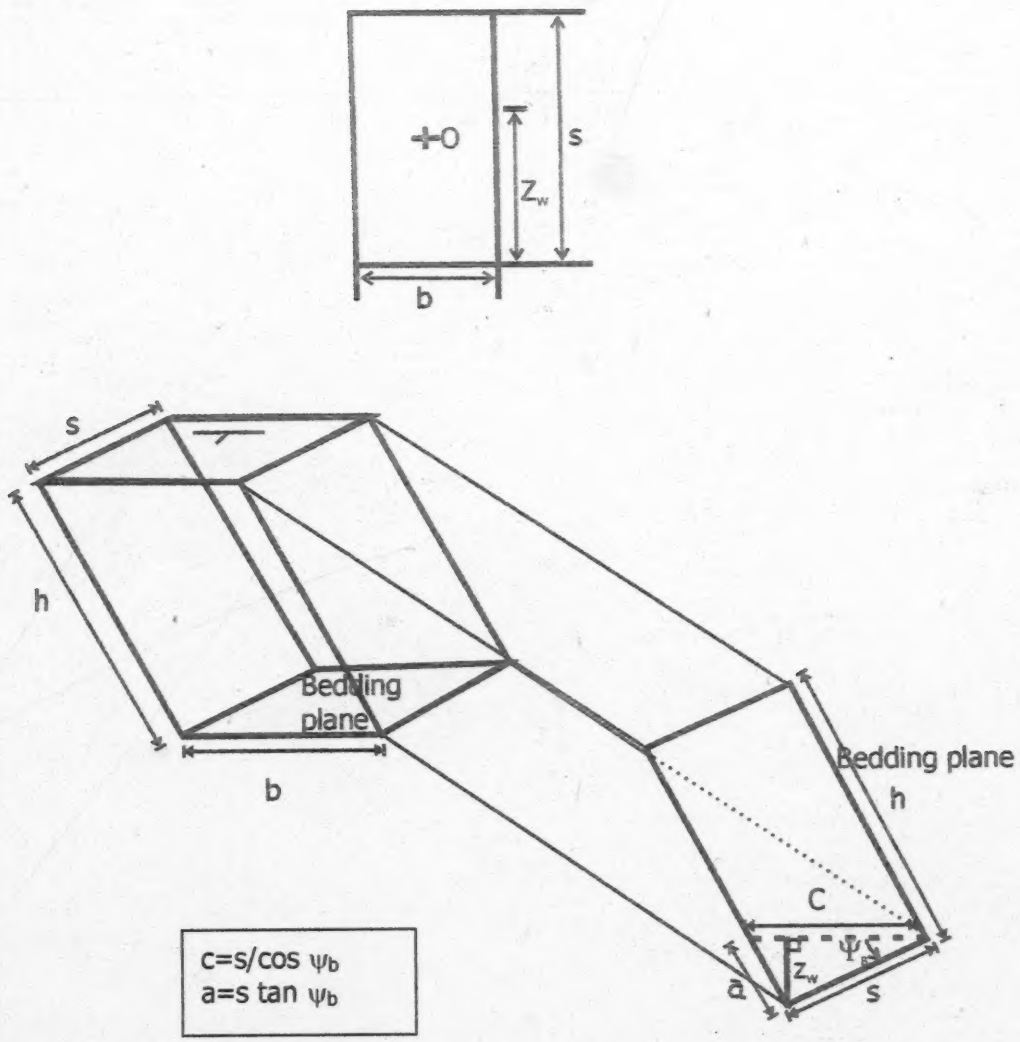

Figure 3.3 – Diagram of blocks that are bounded by bedding planes and kathetal joints. Upper block represents the situation where bedding is vertical, and the view is looking at the bedding plane. The lower block represents the situation where bedding is inclined, and the three dimensional view as well as the view along the strike of the bedding are shown.

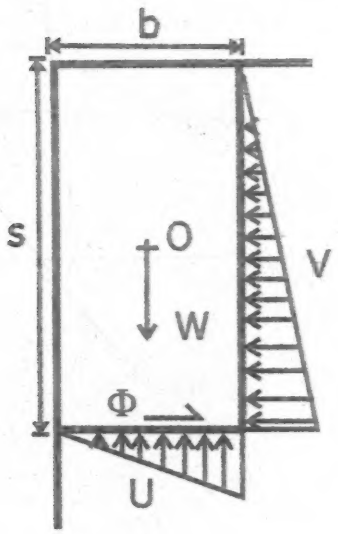

Figure 3.4 – Diagram of a block bounded by a bedding plane and a kathetal joint set showing the pressures acting on the block to drive and resist sliding. The bedding in this situation is vertical, with s=strike joint separation and b=dip joint separation.

Substituting these parameters into equation 3.2

$$FS = \frac{[(2bs\gamma_r) - (\gamma_w bs)]\tan\phi}{\gamma_w s^2}$$

Simplifying the above

$$FS = \frac{b(2\gamma_r - \gamma_w)\tan\phi}{\gamma_w s} \qquad \text{(Eq. 3.3)}$$

As the factor of safety in the limit equilibrium model is equal to the sum of the resisting forces divided by the sum of the driving forces, when the factor of safety is set to 1, slope movement should occur, and a critical block ratio (deFreitas and Watters, 1973) can be derived as follows

$$\frac{s}{b} = \frac{(2\gamma_r - \gamma_w)\tan\phi}{\gamma_w} \qquad \text{(Eq. 3.4)}$$

Given the unit weight of the rock, the unit weight of the water and the friction angle of the material, a height to width ratio of a block that would slide on an orthoclinal slope can be calculated from Equation 3.4.

From the above information, a prediction can be made of the slope angle for the orthoclinal slope, based on an assumption that the sliding of blocks is due to a build up of water pressure in a dip joint. This slope angle, β, can be estimated by

$$\beta = \tan^{-1} s/b \qquad \text{(Eq. 3.5)}$$

as illustrated in Figure 3.5.

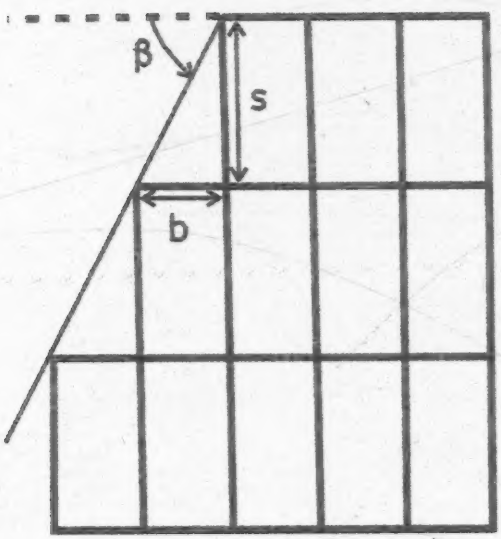

Figure 3.5 – Diagram showing the generalized slope angle, β, as controlled by the block dimensions b, the dip joint spacing, and s, the strike joint spacing, for the situation where bedding is vertical.

γ r	s/b	β
20	1.77678	60.62849
22	2.01219	63.57398
24	2.24761	66.01528
26	2.48302	68.06359
28	2.71843	69.80349
30	2.95384	71.29689
32	3.18926	72.59105

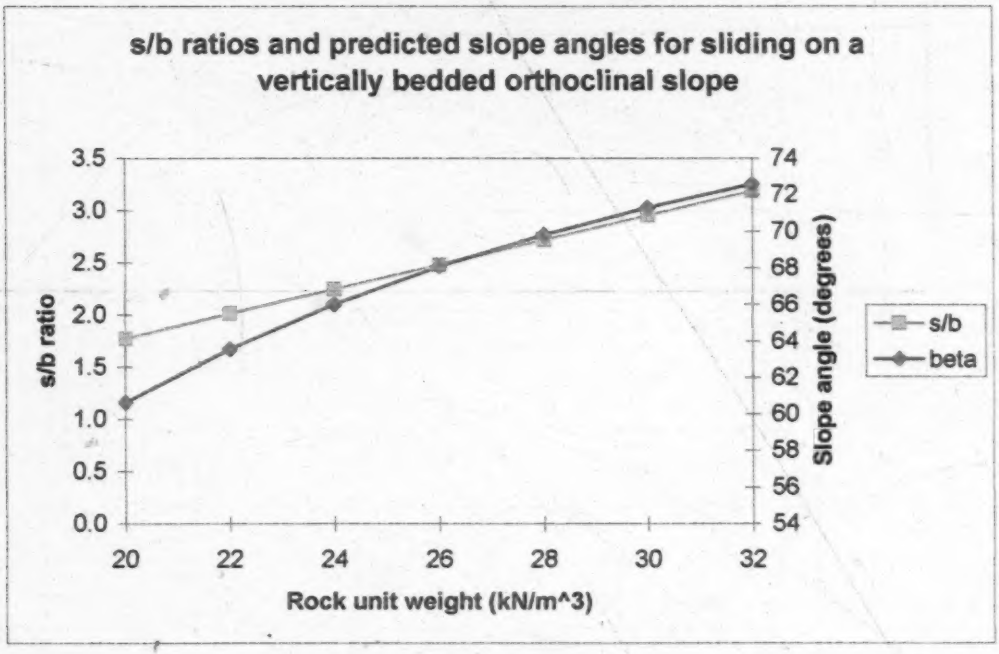

Table 3.1 – Range of s/b ratios as calculated with Equation 3.4, and corresponding predicted slope angles, β, as calculated with Equation 3.5, for a range of rock unit weights, γ_r.

Knowing that γ_w=9.81kN/m^3, and setting ϕ=30° (Norrish and Wyllie, 1996), β can be calculated for a range of γ_r values (Table 3.1). For rock with a unit weight of 25.5 kN/m^3 (Hoek and Bray, 1976) sliding can take place on slopes with a slope angle greater than 67°. Alternatively, for rock with a unit weight of 25.5kN/m^3, a block ratio of 2.4 is required for sliding to take place. This means that the strike joint spacing is 2.4 times greater than that of the spacing of the dip joints.

Once there has been sliding motion of the block, the water pressure behind the block drops, as there is a larger space to fill. This results in the opening of a crack, which snow, ice and rock debris may infill (Figure 3.6). As the crack is again filled, the snow, ice, rocks and water are all able to contribute to the movement of the block with a translational mode of movement. As this process occurs over a long period of time, and with repeated cycles of infilling, this process should be visible in the field on orthoclinal slopes.

This analysis is valid for both the case of vertical bedding and horizontal bedding in orthoclinal slopes. In the situation where bedding is horizontal, b is equal to the dip joint separation, h is substituted for s, and is equal to the bedding spacing.

3.2.2 Inclined bedding orientation

Figure 3.2 shows a horizontal view of a simple model of an orthoclinal slope with dipping bedding planes and 2 sets of kathetal joints. Figure 3.1 displays the plan view of this slope.

In order to analyze sliding for a block that is bounded by inclined bedding planes, there are some parameters that need to be defined, and these parameters are defined in Figure 3.3 for the discussion to follow. The parameters that are used in this discussion are h, the bedding spacing; s, the strike joint spacing; b, the dip joint spacing, c, the horizontal width of the block and a, the height of the water in the dip joint on face hb, the strike joint.

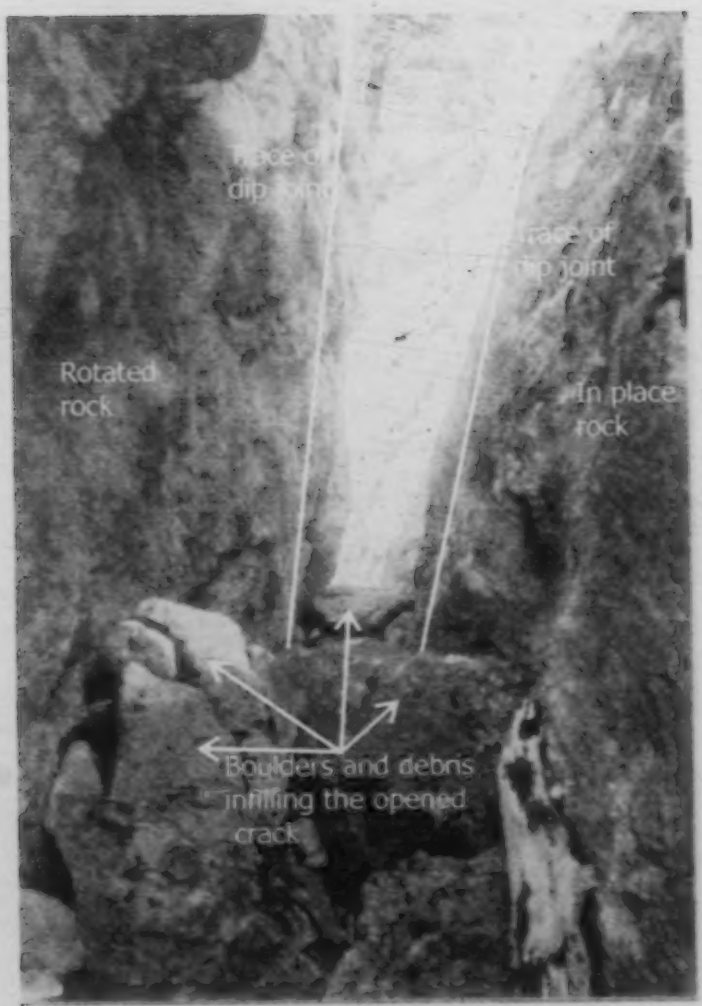

Figure 3.6 – Boulders and debris infilling a crack that has been created by the rotation of a block, opening the dip joints and allowing for the infilling of the open space. Photograph is taken at the Morro Creek orthoclinal block as shown in Figure 3.13.

In section 3.2.1, the factor of safety is determined for sliding on a single plane out of an orthoclinal slope from Equation 3.2. Assuming that the friction angle is the same for both face sb (the bedding plane) and face hb (the strike joint) (Figure 3.3), the case for sliding of a block with inclined bedding in an orthoclinal slope could be treated as a slide on a single plane, rather than as a wedge movement. The wedge factor is multiplied by the value of the factor of safety for planar failure, Equation 3.2, in order to determine the factor of safety for a wedge failure. Hoek and Bray (1974, Figure 94) defined the wedge factor, K, as

$$K = \frac{\sin \chi}{\sin(\xi/2)} \qquad \text{(Eq. 3.6)}$$

where χ was the angle between the horizontal plane and the bisector of the wedge (Figure 3.7), and ξ was the angle between the two planes defining the wedge. In the case of an orthoclinal slope with kathetal joints, the angle ξ is always 90°. Because χ is the acute angle between the horizontal and the wedge bisector, and the bisector can not be less than 45° if the planes are orthogonal, the value of χ varies between 45° and 90°. From Equation 3.6, the minimum value of K is 1.0 when χ=45°, and the maximum value of K is 1.41 when χ=90 (when ψ=45°). This indicates that for the analysis of a wedge on an orthoclinal slope, an analysis assuming planar sliding usually gives a low estimate of safe slope angles.

From Equation 3.2, the sliding of a block on an orthoclinal slope is defined by

$$FS = \frac{(W-U)\tan \phi}{V}$$

Parameters W, U and V are defined for a 3-dimensional wedge as shown in Figure 3.3, and as follows

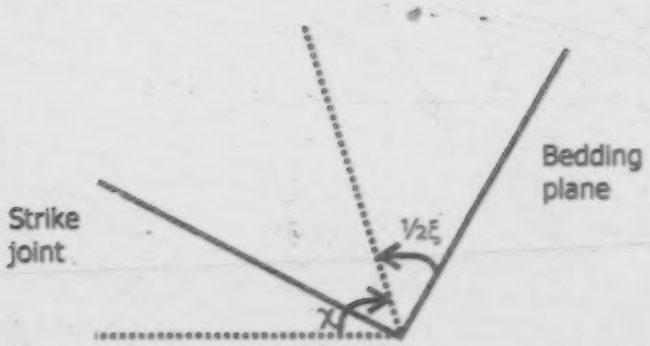

Figure 3.7 – Geometry of an orthoclinal wedge after Hoek and Bray (1973).

$W = bhs\gamma_r(\sin\psi_b + \cos\psi_b)$

$U = 0.5\gamma_w z_w A_r$ where $A=(bs + bs\tan\psi_b)$

$=0.5\gamma_w bs^2\sin\psi_b(1 + \tan\psi_b)$

$V=0.5\gamma_w z_w A_r$ where $A=(0.5s^2\tan\psi_b)$

$=0.25\gamma_w s^3\sin\psi_b\tan\psi_b$

Substituting this into the Equation 3.2

$$FS = \frac{[bhs\gamma_r(\sin\psi_b + \cos\psi_b) - 0.5\gamma_w bs^2\sin\psi_b(1 + \tan\psi_b)]\tan\phi}{0.25\gamma_w s^3\sin\psi_b\tan\psi_b} \quad \text{(Eq. 3.7)}$$

Setting the factor of safety to 1, and simplifying

$$\frac{s}{b} = \frac{[4h\gamma_r(\sin\psi_b + \cos\psi_b) - 2\gamma_w s\sin\psi_b(1 + \tan\psi_b)]\tan\phi}{\gamma_w s\sin\psi_b\tan\psi_b} \quad \text{(Eq. 3.8)}$$

A simple case can be examined where $\psi_b=45^\circ$, $h=s$ and $\phi=30^\circ$ (Figure 3.8).

Knowing that $\gamma_w=9.81$ kN/m^3, substituting these values into Equation 3.8, a range of the different ratios of s/b for different unit weights of rock can be calculated. Making the assumptions in Figure 3.8, the equation simplifies to

$$\frac{s}{b} = \frac{4(2\gamma_r - \gamma_w)\tan\Phi}{\gamma_w} \quad \text{(Eq. 3.9)}$$

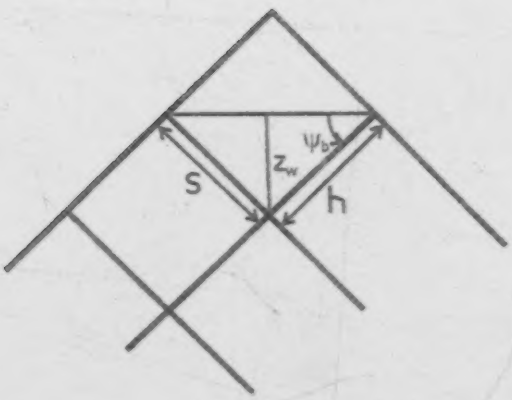

Figure 3.8 – Cross-section of a simple example of an orthoclinal wedge, showing ψ_b=45° and s=h.

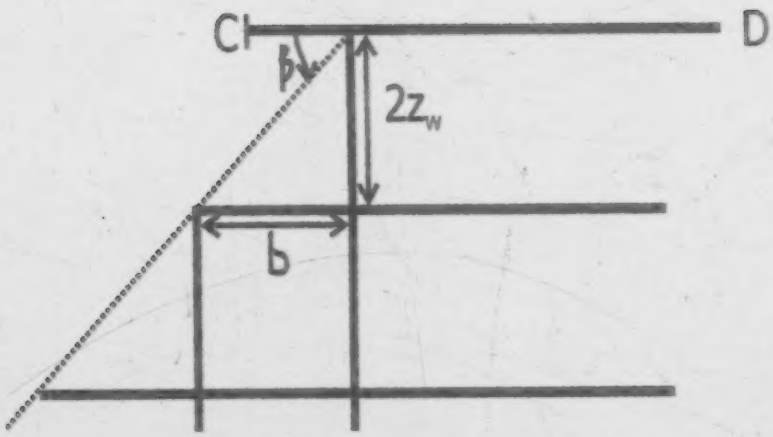

Figure 3.9 – Diagram of the generalized slope angle, β, based on the rock geometry.

γ r	s/b	β
20	7.017117	84.318183
22	8.048769	84.979296
24	8.990421	85.502880
26	9.932073	85.927739
28	10.873724	86.279355
30	11.815376	86.575143
32	12.757028	86.827410

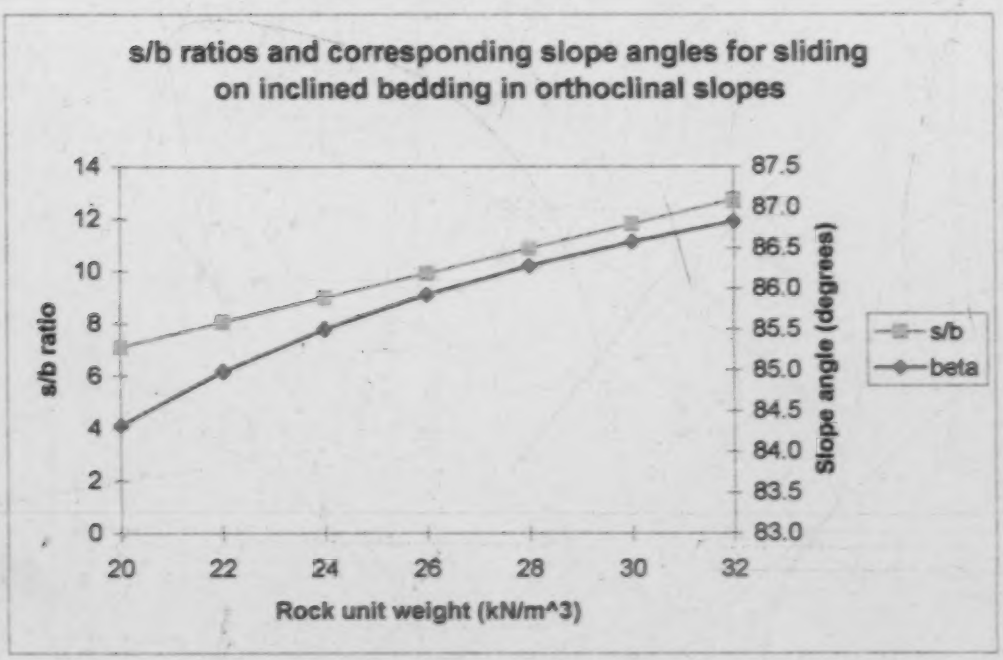

Table 3.2 – Range of s/b ratios as calculated from Equation 3.9, and corresponding slope angles, β, as calculated using Equation 3.10, for a range of possible rock unit weights.

In addition, the average slope angle, β, can be calculated for the geometry of this situation (Figure 3.9). A range of possible slope angles is included in Table 3.2, for a range of rock unit weights. The slope angle is calculated by

$$\tan \beta = \frac{2z_w}{b} \qquad \text{(Eq. 3.10)}$$

Table 3.2 shows that a rock with a unit weight of 25.5 kN/m3 requires an s/b ratio of 9.7 in order to slide, indicating that the strike joint spacing must be 9.7 times greater than the dip joint spacing in order for sliding to take place under water pressures. Alternatively, a slope angle, β, of 85.8° is required for sliding to occur on this orthoclinal slope.

In the situation where the bedding is dipping more steeply than 45°, the limit of the height of the water, z_w, is defined by the more gently dipping kathetal joint. In this situation, the dip of the strike joint needs to be used in the analysis, or, as it is assumed that the joints are orthogonal, $90-\psi_b$ can be used as the limiting angle in the analysis. With this geometry, h is substituted for s, s is substituted for h and b remains as the dip joint spacing in the calculations.

3.3 Toppling on orthoclinal slopes

The other rock slope process discussed by Norrish and Wyllie (1996) is toppling. deFreitas and Watters (1973) examined the mode of toppling, and calculated a critical ratio of block width to block height, in order to determine the dimensions of a block that would topple, depending upon the angle of dip of the bedding plane, ψ. As has already been established, in the case of an orthoclinal slope, the apparent dip of the bedding in the direction of the slope is zero degrees. In the terms of Norrish and Wyllie (1996), used in this discussion, $\psi = 0$, and in the terms of deFreitas and Watters (1973), $\alpha = 0$. Taking $\phi = 30$ degrees, $\psi < \phi$, and only two of the situations described by deFreitas and Watters are applicable:

- Complete stability when $b/s > \tan \psi$

- Toppling only when $b/s < \tan \psi$

Under these assumptions, toppling on an orthoclinal slope requires another force, in addition to gravity. When an external force is added to the analysis, it can be shown that toppling is dynamically possible.

In the next two sections, 3.3.1 and 3.3.2, toppling on vertical bedding planes, as well as toppling on inclined bedding planes, in orthoclinal slopes is kinematically examined.

3.3.1 Vertical bedding orientation

In order for a block to topple on an orthoclinal slope, the driving moment must overcome the moment resisting rotation. In the case of a vertically bedded orthoclinal slope, the driving moment would be due to water pressure in a discontinuity bounding the back of the block, with a height s (Figure 3.10). The resisting moment would be the weight of the block acting about the line b, the strike joint. In order for the driving moment to overcome the moment of the weight of the block, the resultant vector would need to overcome the critical angle, θ, resulting in a rotation of the block (Figure 3.10).

When analyzing toppling, outward moments are driving the rotation of the block around a pivot, O_r, or the centre of rotation of the block (Figure 3.11). The driving force of rotation is water pressure, defined as $V=0.5\gamma_w s^2$. In the analysis of toppling, as a rotation the driving moment is

$$M_d=0.5s(0.5\gamma_w s^2)$$

Which can be simplified to

$$M_d=0.25\gamma_w s^3 \qquad \text{(Eq. 3.11)}$$

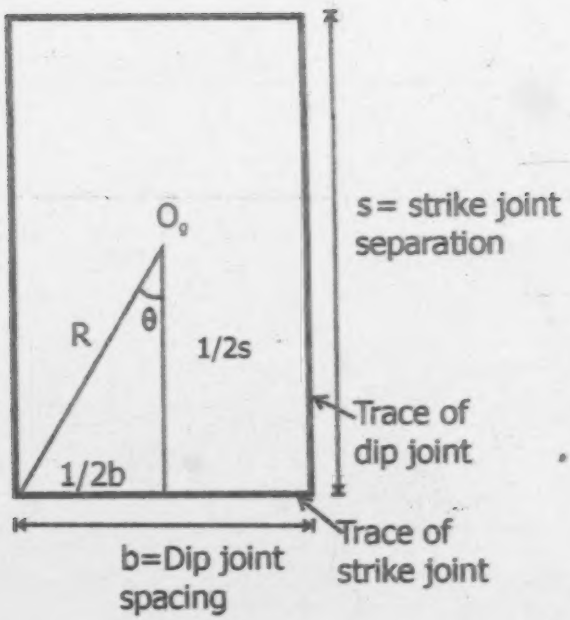

Figure 3.10 – Geometry of a block in a vertically bedded orthoclinal slope that is subject to toppling, looking at the bedding plane, showing s (the strike joint separation), b (the dip joint separation) and θ.

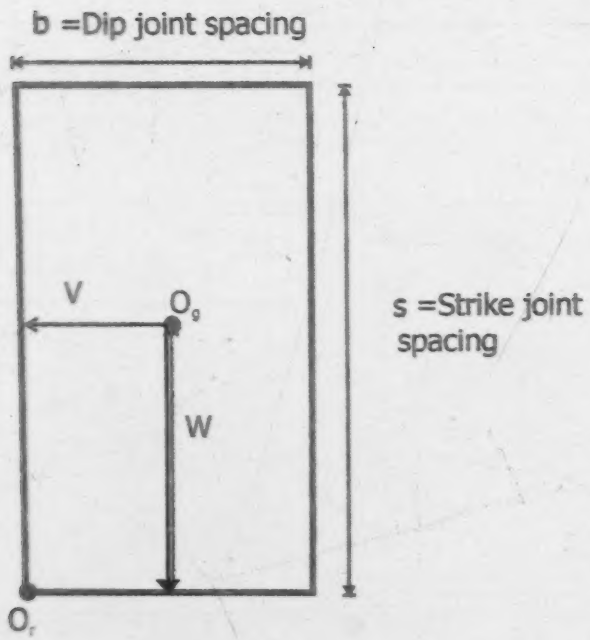

Figure 3.11 – Diagram of a block in a vertically bedded orthoclinal slope looking at the bedding surface, showing the centre of gravity. O_g, the centre of rotation, O_r, and the pressures on the block, V and W.

The force resisting rotation of the block is the weight of the block, $W=\gamma_r bs$. The resisting moment is

$$M_r=0.5b(\gamma_r bs)$$

Simplifying this term,

$$M_r=0.5\gamma_r b^2 s \qquad \text{(Eq. 3.12)}$$

Toppling of this block occurs if the moment of rotation, Equation 3.11, exceeds the moment resisting rotation, Equation 3.12. This can be written as

$$M_d>M_r$$

Or,

$$0.25\gamma_w s^3>0.5\gamma_r b^2 s \qquad \text{(Eq 3.13)}$$

In order for toppling to occur on horizontally or vertically bedded orthoclinal slopes,

$$s/b>(2\gamma_r/\gamma_w)^{.5} \qquad \text{(Eq. 3.14)}$$

Referring back to Equation 3.5, a range of expected slope angles in vertically bedded orthoclinal slopes can be calculated for a range of different densities of rock (Table 3.3). This indicates that for a rock with a unit weight of 25.5kN/m^3, a slope angle of 66.5° is necessary in order for blocks to topple on the orthoclinal slope. A block ratio of 2.3 is required for toppling to occur, indicating that the strike joint spacing must be 2.3 times greater than the dip joint spacing.

γ r	s/b	β
20	2.01928	63.65413
22	2.11783	64.72423
24	2.21201	65.67330
26	2.30233	66.52262
28	2.38924	67.28857
30	2.47310	67.98399
32	2.55420	68.61909

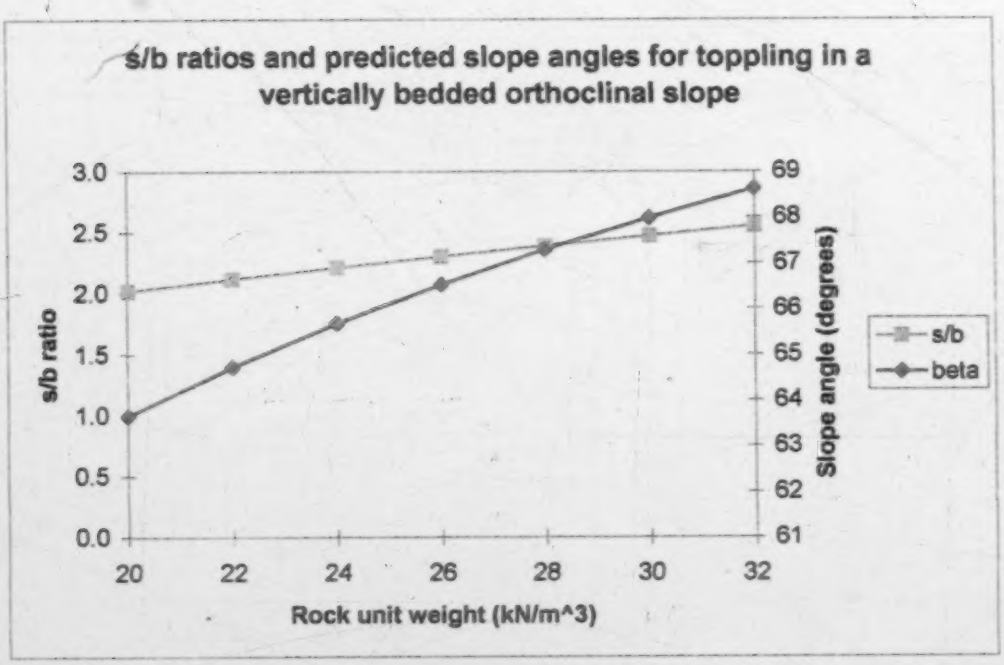

Table 3.3 – Range of s/b ratios as calculated with Equation 3.14, and the corresponding slope angle, β, as calculated with Equation 3.5.

This analysis can also be used where bedding is horizontal, where h is the bedding spacing and is substituted for s in the above equations.

3.3.2 Inclined bedding orientation

Toppling on orthoclinal slopes in inclined bedding is a process that is not well understood as of yet. There are several different potential axes of rotation for topping in a 3-dimensional analysis. For this analysis, assume that the block rotates about the azimuth of the dip that intersects with the block at point A_r (Figure 3.12). In addition, the parameters d and H are defined in Figure 3.12.

For toppling to take place, the moment driving the toppling, M_d, must exceed the moment that is resisting the toppling, M_r, of the block. The driving moment for toppling this block is defined as

$$M_d = 0.5HV$$

where $V = 0.25\gamma_w z_w A = 0.25\gamma_w s(\sin\psi_b)(s^2\tan\psi_b) = 0.25\gamma_w s^3 \sin\psi_b \tan\psi_b$

$H = s(\sin\psi_b) + h(\cos\psi_b)$

$$M_d = 0.125\gamma_w s^3 \sin^2\psi_b (s\tan\psi_b + h) \qquad \text{(Eq. 3.15)}$$

In this case, there is both the weight of the block and the friction on the inclined surfaces that are acting to resist the toppling of the block. In addition, the weight is acting on 2 faces, and so the weight vector must be broken into 2 components. The moment resisting toppling is now defined as

$$M_r = 0.5bW(\sin\psi_b + \cos\psi_b)\tan\phi$$

where $W = bhs\gamma_r$

$$M_r = 0.5b^2 hs\gamma_r(\sin\psi_b + \cos\psi_b)\tan\phi \qquad \text{(Eq. 3.16)}$$

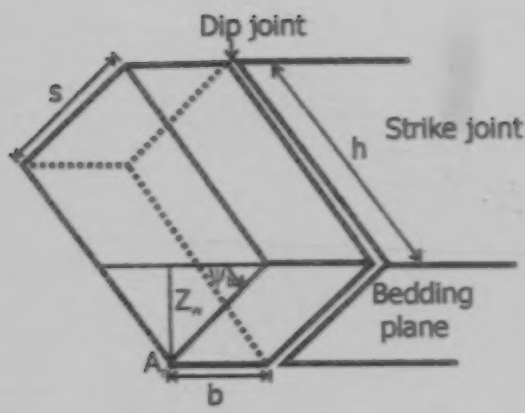

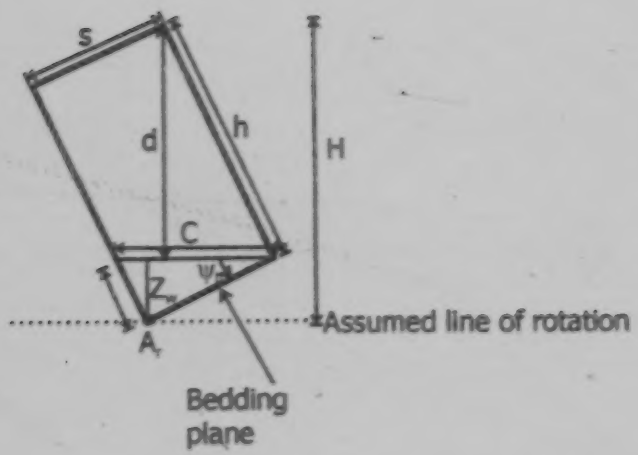

$d = h \cos\psi_b$
$H = d + z_w$
$c = a/\sin\psi_b$

A_r represents the pivot point for rotation of the block, and the block is assumed to rotate about a horizontal line intersecting the block at point A_r.

Figure 3.12 – Diagram of 3-dimensional block geometry.

So, substituting Equations 3.15 and 3.16 into the inequality for toppling, $M_d > M_r$

$$0.125\gamma_w s^3 \sin^2\psi_b (s \tan\psi_b + h) > 0.5 b^2 h s \gamma_r \tan\phi \, (\sin\psi_b + \cos\psi_b)$$

which can be simplified to

$$\frac{s^2}{b^2} > \frac{4h\gamma_r \tan\phi \, (\sin\psi_b + \cos\psi_b)}{\gamma_w \sin^2\psi_b (s \tan\psi_b + h)} \qquad \text{(Eq. 3.17)}$$

A Factor of Safety can be calculated for toppling, by using a ratio of the sum of the resisting forces divided by the sum of the driving forces of toppling

$$FS = \frac{0.5 b^2 h s \gamma_r \tan\phi \, (\sin\psi_b + \cos\psi_b)}{0.125\gamma_w s^3 \sin^2\psi_b (s \tan\psi_b + h)} \qquad \text{(Eq. 3.18)}$$

By making the assumptions that follow, an example calculation can be undertaken, and the angle of slope under different circumstances can be predicted. Assuming that the geometry is the same as that in Figures 3.7 and 3.8, ϕ=30, h=s, γ_w=9.81 kN/m^3, and looking at a situation where ψ_b=45°, the s/b ratio can be calculated for different densities of rock, and then the slope angle, β, can be estimated by

$$\beta = \tan^{-1} [2 (s \sin\psi_b / b)]$$

given that the height of the block in this geometry is $2z_w$=2 s sin ψ_b, and the spacing of the blocks out of the slope is b. The results for these calculations are in Table 3.4, and indicate that for a rock with a unit weight of 25.5 kN/m^3, a block ratio of 2.9 is required for toppling to take place. In order for a block to topple in inclined bedding on an orthoclinal slope, the strike joint spacing must be 2.9 times greater than that of the dip joint spacing. Toppling where the rock unit weight is 25.5 kN/m^3 would result in a slope angle, β, of 71°.

γ r	s/b	β
20	2.58040	74.67546
22	2.70635	75.35728
24	2.82669	75.95548
26	2.94211	76.48586
28	3.05318	76.96035
30	3.16034	77.38812
32	3.26398	77.77637

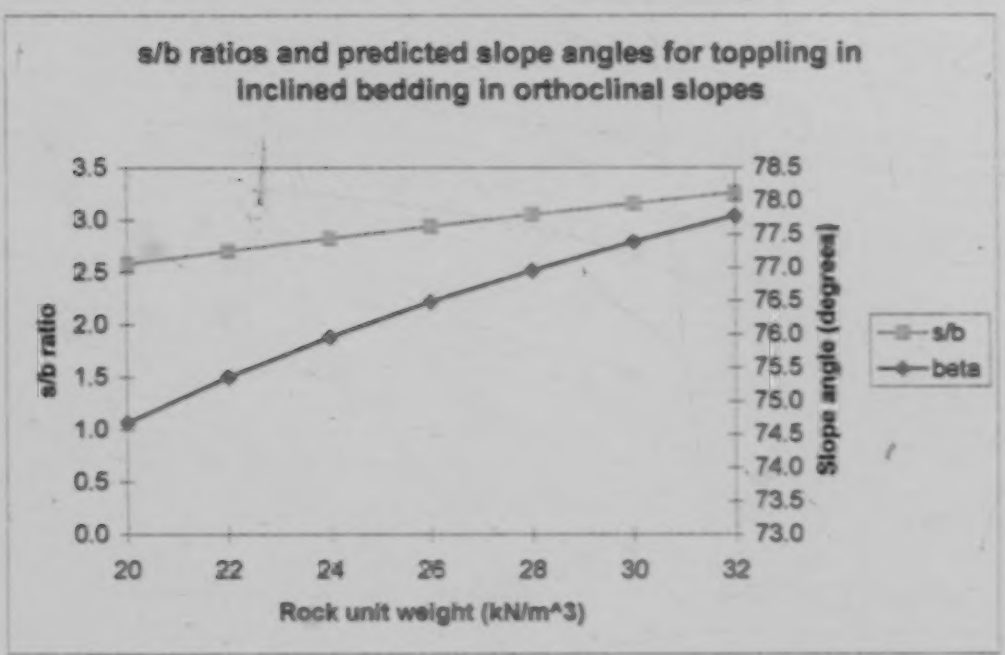

Table 3.4 – Range of possible s/b ratios as calculated with Equation 3.17, and corresponding slope angles, β, as calculated using Equation 3.10.

In a situation where the dip of the bedding is a larger angle than the dip of the strike joint, the dip of the strike joint must be used as the angle ψ. This means that s, the strike joint spacing, and h, the bedding spacing replace one another, while b remains as the dip joint spacing.

3.4 Comparison of sliding to toppling

Tables 3.1 through 3.4 show a range of possible slope angles for orthoclinal slopes based on rock unit weights. According to the data from these tables, toppling is going to be the preferred mode of movement for all situations, except for either vertically or horizontally inclined strata with a rock unit weight less than 23.5 kN/m^3, in which case sliding occurs first (Tables 3.1-3.5). In addition, Table 3.5 gives a general range of slope angles in orthoclinal slopes that range from 68° to 87°, indicating that orthoclinal slopes are expected to have steep slope angles.

A range of predicted slope angles can also be calculated by assuming a unit weight for rock, and using a range of friction angles. Table 3.6 shows a range of possible slope angles for both sliding and toppling in a situation where the bedding is either vertical or horizontal, for a range of friction angles, ϕ. Sliding occurs first on an orthoclinal slope with vertical or horizontal bedding when the friction angle is less than 30°. At friction angles greater than 30°, toppling is likely to occur before sliding is able to occur.

Assuming ψ_b=45°, h=s, γ_r=25.5 kN/m^3, γ_w=9.81 kN/m^3, a range of possible slope angles for orthoclinal slopes in inclined strata can be calculated for an range of friction angles (Table 3.7). Comparison of the calculated slope angles shows toppling is the more likely mode of movement on an orthoclinal slope in inclined strata because it can occur at lower slope angles, and at lower s/b ratios.

γ r	β (sliding)	β (toppling)
20	84.31818	74.67546
22	84.97930	75.35728
24	85.50288	75.95548
26	85.92774	76.48586
28	86.27936	76.96035
30	86.57514	77.38812
32	86.82741	77.77637

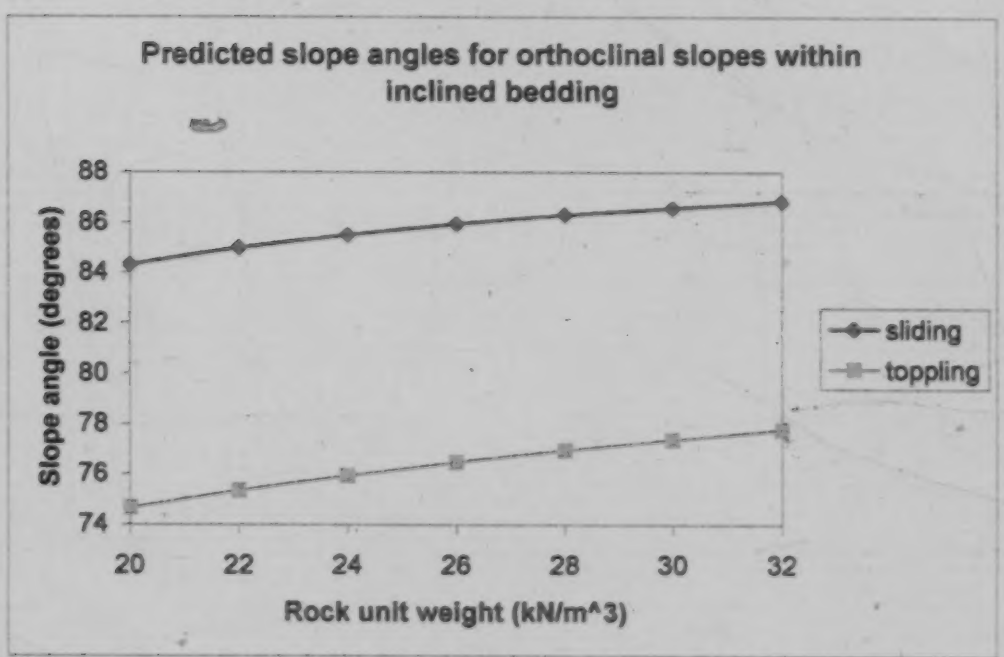

Table 3.5 – Range of possible slope angles of orthoclinal slopes, comparing the predicted slope angles as controlled by toppling motion as opposed to sliding motion. Dolomite has a unit weight of 27.5–28.4 kN/m^3, calcite has a unit weight of 26.5 kN/m^3, and clay minerals have a unit weight in the range of 25.5-27.5 kN/m^3, as an indication of the range of unit weights of some of the rocks found within the study area.

ϕ	β (sliding)	β (toppling)
15	48.36795	66.31868
20	56.80120	66.31868
25	62.94453	66.31868
30	67.58321	66.31868
35	71.21507	66.31868
40	74.15428	66.31868

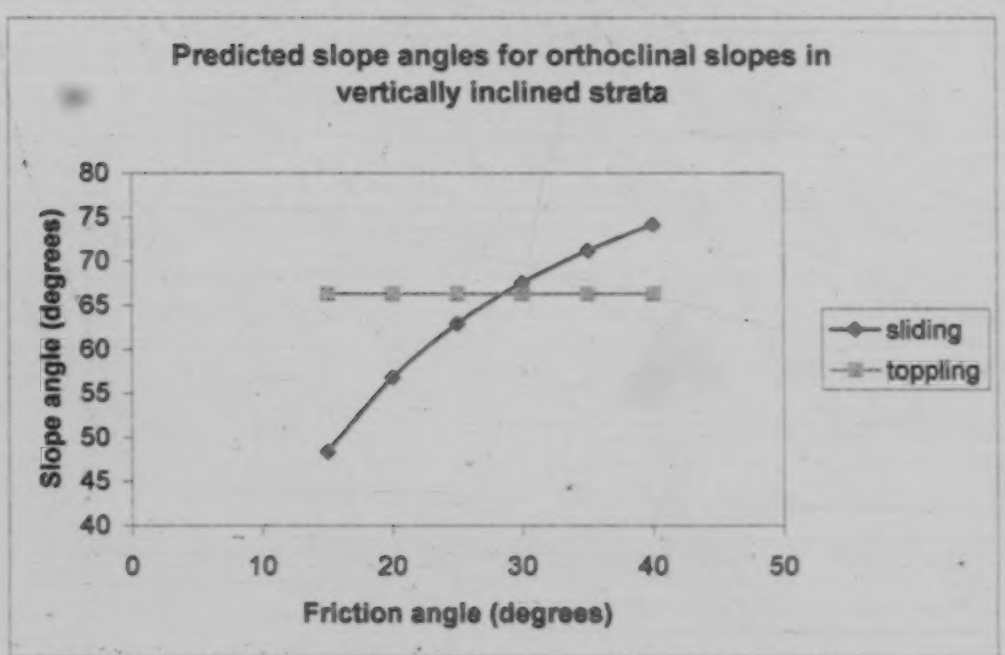

Table 3.6 – Range of possible orthoclinal slope angles, given a range of possible friction angles. Cruden and Hu (1988) indicate that carbonates can have a friction angle that ranges from 21.5° up to 41.3°.

ϕ	β (sliding)	β (toppling)
15	81.07032	70.39236
20	83.40168	73.00406
25	84.84087	74.88837
30	85.82922	76.35892
35	86.55907	77.57247
40	87.12758	78.61818

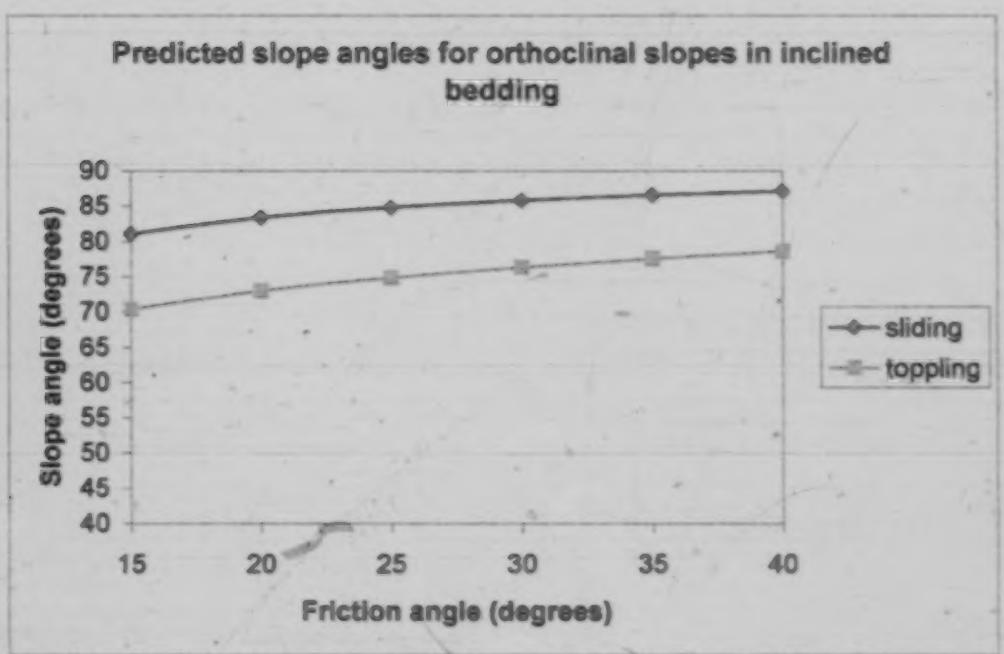

Table 3.7 – Range of predicted slope angles for orthoclinal slopes in inclined strata. Cruden and Hu (1988) found that carbonates have a range in friction angles from 21.5° up to 41.3°.

3.5 Examples of othoclinal movements in the Colin Range

As mentioned in Chapter 2.5, there are two main types of orthoclinal slopes within the study area in the Colin Range, those orthoclinal slopes that were formed during glaciation, and those orthoclinal slopes that were formed by creek erosion post-glacially. Four areas give examples of orthoclinal slope movements that occur in nature (Figure 3.13). The first location with evidence for orthoclinal toppling is the slope formed by Morro Creek through the Devonian and the Mississippian sections of the Colin Range (Figure 3.14). The second area of orthoclinal slopes is along Garrone Creek where slopes occur in the Upper Cambrian, Devonian and the Mississippian strata (Figure 3.15). The third orthoclinal slope is a part of the cut to accommodate the now abandoned Grand Trunk Pacific Railway through Jasper (Parks Canada, 2000), and this slope occurs in the Devonian strata, mainly in the Palliser formation (Figure 3.16). The final slope is that of the northwest side of Morro Peak (Figure 3.13).

From observations, the orthoclinal slopes have slope angles that range from 34°, on the south side of Morro Creek, up to 90° adjacent to Garrone Creek, in the examples that are discussed here. At other locations within the study area, orthoclinal slope angles were found to be as gentle as 17° on slopes that were formed during glaciation of the area, and do not show evidence of post-glacial modification of the slopes.

3.5.1 Morro Creek

Within Morro Creek the orthoclinal slope angles ranged from 34° in the Mississippian Shunda formation to 81° in the Devonian Palliser formation. Among several examples of orthoclinal toppling, the most striking is a large block that has rotated in a direction perpendicular to the dip direction of bedding within the Turner Valley formation. The UTM location of this block is 11U

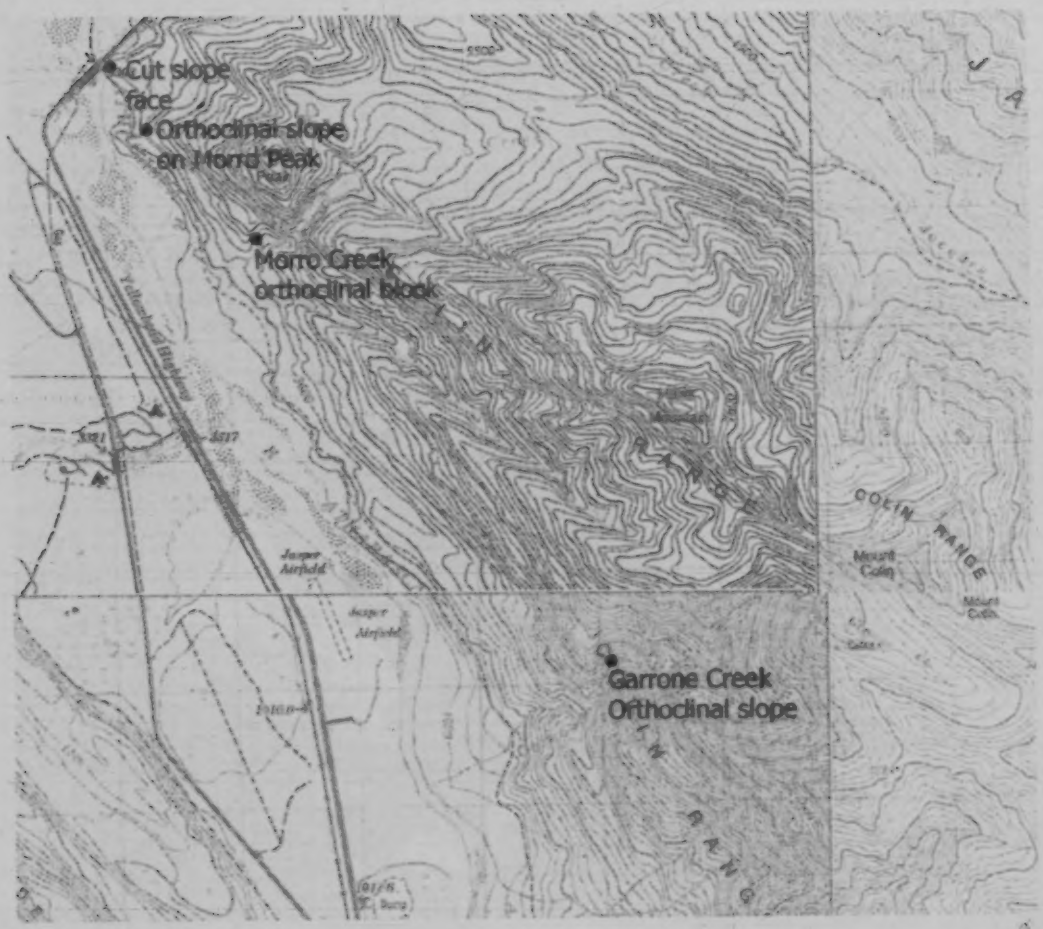

Figure 3.13 – Map showing the areas where orthoclinal slope movements are documented within the study area. Map taken from the 1:50 000 topographic maps of the area.

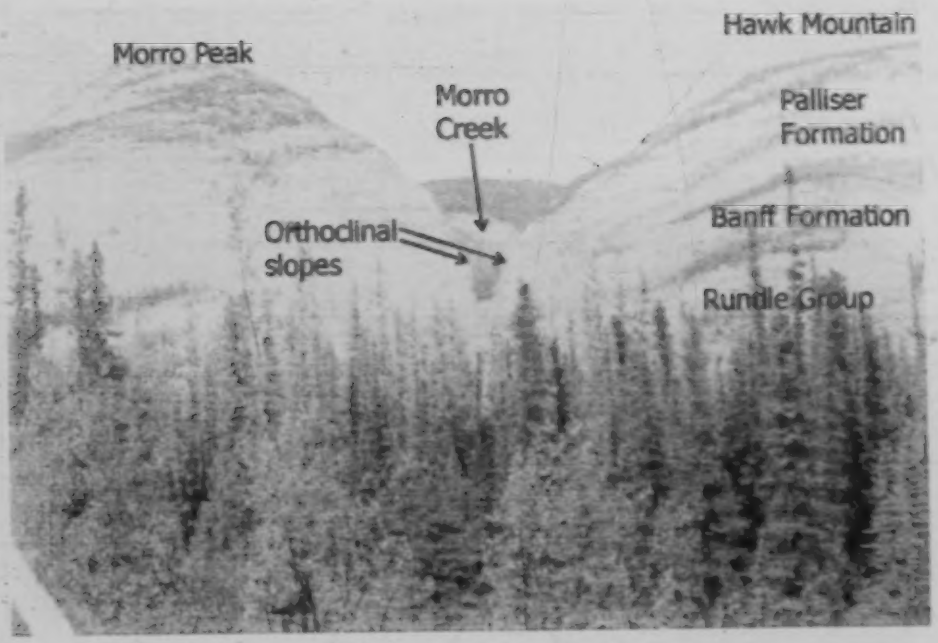

Figure 3.14 – View of the canyon of Morro Creek taken from the Snaring River Bridge on the secondary road. The bedding is dipping to the southwest at 70°, and the canyon is cut at a right angle to the bedding.

Figure 3.15 – View from the east into the canyon of Garrone Creek (Figure 3.13). The canyon is 3m wide at the base at this location, and the canyon walls slope at angles up to 90°.

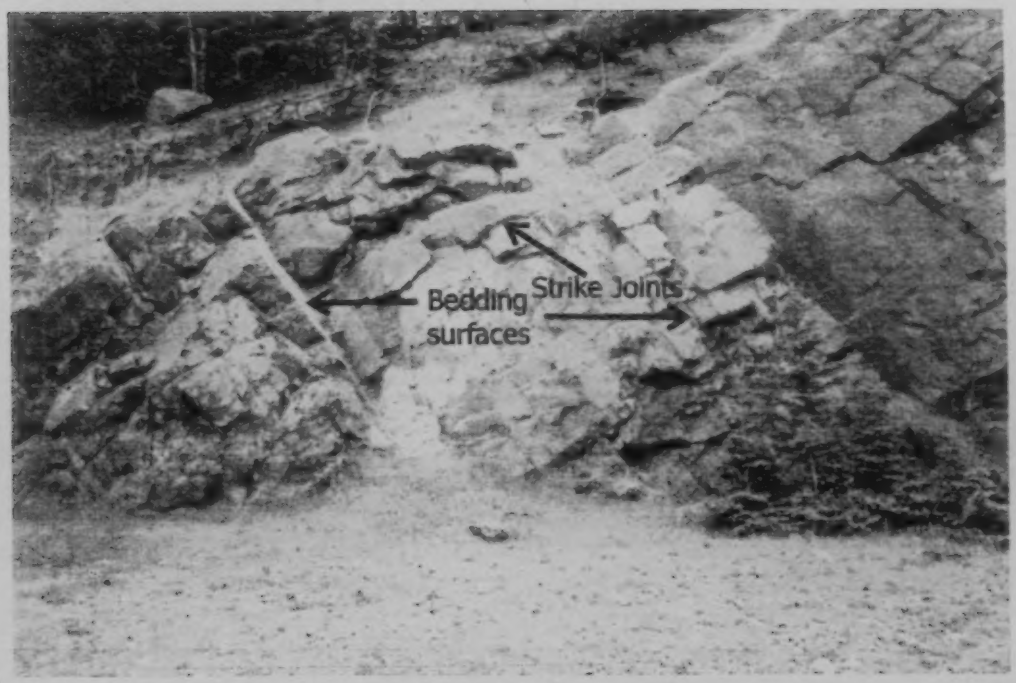

Figure 3.16 – Photograph of the cut slope adjacent to the Athabasca River (Figure 3.13). Photo is taken on a bearing of 130°.

0427931 5875736. The bedding is dipping 60° toward 222°, and the bedding thickness, or spacing, is 3m. As ψ_b is greater than 45°, h and s are reversed in the calculations. The dimensions of the block are H=25m (the height from the line of rotation to the uppermost part of the block), s=44.8m from definition (Figure 3.12, with s and h reversed), h=3m (bedding spacing) and b=1.67m (the width of the block in the direction of strike) at the base. Based on the orientation of the bedding, Equation 3.18 can be used to determine a factor of safety for this block. In order to calculate the factor of safety for this block, some assumptions need to be made. The parameters that are used are as follows:

$\gamma_w = 9.81$ kN/m^3

$\gamma_r = 25.5$ kN/m^3 (Hoek and Bray, 1976)

$\phi = 31°$ (middle of range for carbonates, Cruden and Hu, 1988).

Substituting these into Equation 3.18, the upper limit factor of safety for this block is calculated to be 9.0, using a dip angle of the shallow discontinuity of ψ=30°. Based on this calculation, this block should not topple, yet there is evidence of rotation of this block.

Evidence for the toppling of this block is observed as the block has already moved out from the original location a total of 82cm at the top. The base of the block, however, has been stopped from moving by a large block of Gog Quartzite that has fallen into the creek and wedged the block into place (Figure 3.17). It appears that the flow of the creek has undercut the block of Turner Valley Formation rock, creating instability at the base of the block. The hinge point can not be seen at this location, as it is obscured by gravel in the creek. Toppling began to take place, yet was arrested by the quartzite block in the creek. Figure 3.18 is a photograph of the top of the block, where the opening of the crack is evident. Figure 3.19 is a photograph of the bedding face of this block, showing the differential movement at the top of the block from the base of the block, as well as the other debris fallen into the opened crack on the crest of the slope. Tree roots were observed to be growing into the crack at the base of the block;

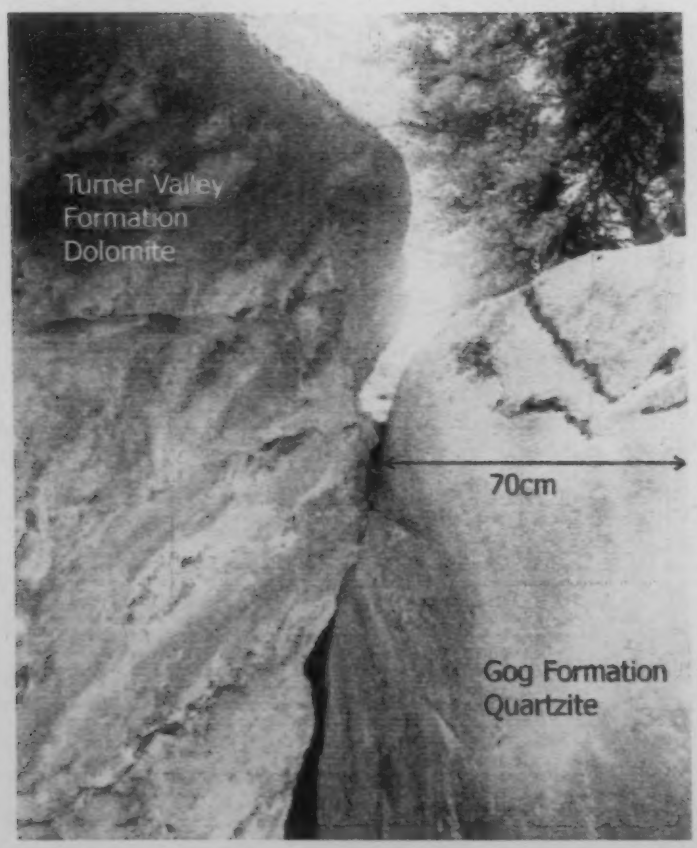

Figure 3.17 – Block of Gog Quartzite on the right side of the photograph that is preventing a block of Turner Valley Formation rock from rotating into Morro Creek.

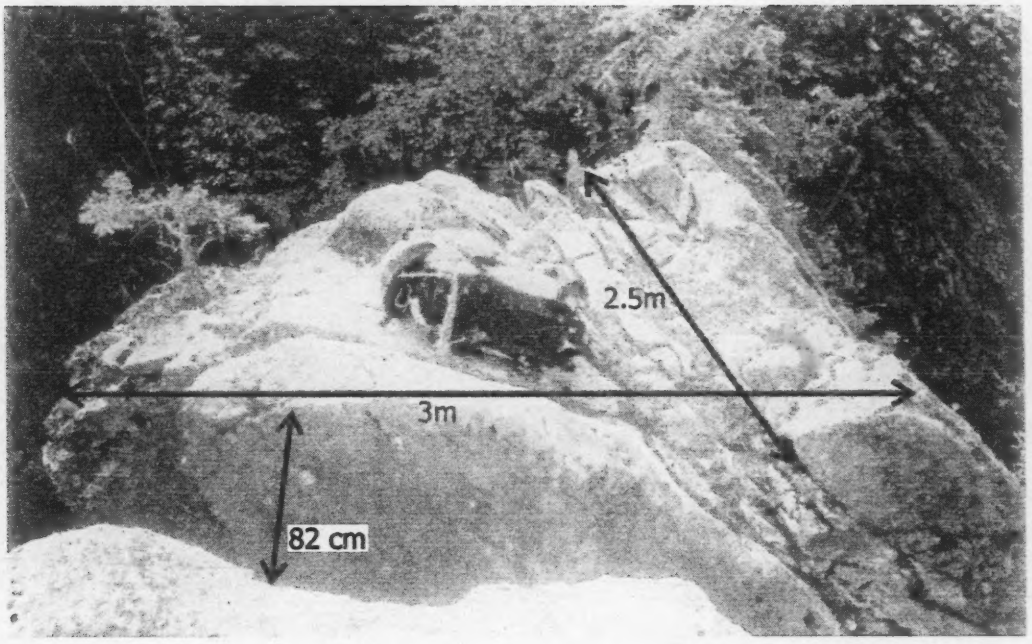

Figure 3.18 – Photograph of the top of the block that is in the process of toppling into Morro Creek.

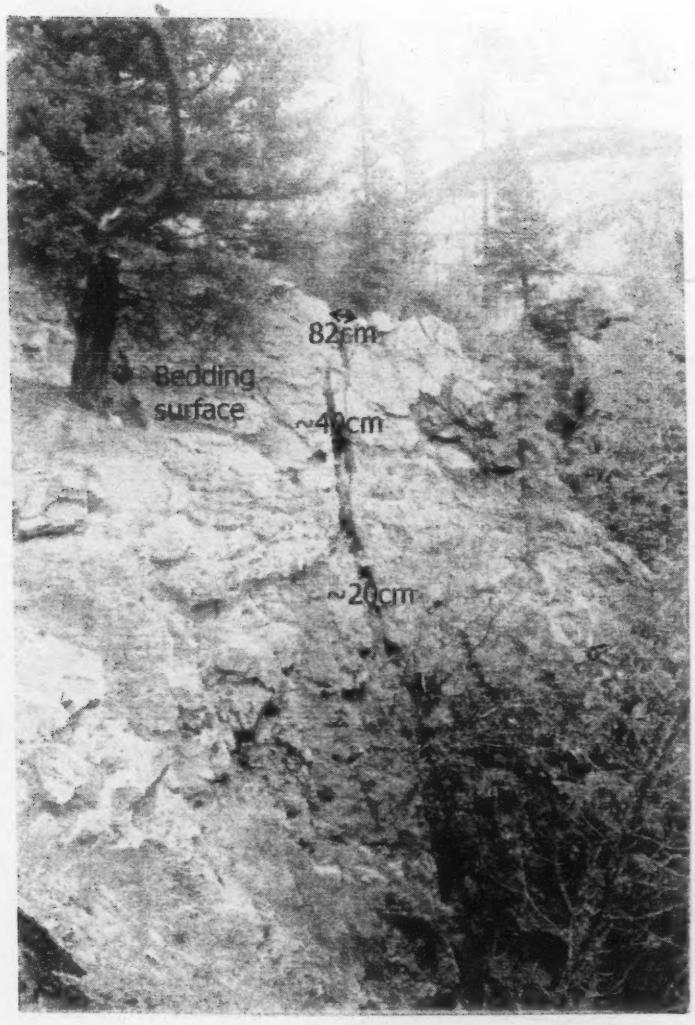

Figure 3.19 – Toppling block showing rotational type movement of the block to the right of the photograph, into Morro Creek. The photograph is taken looking at the bedding surface from the direction of dip.

the growth of these tree roots might enlarge the crack at this location, yet further rotation of this block is not possible, as long as the boulder of Gog Quartzite remains lodged at the base of the block. This block has rotated on an orthoclinal slope, yet the driving moment of the toppling is not water pressures, as shown by the factor of safety calculations; the pressure of the tree roots is likely driving the rotation of this block.

3.5.2 Garrone Creek

The canyon of Garrone Creek is a narrow and steep walled canyon that is cut through strata of the Cambrian Lynx formation, the Cambrian-Ordovician Survey Peak formation, and the Mississippian Turner Valley and Mount Hawk Formations. Slope angles within the canyon range from 74° up to 90° where the creek cuts through more resistant rocks creating orthoclinal slopes (Figure 3.15). At one location, where the less resistant rocks of the Triassic Sulphur Mountain Formation are encountered, the creek takes a 90° turn to follow the strike for a distance, rerouting around the Sulphur Mountain Formation rocks, and the slopes here are more gentle (Figure 2.3). The canyon of this creek is narrow, and ranges in width from 1-4m at the base of the slopes adjacent to the creek. According to the topographic maps of the area, the canyon walls are up to 100m in height.

Within the Cambrian Lynx Formation, at location UTM 11U 431000E and 5871900N, several fresh blocks of rock in the creek at the base of the slope (Figure 3.20) have surfaces which measure 18cmx105cm, 24cmx75cm, 18cmx60cmx75cm and 15cmx30cm. All the blocks found at the base of the slope had orthogonal corners, with no rounding, indicating a local source. One of the blocks was standing on end, indicating that high water had not yet flowed through this canyon since the deposition of this block at this location, or else the block would not be stable balanced on its narrow side.

Figure 3.20 – Several blocks in Garrone Creek that look to have fallen recently. The blocks are angular, not rounded, and the block on the right is balanced on a thinner side. The long dimension of the block is parallel to the bedding, and the bedding spacing is 18cm.

3.5.3 Grand Trunk Pacific Railway Cut

Along a cut slope that faces onto the Yellowhead highway, at River Rock, in the Devonian Palliser Formation rocks, the slope angle is 51°, a gentler slope than the slopes of Garrone Creek and Morro Creek. Several blocks were observed to be moved out from their original location, and the blocks are now suspended in new locations (Figures 3.21-3.22). Table 3.8 gives the dimensions of five of the blocks and the calculated safety factors for both sliding and toppling. The factor of safety calculations are carried out for both ϕ=21° for a lower limit, and ϕ=41° for an upper limit (Cruden and Hu, 1988). Based on the calculated safety factors, these blocks were not moved by water pressures, as all of the factors of safety are calculated to be greater than one. The movement of these blocks may have been driven by the blasting of the rock, by frost heave, freeze and thaw or ice wedges (Selby, 1993).

3.5.4 Northwest slope of Morro Peak

The northwest slope of Morro Peak (Figure 3.13) is an area with several bolted climbing routes used for instruction in rock climbing. In this area, the slope is the type of slope predicted in Chapter 3.3.2, with blocks defined by the bedding and the joint spacing controlling the angle of slope, showing a stepped pattern. The angle of slope at this location is 50°. The base of this slope is covered with both fresh talus and older talus. The blocks of the fresh talus have fresh, dark gray colours, no lichen and no karren (Bates and Jackson, 1984) on their surface, and can be found against the trunk of trees ranging in height from 20 m down to 40-50cm. The older talus is oxidized to a pale gray color, shows karren that are formed in place and also are covered by lichens. There is evidence of damage to trees by rock fall in the area, including the fresh scarring

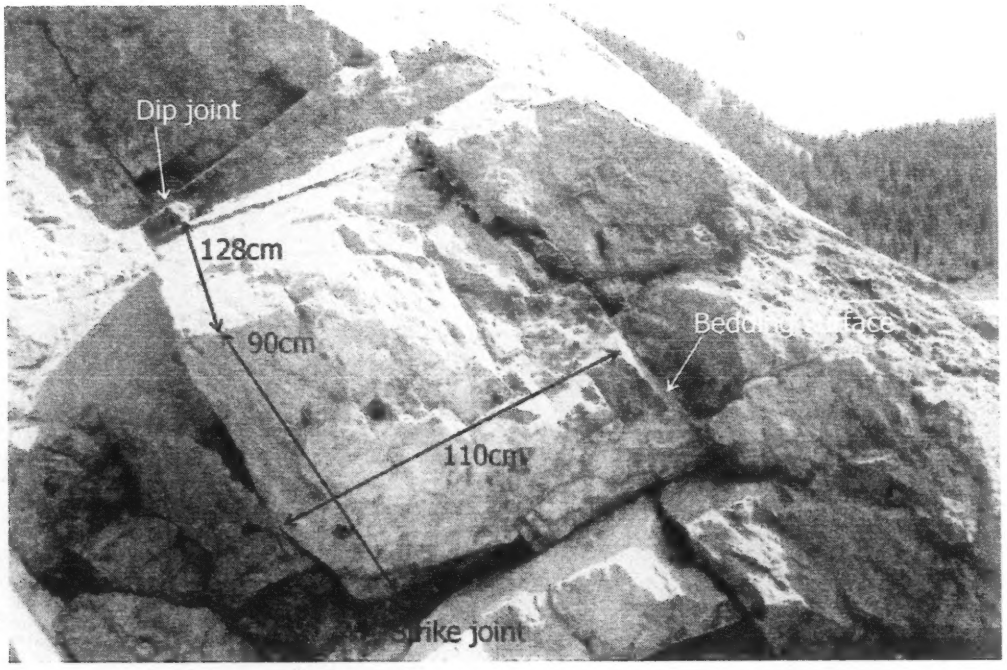

Figure 3.21 – A block on the cut face along the Yellowhead Highway, that has moved out from the slope in the direction of strike, to the northwest.

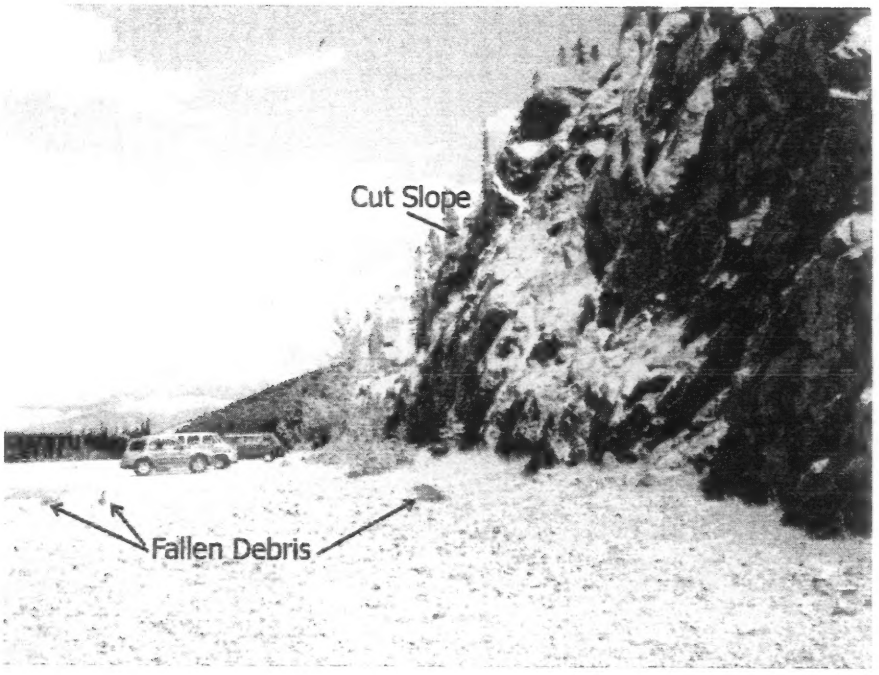

Figure 3.22 – View along the cut slope, looking northeast, showing the slope and several blocks at the base of the slope that have come off of the slope.

ψ (beddi ng) degrees	ψ (less than 45) degrees	bedding spacing (h) (cm)	strike joint spacing (s) (cm)	dip joint spacing (b) (cm)	FS(toppl ing) eqn. 3.16 ϕ=21	FS (sliding) eqn. 3.7 ϕ=21	FS(toppl ing) eqn. 3.16 ϕ=41	FS (sliding) eqn. 3.7 ϕ=41
60	30	32	34	38	57	7	256	15
56	34	77	91	73	28	5	126	10
74	16	168	87	180	135	10	610	22
67	23	30	23	28	54	6	244	14
51	39	110	90	128	19	2	88	5

Table 3.8 – Factor of safety calculations for toppling and sliding on the cut slope within the study area. ϕ=21° is used as a lower limit of friction angle, and ϕ=41° is used as an upper limit for the friction angle of the material.

of the trees, secretion of sap to heal open wounds on the tree trunks, and a build up of colluvial material at the base of the trees. The measurements of some of the blocks that show evidence of movement are included in Table 3.9, along with the calculated safety factors. On this slope at various locations there is evidence for complex movements of these blocks, as there is a combination of movement perpendicular to the dip direction of the bedding, as well as in the dip direction of the bedding, with the infilling of opened joints and cracks with boulders and vegetation.

3.6 Conclusions

Small scale sliding and toppling can take place on orthoclinal slopes, with an external driving force, such as water pressure or ice jacking. Toppling may take place at lower pressures than sliding does, as well, toppling may take place on slopes that are not as steep as those required for sliding to occur, with the exception of the situation where bedding is vertical and the friction angle is less than 29°. Both toppling and sliding on orthoclinal slopes require steep slope angles, and the models suggest slope angles greater than 60° for sliding and 63° for toppling where bedding is vertical, or slope angles greater than 84° for sliding and 68° for toppling where bedding is inclined.

Based on observations in the field, slope movement is found to occur in a direction perpendicular to the dip direction of bedding. This process is likely to be a slow process, as it requires the build up of water or ice pressures, in order to drive the movement of blocks. Not all of the displaced blocks show evidence for toppling being the mode of movement, as rotational motion was not always observed. Yet, the presence of one large block within Morro Creek indicates that toppling does occur in a direction perpendicular to the dip direction of bedding where a block is kinematically free to do so (Chapter 3.5.1).

ψ (beddi ng) degrees	ψ (less than 45 degrees) degrees	bedding spacing (h) (cm)	strike joint spacing (s) (cm)	dip joint spacing (b) (cm)	FS(toppl ing) eqn. 3.16 ϕ=21	FS (sliding) eqn. 3.7 ϕ=21	FS(toppli ng) eqn. 3.16 ϕ=41	FS (slidin g) eqn. 3.7 ϕ=41
72	18	60	110	120	1186	64	5373	156
76	14	100	213	90	572	56	2588	126
73	17	70	130	60	260	31	1177	71
70	20	15	110	95	25101	716	113684	1621
78	12	35	150	45	3358	222	15211	501

Table 3.9 – Factor of safety calculations for the northwest slope of Morro Peak for several blocks that were measured in the field, and noted to show motion in the orthoclinal direction.

Observations in the field indicated that erosionally formed orthoclinal slopes exist at angles ranging from 34° up to 90°. Table 3.5 shows the predicted slope angles for orthoclinal slopes in dipping strata, and indicates that slope angles should range from 74° for toppling with a friction angle of 21° up to 88° for sliding with a friction angle of 41°. The range of slope angles corresponds, for the most part, to the slope angles that were observed in nature. Slopes observed in nature were found to have slightly greater angles than those that were predicted by the equations in section 3.4. This may be due to the pore water pressure in joints not being large enough to lead to the toppling or sliding of blocks on these slopes, indicating that other forces such as ice wedges, freeze and thaw, human and animal impacts or vegetation have caused these movements (Selby, 1993). While the model is a start, is does not explain most of the blocks in the field that were observed to have moved.

A hazard is present on orthoclinal slopes at three locations within the study area. The first place where a hazard is present is within the canyon of Garrone Creek. While the volume of material that may move is not great, the high, steep slopes into the canyon indicate that any material that falls is hazardous. In addition, the presence of freshly toppled material within a narrow, high-walled portion of the canyon is indicative of a hazard. While Garrone Creek is not frequently traversed, it is along the path to the Mount Colin Centennial Hut run by the Alpine Club of Canada (Alpine Club of Canada, 2002). If a new path were to be constructed through this portion of the creek, a hazard warning should be posted. In addition, the area on the northwest side of Morro Peak, where climbers use the slope for practice, should have a hazard warning posted, and climbers should be encouraged to wear helmets while climbing in this area. Users of the Morro Creek canyon rappel should be aware of the rock fall hazard on the steep and high canyon walls through the Devonian Sassenach and Palliser Formations, where bolts have been placed for the rappel.

4 Movements on cataclinal slopes

4.1 Introduction

Chapter two described the different types of slopes and some of the movements on slopes that were discussed by Cruden and Hu (1996), who devised a process diagram to show where different slope movements were kinematically possible (Figure 4.1). This chapter focuses on the different types of movement on cataclinal slopes that are observed in the Colin Range of Jasper National Park.

Evidence for three types of movement is noted on the cataclinal slopes of the Colin Range: toppling, exfoliation and sliding on bedding. Toppling, the rotational movement of a block around a pivot point, was found to occur within the Devonian Palliser Formation, the Mississippian Banff, Turner Valley and Mount Head Formations. Block topples were found to occur within all of these formations, on both steep slopes, and on slopes less than 30°, the slope angle used as the lower bound of toppling on Figure 4.1. Multiple-block topples were found to occur within the Banff Formation on slopes of less than 30°. Toppling on cataclinal slopes is discussed in section 4.2.

Evidence for exfoliation was found within the steeply dipping rocks of the Devonian Palliser Formation on the cataclinal slopes of Morro Peak and Mount Colin. The slopes where exfoliation had taken place are located adjacent to a creek, where slopes are steep and bedding planes daylight above the depression on a shallow slope. Exfoliation is discussed in section 4.3.

A relict translational slide within the gently dipping rocks of the Palliser Formation at the south end of the Colin Range has a recognizable scarp, main body and an extensive foot. The translational slide is discussed in section 4.4.

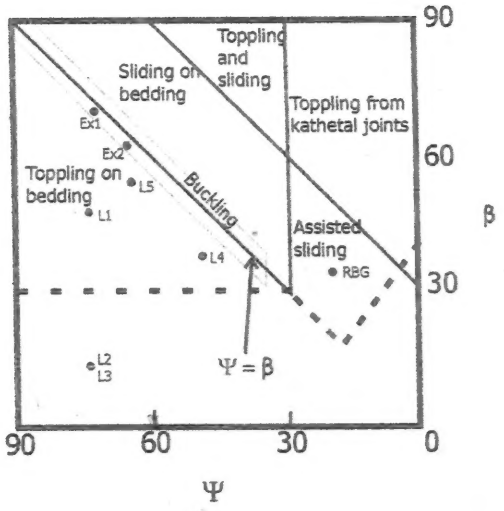

Figure 4.1 – Part of the process diagram from Cruden and Hu (1996, Figure 3), showing the locations of movements that are discussed in this chapter. The plots labeled as L1-L6 refer to the locations of toppling, with L2' and L3' plotted with the localized slope angle. Ex indicates where exfoliation plots on the diagram, and RBG indicates roughly where the Rock and Boulder Gardens plot on the diagram. Ψ is the dip of the bedding, and β is the slope angle.

4.2 Toppling on cataclinal underdip slopes

deFreitas and Watters (1973) stated that "toppling occurs when the centre of gravity of a unit of rock overhangs a pivot point within the unit" (pg. 497). deFreitas and Watters (1973) assumed that toppling depended upon the orientation of the base of the unit surface. Norrish and Wylie (1996) stated that "toppling failures most commonly occur in rock masses that are subdivided into a series of slabs or columns formed by a set of fractures that strike approximately parallel to the slope face and dip steeply into the face" (pg. 410).

By definition, beds in rocks that form cataclinal slopes do not dip into the face of a slope, but rather dip in the same direction as the slope (Cruden and Hu, 1996). The conditions for toppling on cataclinal slopes were given by Cruden (1989) to be

$$\beta + (90 - \phi) > \psi \qquad \text{Eq. 4.1}$$

where β is the angle of slope, ϕ is the internal angle of friction and ψ is the angle of dip of the bedding and demonstrated that toppling is kinematically possible on cataclinal slopes (Cruden, 1989). A process diagram demonstrating the range of slope angles, β, and bedding dips, ψ, where toppling is likely to occur on a cataclinal slope is shown in Figure 4.1.

The majority of the slopes within the study area are cataclinal underdip slopes (Figure 2.7). The cataclinal slopes within the study area are composed of dip slopes alternating with shallow underdip slopes, covered with a thin veneer of till and colluvial material, often with a vegetated cover.

The dominant type of movement observed on cataclinal underdip slopes in the field is toppling, with block topples, where the angle of the bedding changes abruptly between blocks, occurring most frequently (Cruden and Hu, 1994). As discussed in Chapter 2, the geology in the region involves beds that are steeply

dipping toward the southwest, with 2 sets of kathetal joints, strike joints and dip joints. Toppling occurs in the bedding direction on cataclinal slopes, and the kathetal joints control the shape of the toppling block. Joint set 1 is the joint set that has the greater dip, also known as the dip joints, as the strike of the joint is in the direction of dip of the bedding. Joint set 2 is the joint set with the smaller angle of dip, also known as strike joints, with the strike of the joints the same as the strike of the bedding. Rotation takes place about an axis of rotation parallel to joint set 2; where sliding surfaces are subsequently formed, sliding surfaces are developed along joint set 2.

4.2.1 Site 1

The first location with evidence for toppling on a cataclinal slope is marked as location 1 on Figure 4.2. The site is located between the UTM coordinate 11U 0427250 5876912 and 11U 0427289 5876884. The rock at this location is the Devonian Palliser Formation, with an average dip of 71° toward 219°. The bedding thickness ranges from 10cm to 30cm. Dip joint spacing ranges from 20cm to 270cm with an average orientation of 87° toward 131°, while strike joint spacing ranges from 40cm to 310cm with an average orientation of 6° toward 078°. The slope is 44° toward 217°, with local slopes up to 71°.

The base of the slope is covered by accumulated talus, and further down slope, trees are growing in a depression where the Banff Formation has been eroded, and talus is found to be resting among these trees, along with organic debris. Some of the trees show damage by rock fall; bark is scratched off and at places the trees are secreting sap to heal open wounds. Some of the talus is dark gray, with a fresh smell, mineral precipitation on one or more surfaces and shows no signs of post-depositional solution. Other talus blocks are light gray in colour and show solution features that developed in the current orientation of the block.

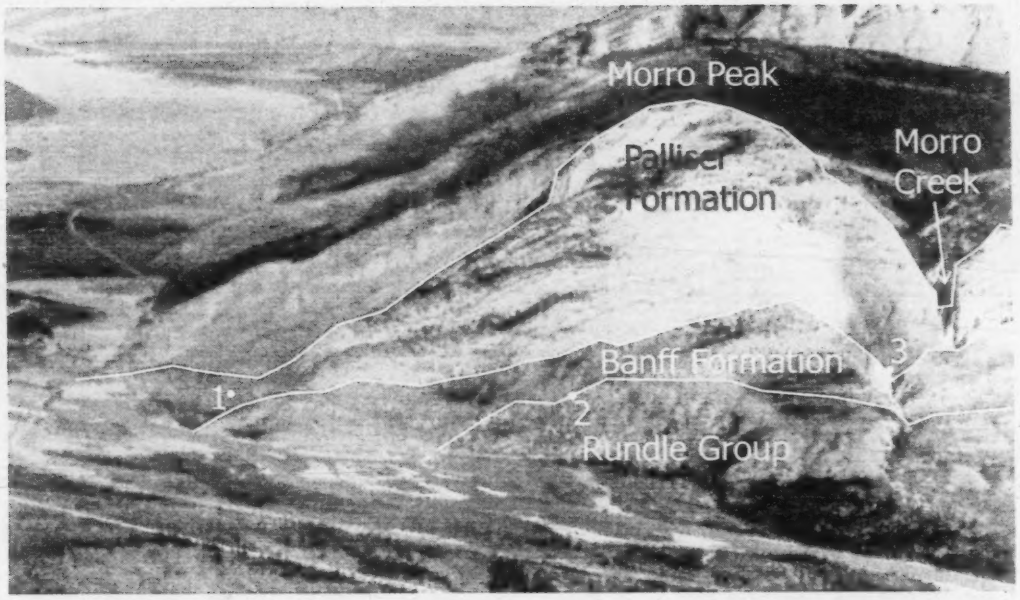

Figure 4.2 – Oblique photograph showing Morro Peak from the southwest, showing the cataclinal slopes of Morro Peak. The locations of sites 1-3 are shown on the photograph, with the formations that they occur in. Photograph number 470, M.P. Bridgland, 1915.

At location 1, there are several blocks that have rotated to steeper dips than the dip of the bedding on this slope (Figure 4.3). Where a block has rotated, space is created between the block and the underlying bed, and is infilled with rock debris (Figure 4.3). From the above information, the orientation of the bedding and the slope angle are plotted on Figure 4.1, and indicate that the mode of movement on this slope is toppling in the cataclinal direction. The mode of movement on this slope is individual block topples, with the size and the shape of the blocks being controlled by the orientation and the spacing of bedding and the kathetal joint sets.

4.2.2 Site 2

Location 2 (Figure 4.2) is on the lower west slope of Morro Peak, and lies within Banff Formation and Rundle Group rocks. The average bedding at this location is dipping 76° toward 194°. The slope is composed of alternating dip slopes and underdip slopes to create a shallow cataclinal underdip slope. The bedding spacing in this slope ranges from 0.5cm in the shaly Banff Formation up to 60cm within the crinoidal layers of the Banff Formation. The average orientation of the dip joints in this slope is 88° toward 306°, with a spacing of 30cm to 70cm. The average orientation of the strike joints is 5° toward 045°, with a spacing ranging from 30cm to 80cm. The majority of this slope has a very low slope angle, and is covered with glacial till and angular colluvial deposits.

Along the Overlander Trail across this slope, between UTM 11U 0427659 5876251 and 11U 0427532 5876543 numerous angular blocks of rock overlie the bedrock (Figure 4.4). Vegetation on this slope consists of bearberry and some coniferous trees; ungulates graze in this area (Figure 4.4). Directly upslope from the trail, at an outcrop of the Pekisko Formation (Figure 4.5), blocks that are defined by the bedding and the kathetal joint set have been rotated and now dip at an angle that is steeper than that of the underlying bedding (Figure 4.4).

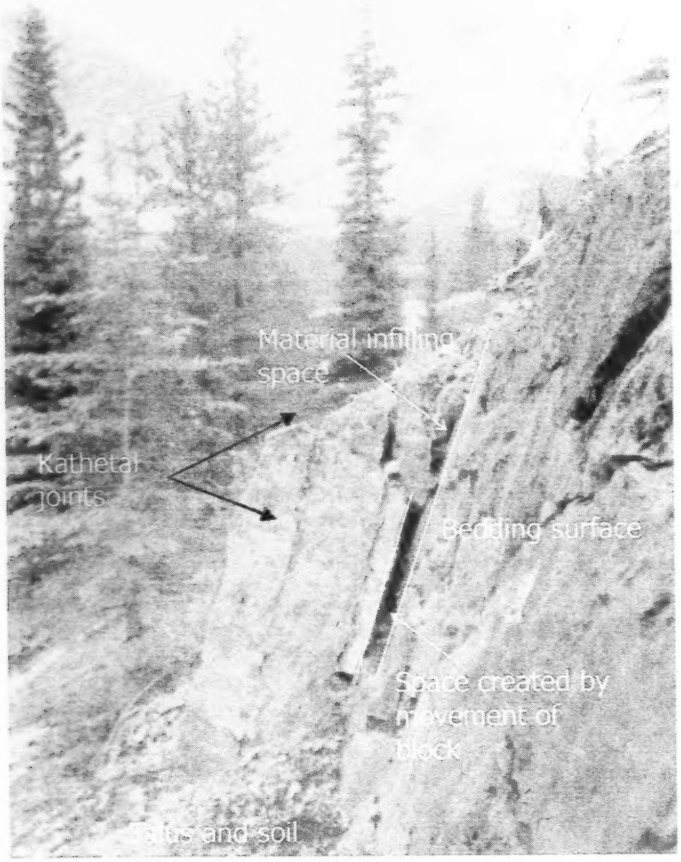

Figure 4.3 – Toppling block located at location 1, at the north end of the slope.

Figure 4.4 – Downslope at Location 2, showing the blocky talus deposits, the sparse vegetation and the use of the slope by Big Horn Sheep. The slope ends on the Athabasca Flood Plain, and blocks of rock can be seen resting on the flood plain.

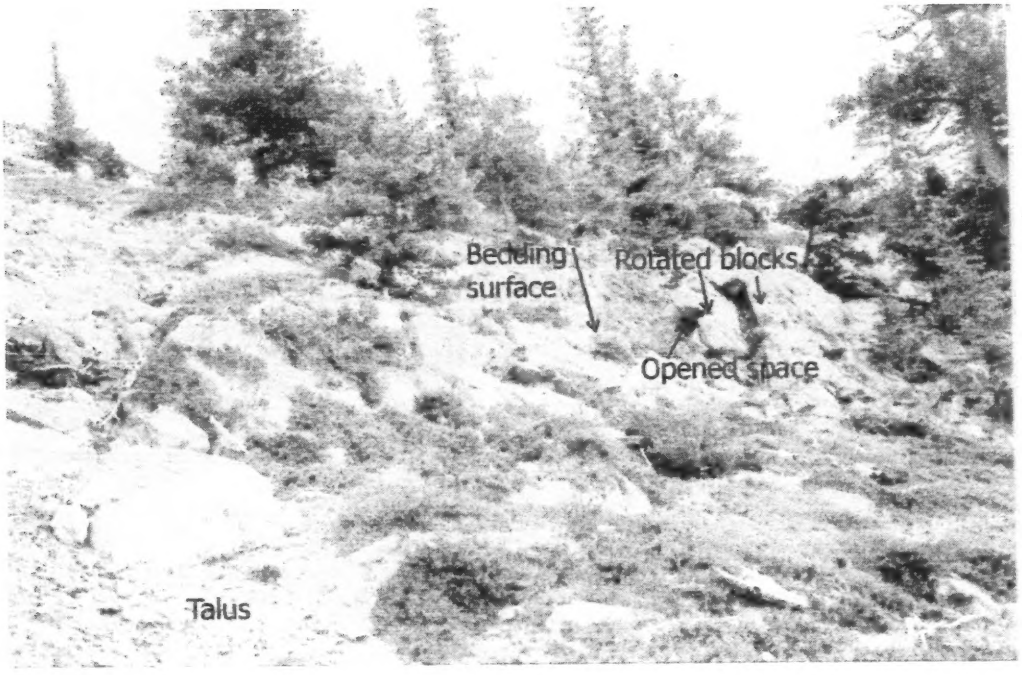

Figure 4.5 – Outcrop of Pekisko Formation along the Overlander Trail at Site 2. The in place bedding is shown, as well as the bedding that is showing some rotation.

The regional slope angle from the NTS maps is 17°. As rotation of the blocks can be interpreted from the orientation of some of the blocks dipping at an angle that is steeper than that of the bedding underlying it, toppling is the inferred method of movement on this slope. Figure 4.1 shows point L2, which plots below the area for toppling on bedding. The lower boundary for toppling on bedding was taken to be the angle of internal friction of the material (Cruden and Hu, 1996), yet it can be shown that small scale toppling will occur on cataclinal slopes with a regional slope angle less than the internal angle of friction of the material. With the presence of the overlying surficial materials at this location, it is likely that the overlying material is subjected to downslope creep, and this may add a driving force to the toppling of these blocks.

4.2.3 Site 3

Site 3 is also located on the west slope of Morro Peak, and is shown on Figure 4.2. This location lies within the shale of the Banff Formation, near the contact with the Palliser Formation, adjacent to Morro Creek at UTM 11U 0428450 5875800. At this location the bedding dips 76° toward 218°, with an average bedding spacing of 0.5cm. The slope is covered with talus (Figure 4.6), and blocks of rock have rotated to have dips up to 90°. The mapped slope is 17° toward 222°.

At this location, the mode of movement is interpreted to be multiple-block topples (McAffee and Cruden,1996); the thin bedded rock has a block ratio greater than 2. Cruden and Hu (1994) discussed the control of toppling on cataclinal underdip slopes by slope angle, bed thickness and joint spacing, and McAffee and Cruden (1996) classified types of topples on cataclinal slopes based on the block ratio, the ratio of the height of the block to the width of the block. The bedding within the shale is on the order of 0.5cm thick, so, when the strike joint spacing is greater than 1 cm, the block ratio is greater than 2. Intact bedding and rotated bedding orientations are shown in Figure 4.6.

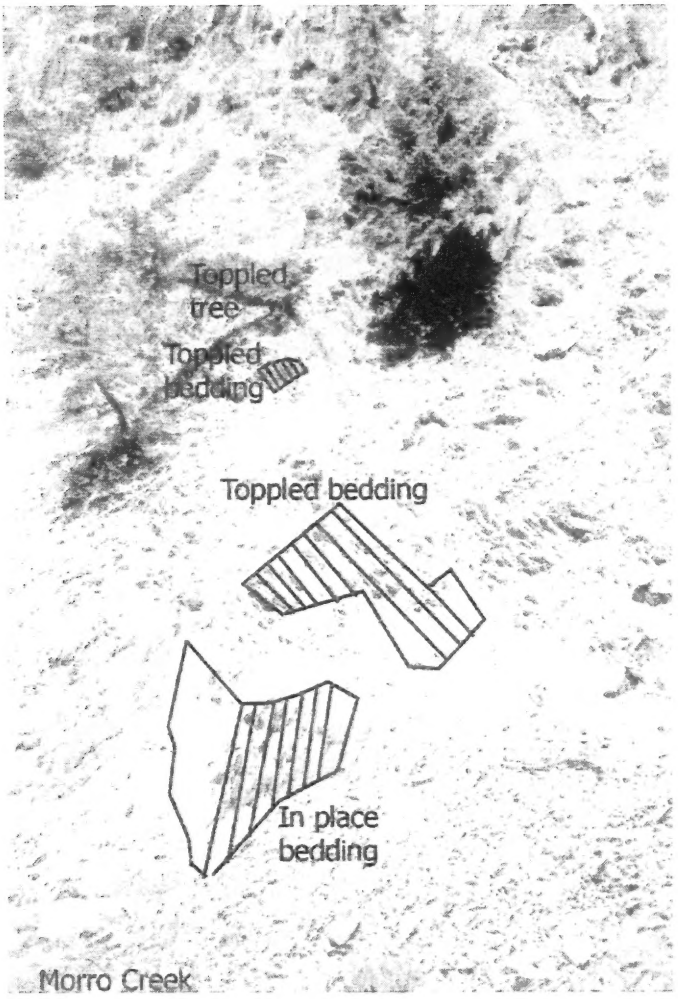

Figure 4.6 – Rotated bedding at Location 3, within the shales of the Banff Formation. The toppled tree is 1.5m high.

4.2.4 Site 4

Location 4 is on the lower west slope of Mount Hawk, between Garrone Creek and the unnamed drainage to the south of Morro Creek (Figure 4.7). The slope is 35° toward 222°. The bedrock of this slope consists of rocks of the Rundle Group which have an average dip of 51° toward 224°. Portions of this slope appeared to be locally plagioclinal from oblique photographs, yet they are formed of both cataclinal and orthoclinal slopes. The bedding spacing ranges from 30 to 40cm, with two joint sets; joint set 1 has spacing of 35-125cm, and joint set 2 has spacing of 10-60cm. The average orientation of joint set 1 is 88° toward 311°, and the average orientation of joint set 2 is 16° toward 036°.

Within the Turner Valley Formation, at UTM 11U 0428650 5874650, a block has been rotated 18° toward vertical from the bedding orientation of the slope (Figure 4.8). The space behind the block has been infilled with rock debris, soil and vegetation. This block is toppling from an underdip cataclinal slope, and the orientation of this block is plotted on Figure 4.1 as L4, and plots within the region for toppling on bedding..

4.2.5 Site 5

Site 5 is on the west side of Mount Hawk, within the Banff Formation (Figure 4.7), on a slope at 57° toward 223°. The bedding at this location dips between 63° and 77°, toward 204° to 219°. The bedding ranges from 5 mm thick in the shales of the Banff Formation up to 35cm thick in the crinoidal beds. Joint set 1 spacing ranges from 80cm to 110cm, and joint set 2 spacing ranges from 45cm to 50cm. Talus is common at the base of this slope, and covers major portions of the slope (Figure 4.9). Within the shales, at UTM 11U 0428784 5875692, blocks have been rotated from the original orientation of the bedding through the vertical to now dip in the opposite direction (Figure 4.9). Within the crinoidal layer 20m downtrail of the shale outcrop, there is an outcrop of the

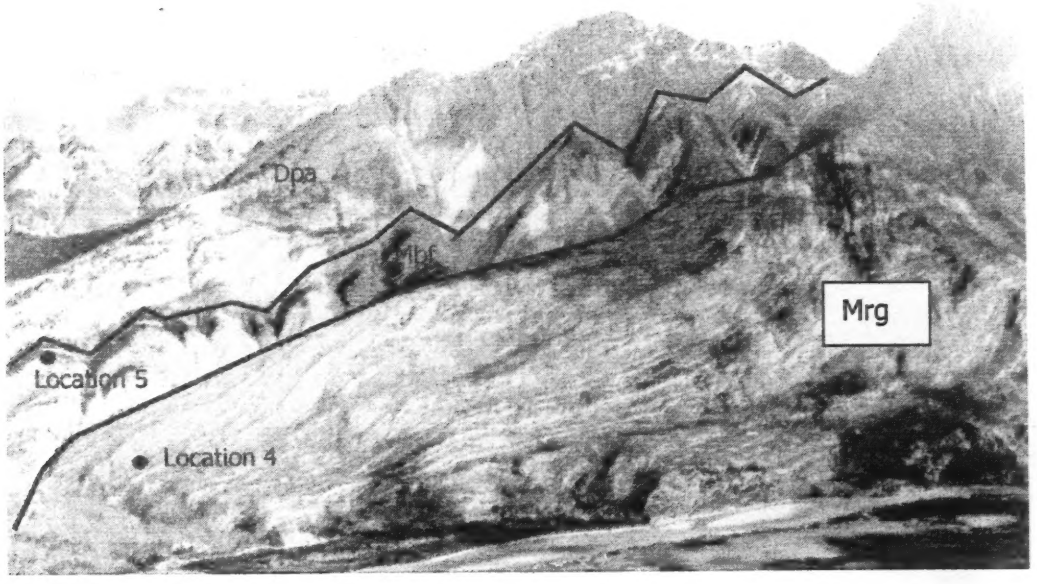

Figure 4.7 – Oblique photograph showing locations 4 and 5 and the bedrock geology. Bridgland Repeat Photography collection, photo B474, showing Mount Hawk, and Mount Colin on the right side of the photograph.

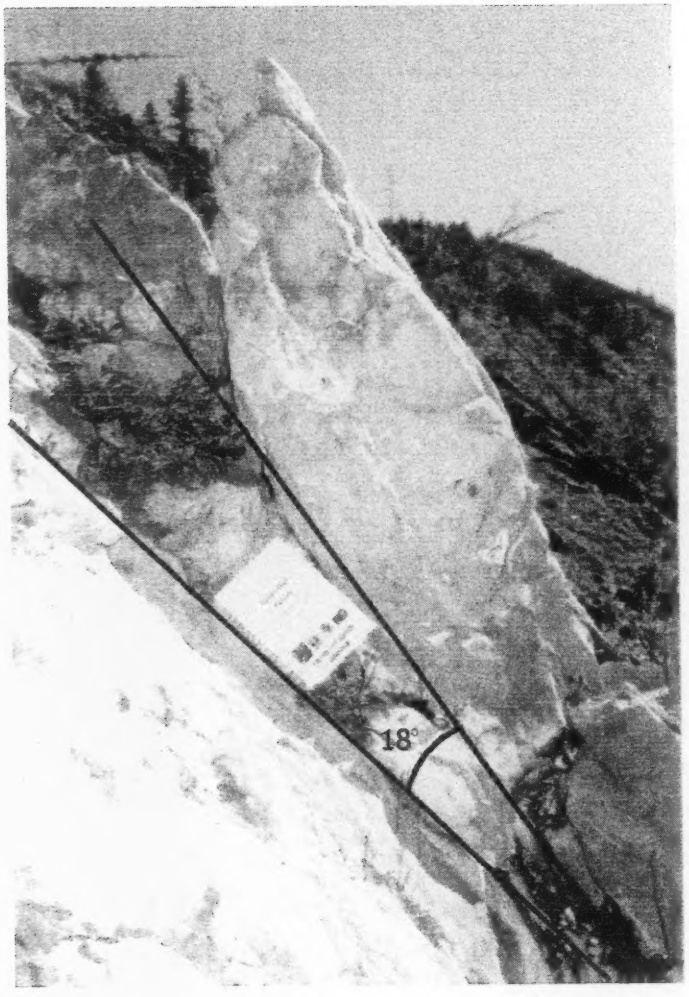

Figure 4.8 – Rotated block within the Turner Valley Formation at Location 4. The space that has been opened up by rotation has been subsequently infilled with debris, soils and vegetation.

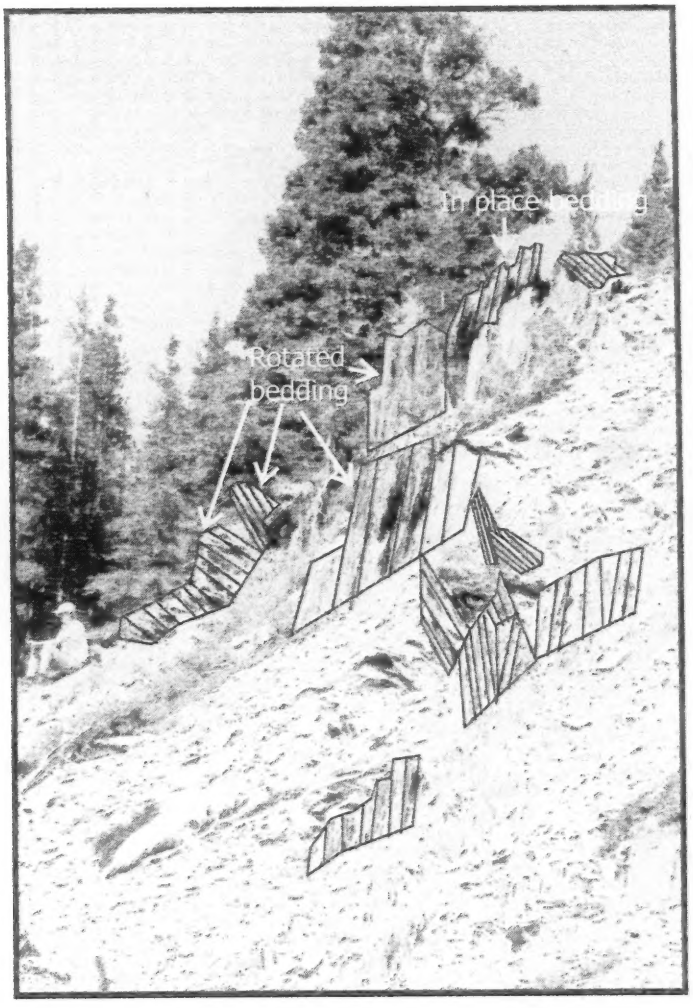

Figure 4.9 – Rotated blocks within the Banff Formation shales at Location 5.

Banff Formation showing individual blocks that are bounded by bedding planes and kathetal joints rotated through 90° (Figure 4.10).

Site 5 is plotted on Figure 4.1, and falls within the area of toppling from bedding on cataclinal slopes. Within the thinly bedded Banff Formation the rock is moving as multiple-block topples, with a height to width ratio of 3 (McAffee and Cruden, 1996). Where the more thickly bedded crinoidal layers are present within the Banff Formation, the widths of the blocks are between 10cm and 20cm, and the heights of the blocks 45cm to 50cm, giving a block ratio between 2.25 and 5, yet they occur as block topples.

4.2.6 Overview of Toppling on Cataclinal Slopes

Sites 1 and 2 are located along the Overlander Trail, which is frequently used by hikers, bikers and ungulates. Site 3 is located adjacent to Morro Creek, which is at times used by rock climbers, as an approach to the Morro Creek Canyon rappel, and as an approach to the Guides Route Climb up the face of Morro Peak. Site 4 is not located in a recreational area, and approach is impeded by fallen trees and the lack of a trail, yet ungulates are common. Site 5 is located along the approach to Mount Hawk, along the trail. The use of trails adjacent to sites 1-3 and 5 indicate that toppling is a potential hazard to those using these trails.

Two different modes of toppling were found to occur on cataclinal underdip slopes within the study area, block topples and multiple block topples. Multiple block topples were found to occur on shallow sloping cataclinal underdip slopes, within the thinly bedded Banff Formation shales. As shown in Figure 4.1, locations 3,4 and 5 plot within the region for toppling on cataclinal slopes for the dip of the bedding and the overall slope in the region. Sites 1 and 2 plot in the area below where toppling is known to occur, yet the lower boundary of this area is dotted, and was arbitrarily included as a lower bound based on the internal friction angle of the material.

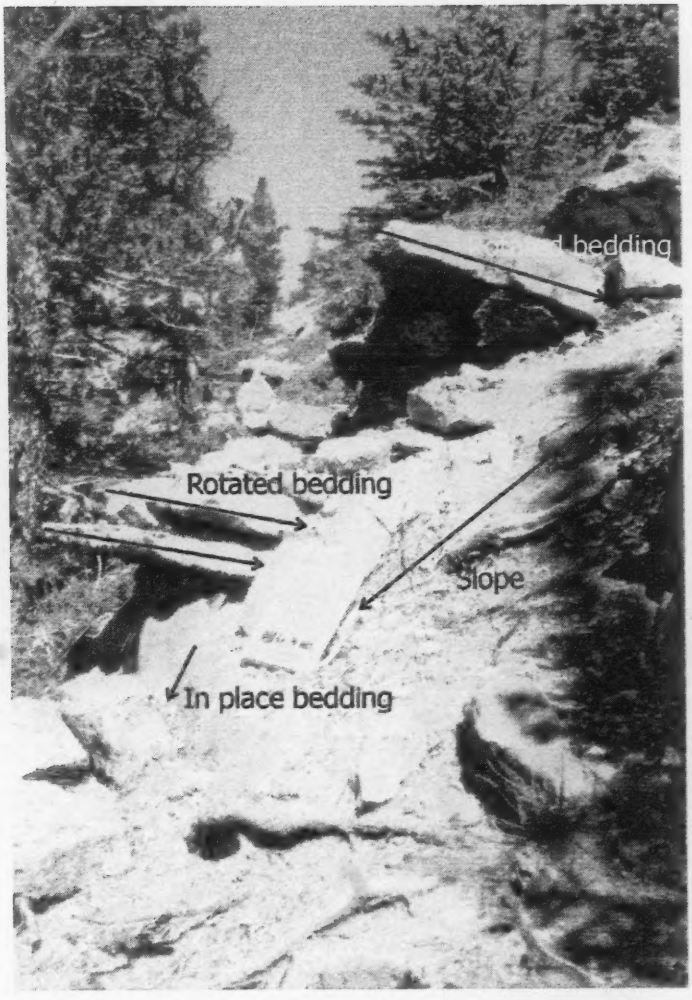

Figure 4.10 – Rotated bedding at Location 5 within the crinoidal limestone of the Banff Formation.

Toppling occurs on cataclinal underdip slopes in increments, and blocks are moved when disturbed by forces exerted by high water pressure, snow, ice and ungulates. The toppling blocks are stable when the disturbing forces are not acting on the blocks. These slopes can be considered safe during dry and warm climatic conditions.

4.3 Exfoliation of cataclinal underdip slopes

In areas of steep, cataclinal, underdip slopes, a different type of slope movement occurs, characterized by a circular to inverted teardrop shaped alcove on the slope surface. The two locations of this phenomenon are shown in Figure 4.11, and both occur within the Devonian Palliser Formation on the west slopes of the Colin Range.

Site 1 is on Morro Peak, at UTM 11U 0428500 5875800, where Morro Creek flows out of the steep-walled canyon through the Palliser Formation and into the less-resistant rocks of the Banff Formation, along the toe of the cataclinal underdip slope. The bedding at this location dips at 70° in the direction 221°, with a bedding thickness of 10cm to 35cm. Joint 1 spacing ranges from 20cm to 60cm, and the joint 2 spacing ranges from 20cm to 180cm. At this location two tear-drop shaped to circular concavities are found in the slope (Figure 4.12 and 4.13). These concavities occur one above the other, with the depression in Figure 4.12 occurring higher up on the slope than that of Figure 4.13.

The upper concavity occurs on a dip slope portion of the cataclinal underdip slope, with a shallow angle slope both above and below the concavity. The lower depression occurs below the ledge seen in Figure 4.12 at the base of the upper depression. Precipitated salts are present along the bedding planes that are exposed on the surface, at the top of the depressions. In a cross-sectional view, the slope profile exposes bedding planes along the slope, where vegetation is present on the shallow slopes that are formed (Figure 4.14). Talus

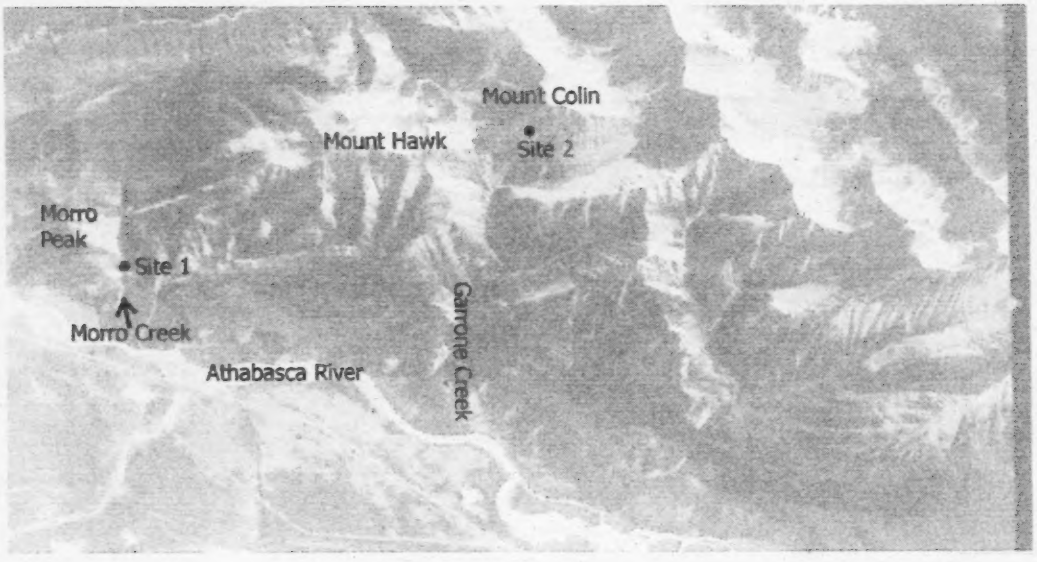

Figure 4.11 – Aerial photograph showing the location of Sites 1 and 2. Aerial photograph #A23015-138, originally at a scale of 1:60 000.

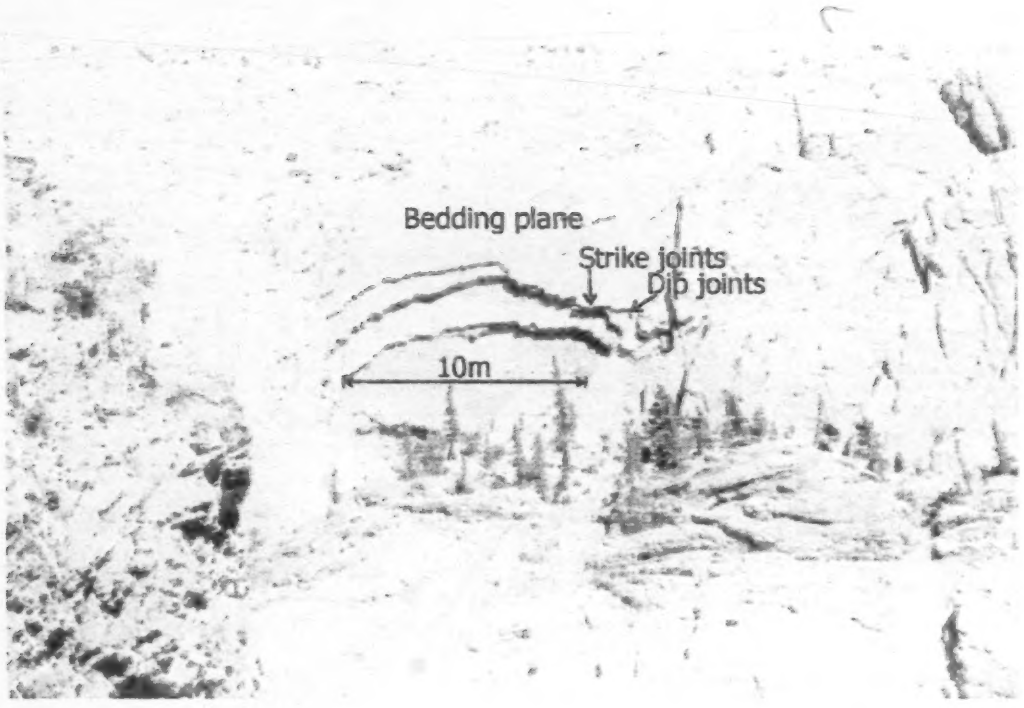

Figure 4.12 – Upper exfoliation at Site 1, showing the dip slope bedding planes, strike joints and dip joints, with the underdip slope visible in the foreground.

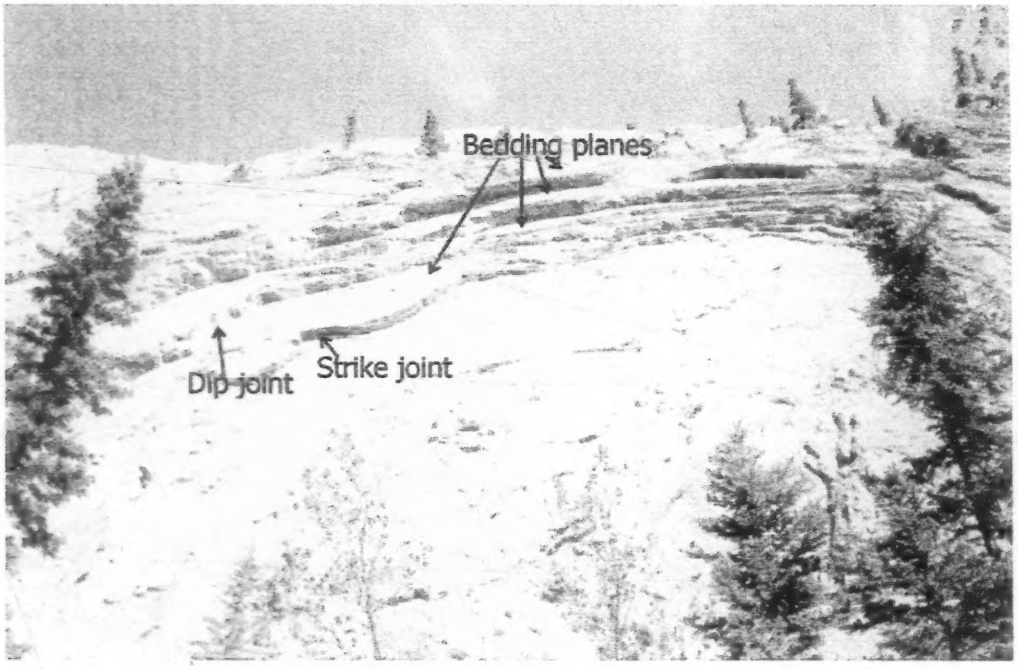

Figure 4.13 – Lower exfoliation at Site 1, taken from the bottom of the feature looking up along the dip of the bedding, showing the bedding planes that daylight in the feature, and the strike and dip joints.

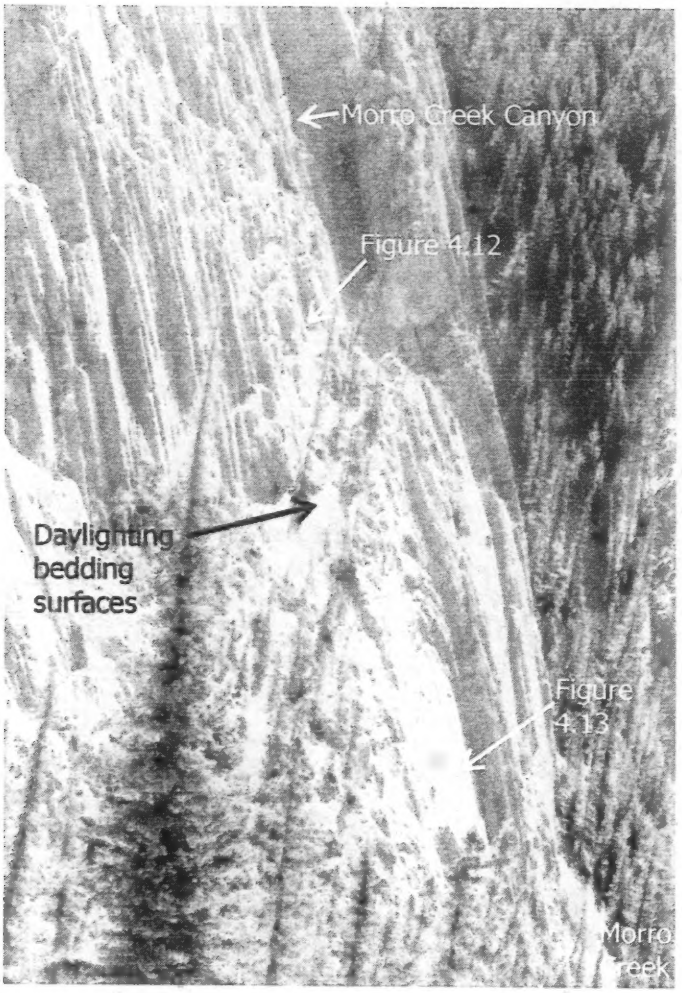

Figure 4.14 – View along the strike of bedding of the area of exfoliation at Site 1. The location of Figures 4.12 and 4.13 are shown, along with the daylighting bedding planes above the concavities and the location of Morro Creek and Morro Creek Canyon.

is present on these shallow slopes, as well as at the base of the slope. The talus at the base of the slope ranges in size from very small block up to blocks 50cm by 70cm. The talus here appears to be fresh, with a dark gray color, no lichen and no well developed karren on the surface. Tree trunks at the base of the slope show evidence of damage, including scarring that has healed, and fresh wounds that are emitting sap (Figure 4.15).

Site 2 is located on the dip slope face of Mount Colin, at UTM 11U 0433575 5872900. The bedding at this location dips 60° toward 215°. Circular to tear-drop shaped concavities in the slope are within the Palliser Formation, adjacent to Garrone Creek in a steep walled valley (Figures 4.16 and 4.17). The concavities at this location cut more bedding planes than within Morro Creek. Bedding thickness was not measured on this inaccessible slope. The base of the slope is covered with talus of Palliser Formation rocks.

At this site, no ledges are present above the concavities, yet as this slope is near to the summit of Mount Colin, the bedding planes daylight at the top of the slope. This site is located above the tree line, so vegetation is not present above the concavities in the slope.

The circular to tear-drop shaped concavities are interpreted to be the result of exfoliation along the bedding planes of the rocks, with joint control of the sides and the top of the depressions. Both locations have bedding planes that daylight above the feature on a shallow slope, where water is able to infiltrate along the bedding planes. All of the examples of exfoliation were found in the Devonian Palliser Formation, a formation that is known for karst development (Thompson, 1976). As the water infiltrates along the bedding planes, it is able to dissolve some calcite from the rocks, and enlarge the bedding plane gapes, reducing cohesion, and the asperities along the bedding planes. One possible mode of movement of the rock is due to the outward force of the water on the bedding planes. This may initiate the buckling of the rock under its own weight (Hu and Cruden, 1993). Another driving force is the freezing of

4.15 – Recent tree damage at the base of the slope of Site 1, below the areas of exfoliation. Talus blocks can be seen where there is a build up of talus up slope of the tree trunk.

Figure 4.16 – An example of exfoliation at Site 2, on the dip slope face of Mount Colin. The depression of the exfoliation is 3.5m deep.

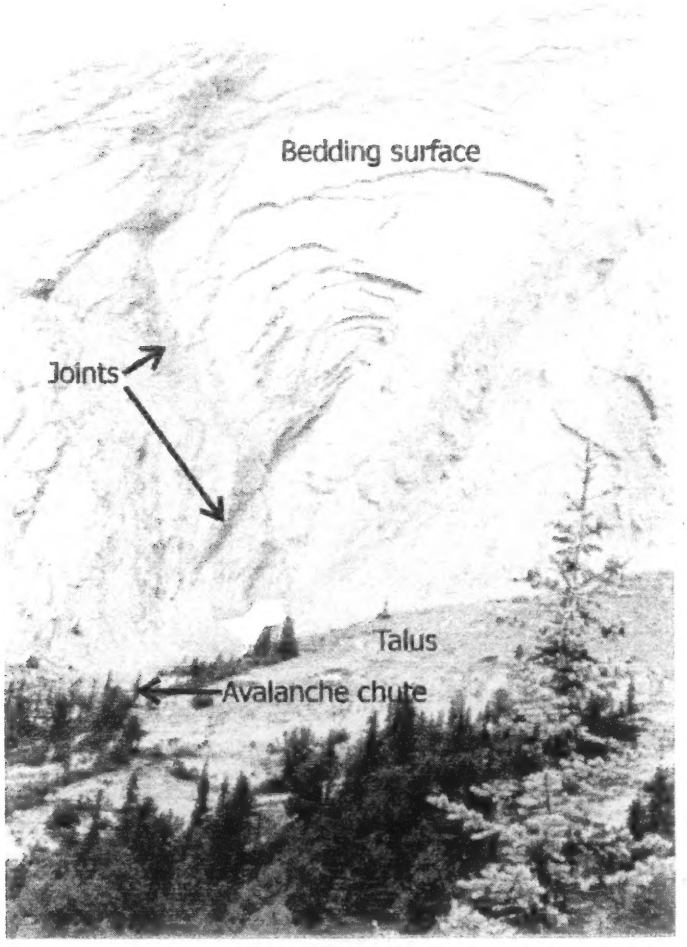

Figure 4.17 – Another example of exfoliation at Site 2, to the south of Figure 4.15. An avalanche chute extends downslope from the narrow base of the exfoliation.

water along the bedding planes, resulting in an outward force as the water expands on freezing.

The typical shape of an exfoliation is that of a concavity (Figure 4.18). Both of the sites where exfoliation occurs are located near the base of steeply dipping slopes located within valleys. Water can infiltrate down channels along bedding planes. With the shading of these slopes at their bases within valleys, water may then freeze, exerting outward forces on bedding plane. With little to no resistance from overlying beds, which have been removed, rocks are able to buckle outward along the kathetal joints, driven by water pressure, and fall or slide out of the plane of the slope (Figure 4.18). The material that is upslope of the concavity is held in place by cohesion and friction along the bedding planes and lateral constraints, leading to a planar sliding hazard. At site 2, some of the upslope material has been removed from the slope.

Exfoliation occurs in steeply dipping beds on cataclinal, underdip slopes and cataclinal dip slopes, where bedding planes are exposed on a shallowly-dipping, cataclinal, underdip slope above the exfoliation. The presence of vegetation at site 1 indicates that the bedding planes are open, as tree roots are able to penetrate into the bedrock, opening the bedding planes for further infiltration of water. At site 2, the steeply dipping bedding planes daylight at the surface above the tree line, indicating that freeze and thaw is a possible driving mode of exfoliation at this location. The size and the shape of the exfoliated area are controlled by joint sets, with joint set 1 controlling the lateral extent of the movement and joint set 2 controlling the height of the exfoliation (Figure 4.13). The continued loosening of rock on the top of the exfoliation causes retrogression upslope and the eventual disappearance of the landform. These are areas of particularly active rock fall, based on the amount of talus at the base of these slopes. The orientations of the slopes and bedding have been plotted on Figure 4.1, and these landforms plot in the area for buckling of rock on cataclinal slopes.

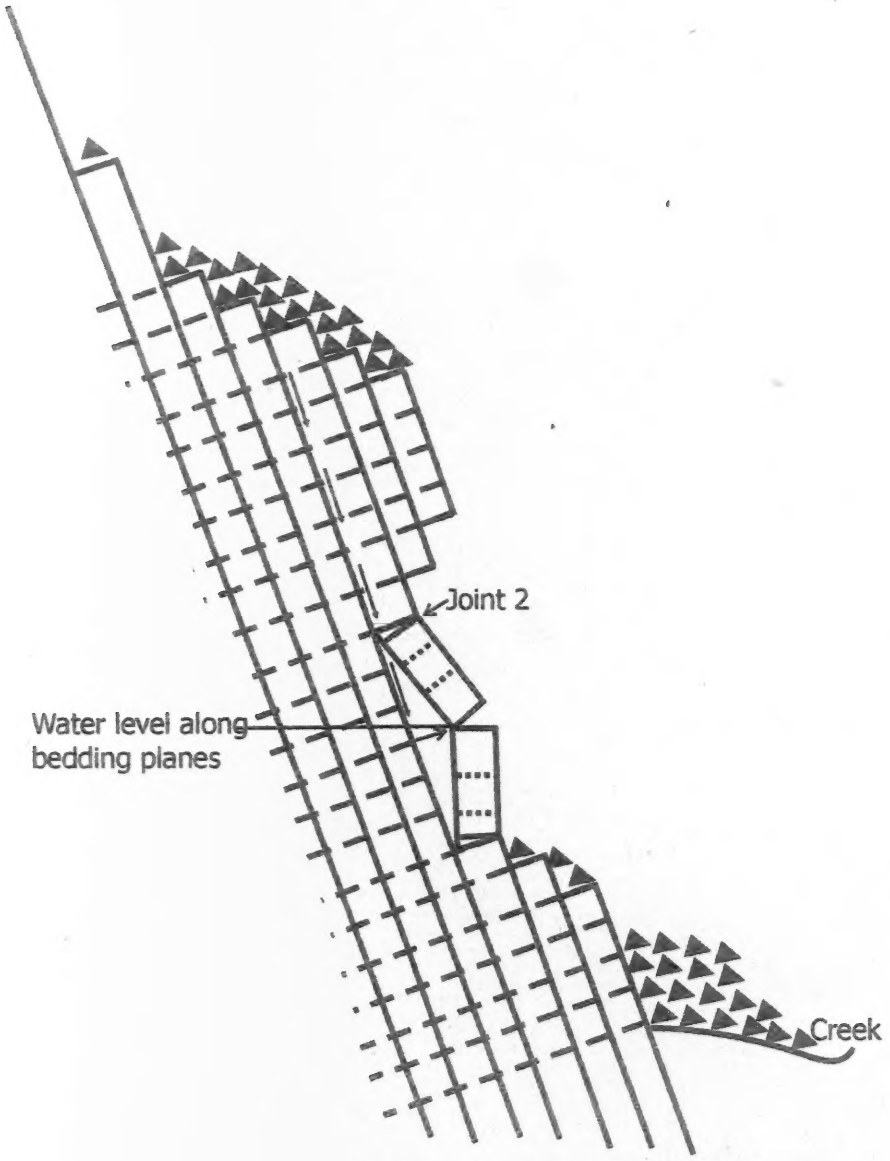

Figure 4.18 – Idealized cross-section across an exfoliation. The solid lines indicate the bedding planes, and the dashed lines indicate joint set 2, the strike joints, and the triangles indicate talus. Small black arrows show the movement of water along the bedding planes, down to the water table, and a possible mode of movement of the blocks out of the slope.

4.4 The Rock and Boulder Gardens

4.4.1 Introduction

The Rock and Boulder Gardens (Robinson, 1999), unique areas within the Colin Range, create a wedge-shaped depression up-slope of an elevated area of colluvial materials (Figure 4.19). The site can be divided into three separate areas, the scarp area, also known as the Rock Gardens (Robinson, 1999), the labyrinth, known as the Boulder Gardens (Robinson, 1999), and the colluvial deposits down slope.

The site is located where the Maligne River flows onto the Athabasca River flood plain (Figure 4.19), where the course of flow of the Maligne River within the Athabasca Valley changes from a northward flow to a northwesterly flow (Figure 4.20). The Rock and Boulder Gardens lie above the floor of the Athabasca valley, on the east side of the valley, at the southern extreme of the Colin Range that faces the Athabasca Valley. The Rock and Boulder Gardens are well known to rock climbers for their many routes (Robinson, 1999).

The Rock and Boulder Gardens lie completely within the Palliser Formation, toward the top of the formation (Figure 4.20). In place bedding in the area has a range of dip angles from 14° to 47°, in a direction between 198° and 270°, with an average 24° dip in the direction 224° . A joint survey, undertaken as a part of the study of this area, found that the joints at this location dip steeply. Figure 4.21 is a plot of the poles to the joints in the area. Joint sets are not well-defined, yet the joints tend to have a steep dip to the northwest and northeast. Locally the joints were orthogonal to one another and to bedding.

The surficial geology at this location includes the lateral moraines of the late-intermediate stage of the Athabasca Glacier, as can be seen in Figure 4.22

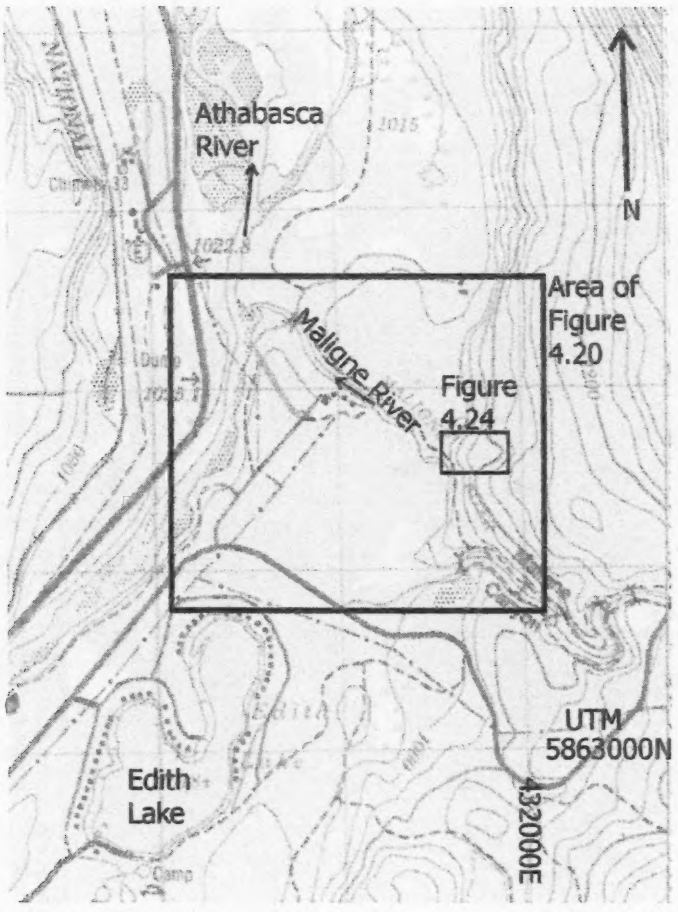

Figure 4.19 – Topographic map enlarged from 1:50 000 scale, showing the location of the Rock and Boulder Gardens study area.

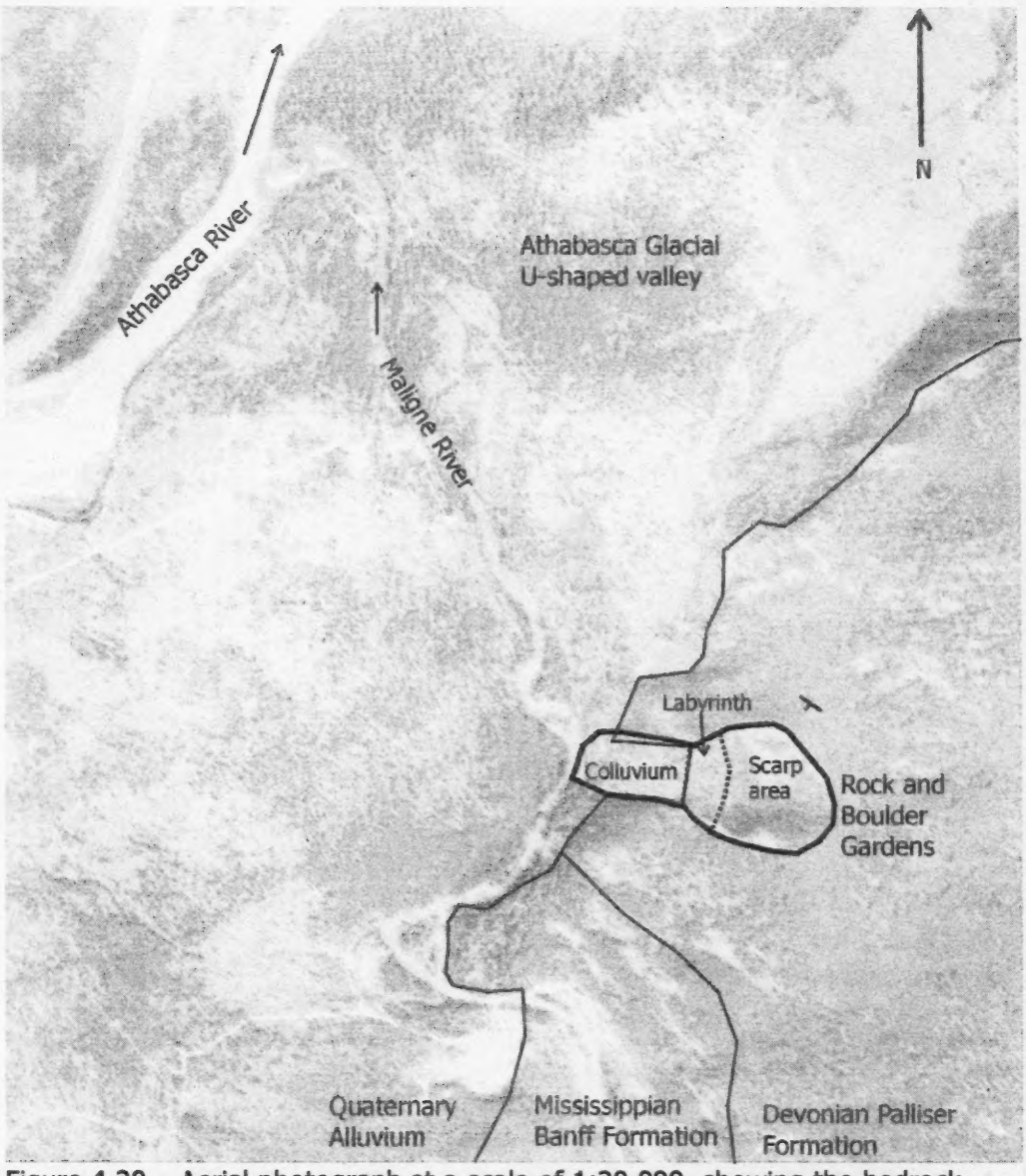

Figure 4.20 – Aerial photograph at a scale of 1:20 000, showing the bedrock geology in the vicinity, the scarp area, the labyrinth area and the colluvial area of the Rock and Boulder Gardens. Photograph courtesy of the Jasper National Park Wardens Office.

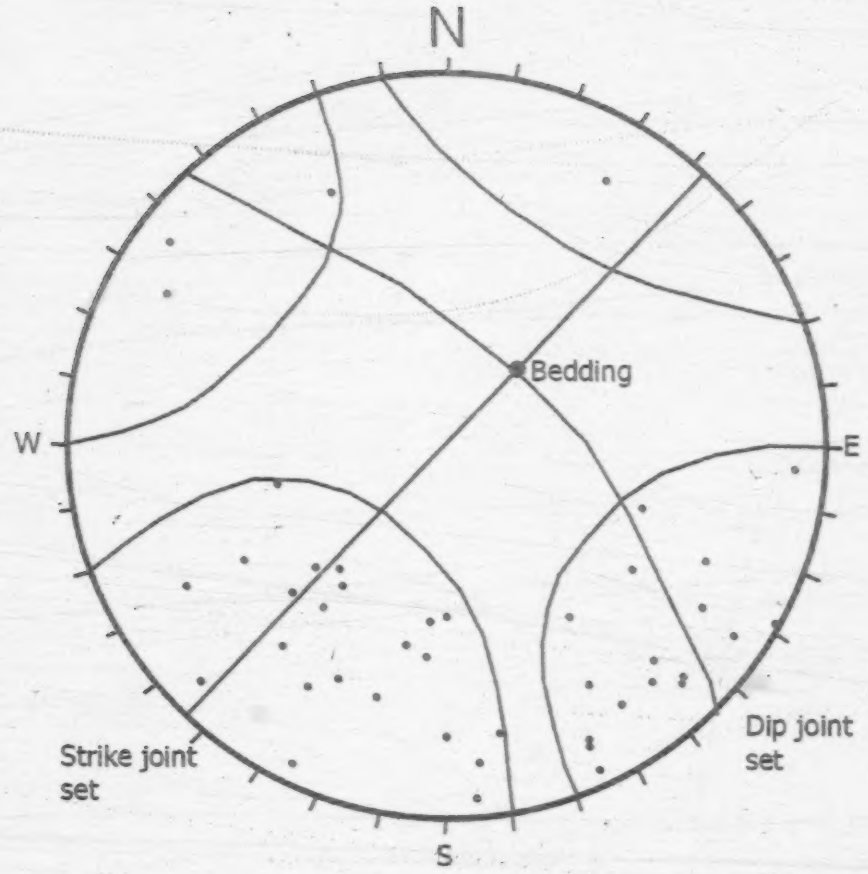

Figure 4.21 – Lower hemisphere equal angle stereographic projection of the poles to the measured joints within the Rock and Boulder Gardens, showing the strike joint set and the dip joint set. The average bedding orientation is plotted.

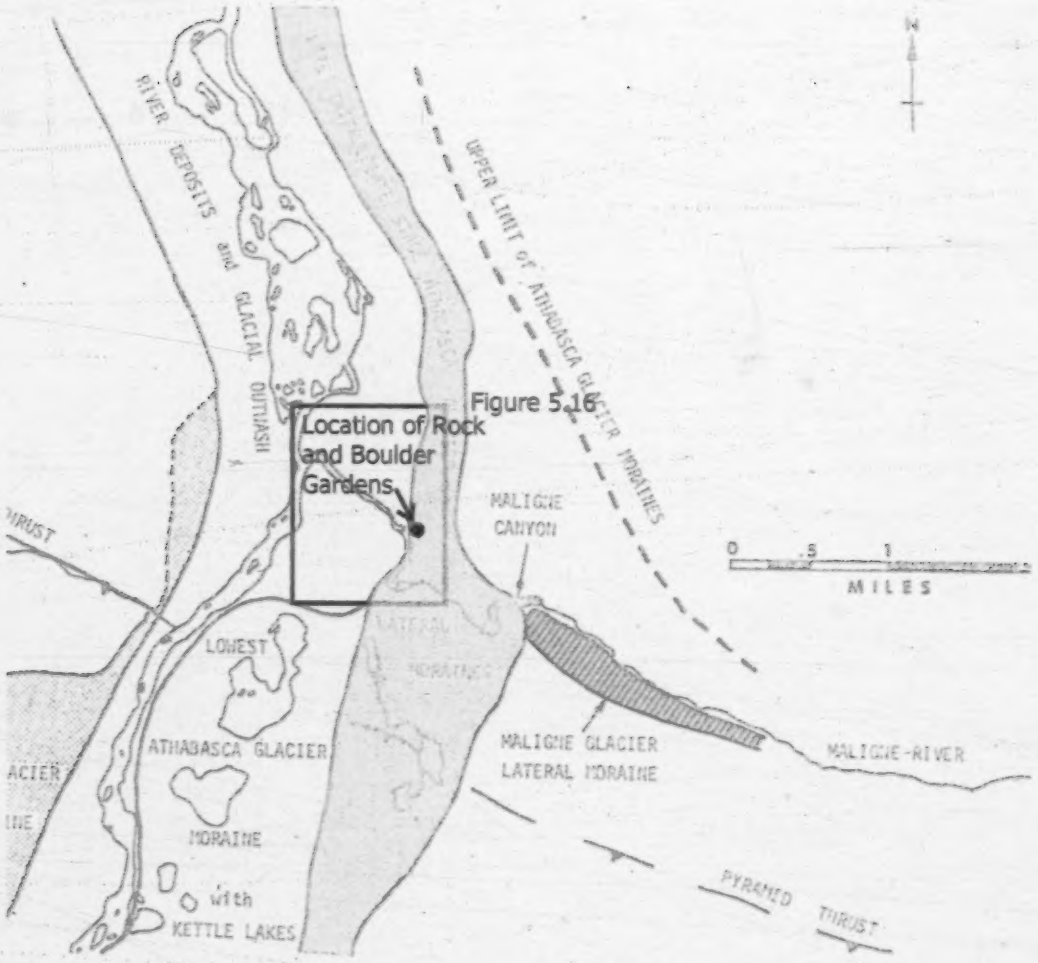

Figure 4.22 – Detailed map of the surficial geology in the vicinity of the Rock and Boulder Gardens (Mountjoy, 1974), showing the location of the Athabasca Glacier Moraine in green and the Maligne Glacier Lateral Moraine in purple.

Figure 4.23 – View from the south scarp toward the north scarp, showing the tree cover in the bowl area. The area with no tree cover is a dip slope. The north scarp of the feature can be seen in the middle ground.

(Mountjoy, 1974). The area is well treed, with the exception of the south-facing scarp (Figure 4.23).

Springs at the base of the slope in this area, within the Palliser Formation, flow into the Maligne River. Maligne Canyon is known to be an area of active karst (Thompson, 1976). Extensive cave systems are likely to exist in the vicinity of this site.

4.4.2 Scarp Area Observations

The scarp area of the Rock and Boulder gardens is the bowl-shaped feature visible on the aerial photos (Figure 4.24). The area is bounded to the south by a steep rock slope of 80° to 90° in the direction of 007°. A much shallower slope of 14° to 47° in the direction of 226° to 246° bounds the feature to the north and the east. To the west of the area is the labyrinth. The boundary between the scarp area and the labyrinth is marked by large, displaced blocks and is densely treed.

The steep south slope of the feature ranges up to 25m in height. This slope is heavily used for rock climbing, as can be seen by the bolts in the rock and the climbers' chalk left on the rock face. The bedding dips 21° toward 218° in this slope. This slope, structurally controlled by the orthogonal joints, (Figure 4.25) is composed of alternating orthoclinal and anaclinal slopes.

The south slope shows signs of recent rock falls. Unweathered boulders and recent tree damage are found at the base of this slope (Figure 4.26). Parts of the slope are covered with mosses and lichens, where climbers are not active. Slopes in this area locally overhang at the top of the slope. The slope here ends to the west where blocks have toppled in the direction 180° away from the direction of dip of the bedding, and the bedding orientation has changed significantly. To the east, the slope height decreases, and the slope angle becomes much less, and ends where a small depression cuts through the raised

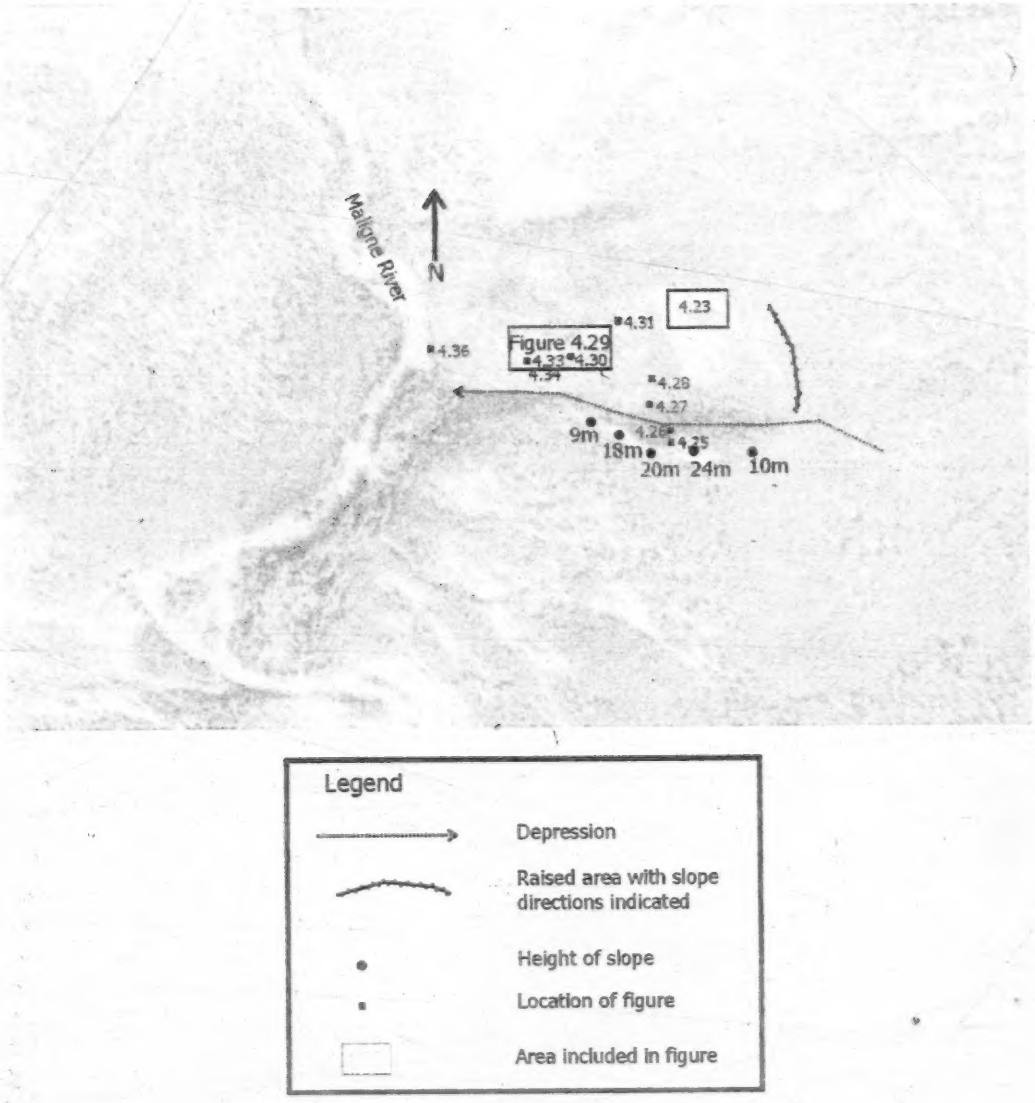

Figure 4.24 – Area from Figure 4.1 enlarged to show the location of figures, the location of a depression through the scarp area, and heights of the south scarp of the Rock Gardens.

Figure 4.25 – Joint control of the south scarp in the Rock Gardens area. Where the dip joint controls the slope, the slope is an orthoclinal slope, and where the strike joints control the slope, the slope is an anaclinal slope.

Figure 4.26 – Tree damage and rock fall debris at the base of the south scarp. The damaged tree has a diameter of 10cm.

area, where the east slope of the graben meets the south scarp (Figure 4.24).

A slope that follows the bedding forms the north boundary of the feature, at an angle of 31° toward 224°. This slope is bounded to the east by a slightly elevated ridge. Its crest is elevated slightly above the main portion of the slope (Figure 4.24). The bedrock on the slope is veneered by thin colluvial deposits, which do not support the dense tree cover of the south and the west slopes. Where tree cover is not present, there are mosses, lichens and rock fragments present on top of the bedrock. Where boulders are present, they are randomly oriented.

Within the scarp area (Figure 4.20) there is a deep, closed wedge-shaped depression bounded by the previously described slopes. Within the depression, there is an assortment of blocks. Within the south portion of the wedge, boulders have toppled from the south slope. Within the northern portion of the scarp, there are boulders that appear to have slid along bedding to rest in the boundary area. There is no indication of current drainage through this depression, and there was no standing water in this region in Summer 2002. The base of the bowl is densely vegetated, and mosses cover the boulders that infill the depression (Figure 4.27).

4.4.3 Labyrinth Observations

The boundary between the labyrinth and the scarp is not distinct. Vegetative cover on the ground obscures the boundary between the randomly oriented boulders that infill the scarp area (Figure 4.28) and the oriented and regularly spaced boulders of the labyrinth (Figure 4.29). The labyrinth is differentiated from the other areas by the regular orientation of individual blocks, separated from one another along gaping joint planes. The labyrinth is a popular rock climbing area known as the Boulder Gardens (Robinson, 1999), from the regular spacing of blocks in the area.

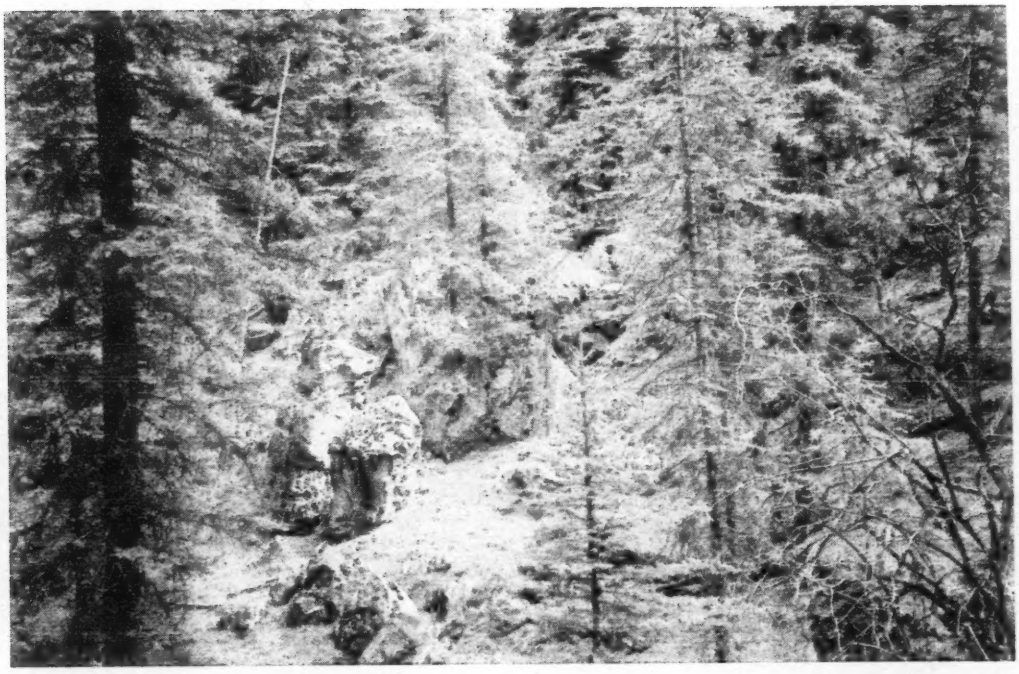

Figure 4.27 – Randomly oriented boulders within the graben at the base of the south scarp.

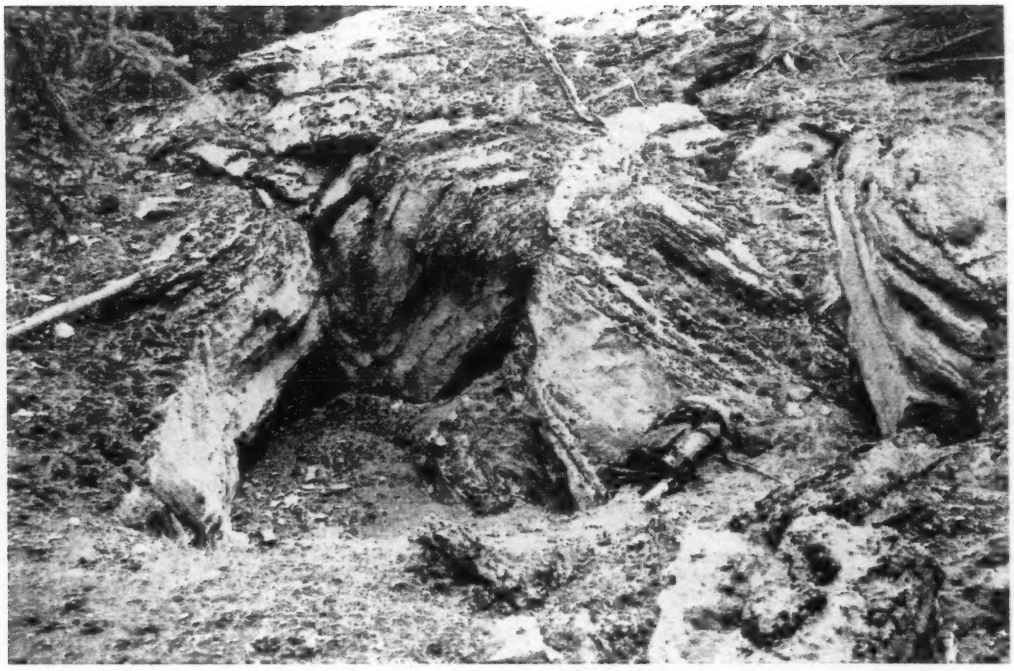

Figure 4.28 – Large, randomly oriented blocks within the transitional area between the scarp and the labyrinth. Backpack is included for scale.

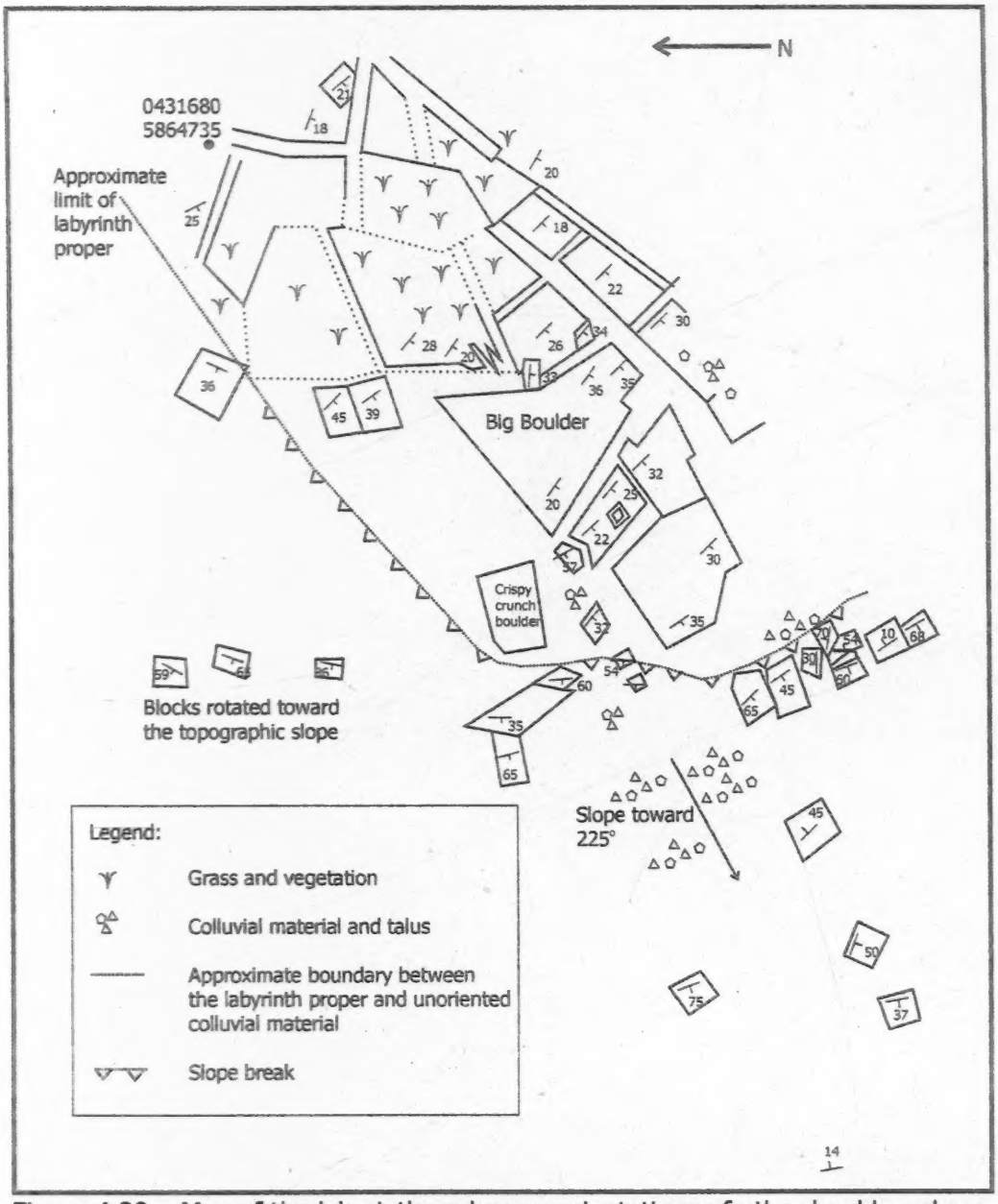

Figure 4.29 – Map of the labyrinth and some orientations of other boulders down slope, at a scale of 1:500.

The boulders in the labyrinth proper are all rectangular prisms, with no rounding, showing clear joint surfaces. The boulders appear to be broken apart. The average bedding orientation within the labyrinth proper was measured to be 24° dip in the direction 224°, using Dips, yet the dip angles and dip directions were found to be quite varied (Figure 4.29), indicating that some of the blocks have rotated. Dip angles varied from 18° to 45° for the blocks that do not appear to have rotated, and up to 65° for the blocks that do appear to have rotated. The dip direction in the labyrinth proper ranges from 198° to 270° for the blocks that do not appear to be rotated, and up to 300° for blocks that appear to not be in their original orientation. Joint orientations for the labyrinth proper do not necessarily show a preferred orientation. One preferred orientation of the joints strikes between 341 and 360°.

A map of the labyrinth produced by traverses along the joints shows the nature of the deposit (Figure 4.29). The largest block within the labyrinth is 11.10m high, 12.0m wide in the direction of dip, and 19.20m wide in the direction of strike of the bedding within the block. This boulder is shown on Figure 4.29 as Big Boulder.

The blocks are separated from one another along joints (Figure 4.29). The separation of joints ranges up to 9.0m with the common spacing between 1 and 2 metres (Figure 4.30). Where joint surfaces separate blocks, pine needles, rock and boulder debris, fallen trees, moss and other vegetation fill in the gapes (Figure 4.31).

Within the labyrinth, slopes that are formed by the separation of the blocks along joints create overhangs along the breaks. Also, at some locations, orthogonal smaller blocks are present on the tops of the larger blocks (Figure 4.32).

The rock within the labyrinth is Palliser Formation limestone. Within this area, the rock shows dolomitic mottling in many areas (Figure 4.33). Bedding is thinner and more recessive in some areas of the labyrinth, yet for the most part the labyrinth is composed of thickly bedded Palliser Formation limestone with

Figure 4.30 – A street within the labyrinth proper. The street narrows to the south, the direction of view of the photograph.

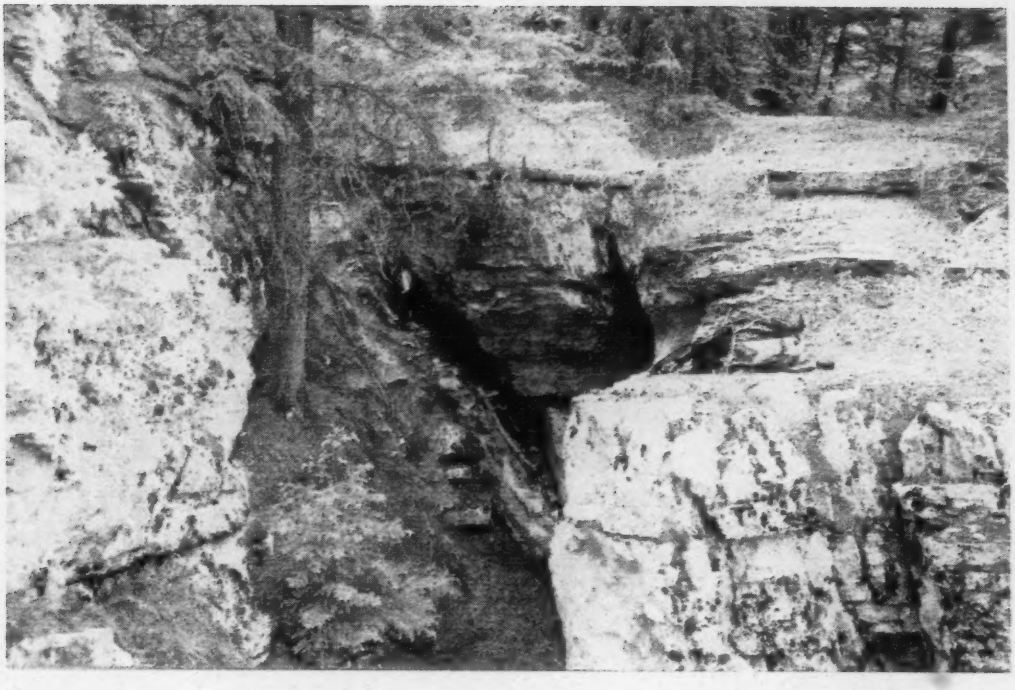

Figure 4.31 – A street infilled with debris (fallen rock, pine needles and branches), with a backpack for scale.

Figure 4.32 – Boulders dipping at 26° resting on top of a rock blocks, indicating that the friction angle of this material is greater than 26°.

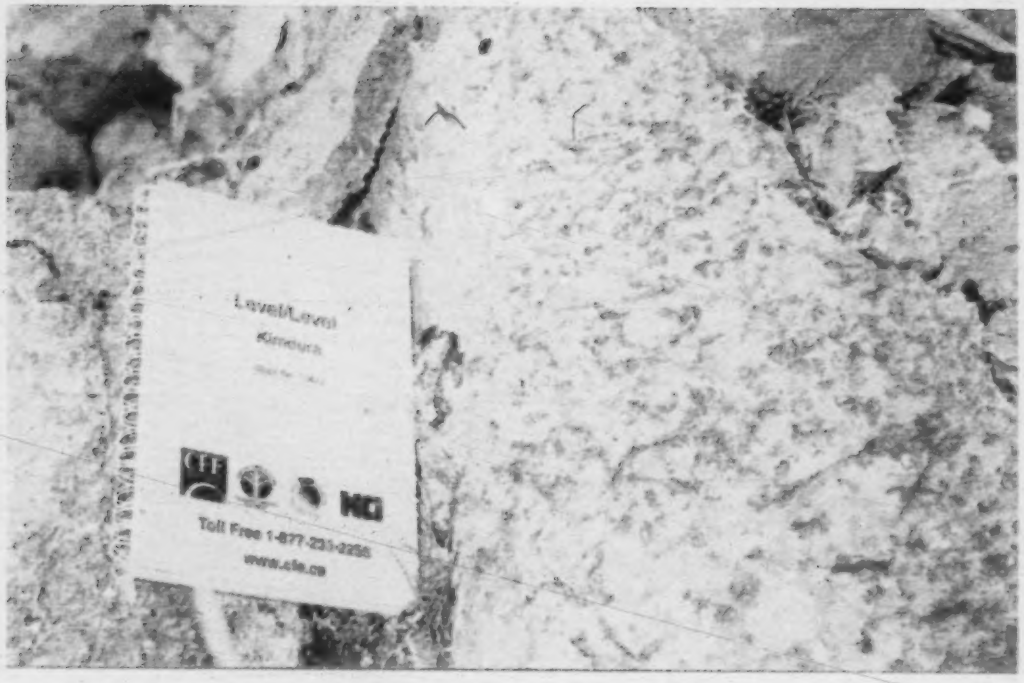

Figure 4.33 – Dolomitic mottling of the Palliser Formation limestone, with a notebook for scale.

thinner bands of dolomitic mottling. Karren are often present on the rocks in the labyrinth, and are developed in place, as there is not a measurable difference in pitch from the vertical for any of the karren that were observed (Figure 4.34). The development of these karren may be able to give an approximate age of exposure.

4.4.4 Down Slope Colluvium Observations

The area of downslope colluvium outlined on Figure 4.24, downslope of the labyrinth, is characterized by a chaotic arrangement of blocks of Palliser Formation limestone. The slope of the downslope colluvium is steeper than the slope of the labyrinth, as the slope is 31° toward the Maligne River. Figure 4.35 is a stereographic plot of poles to bedding orientations as measured within the downslope colluvial area. As can be seen, there is considerable scatter to the bedding orientations within this area, indicating that blocks have rotated about the strike of the bedding and about the strike of the dip joint set.

The area of the downslope colluvium extends from the western margin of the labyrinth proper into the Maligne River, where random blocks of Palliser Formation rock were found (Figure 4.36).

4.5 Interpretations of Rock and Boulder Gardens

The upper colluvial area indicates that this feature is a rock labyrinth (Sokolov, 1963; Simmons and Cruden, 1980), by the sliding of blocks along bedding planes. The scarp of this labyrinth creates a wedge shaped feature in the landscape. Colluvium that has reached the slope break has toppled and some material has been deposited in the Maligne River.

Based on the size of the blocks that were moved in this slide,

Figure 4.34 – Karren on the vertical surface of a boulder within the downslope colluvial area of the Rock and Boulder Gardens, with a notebook for scale.

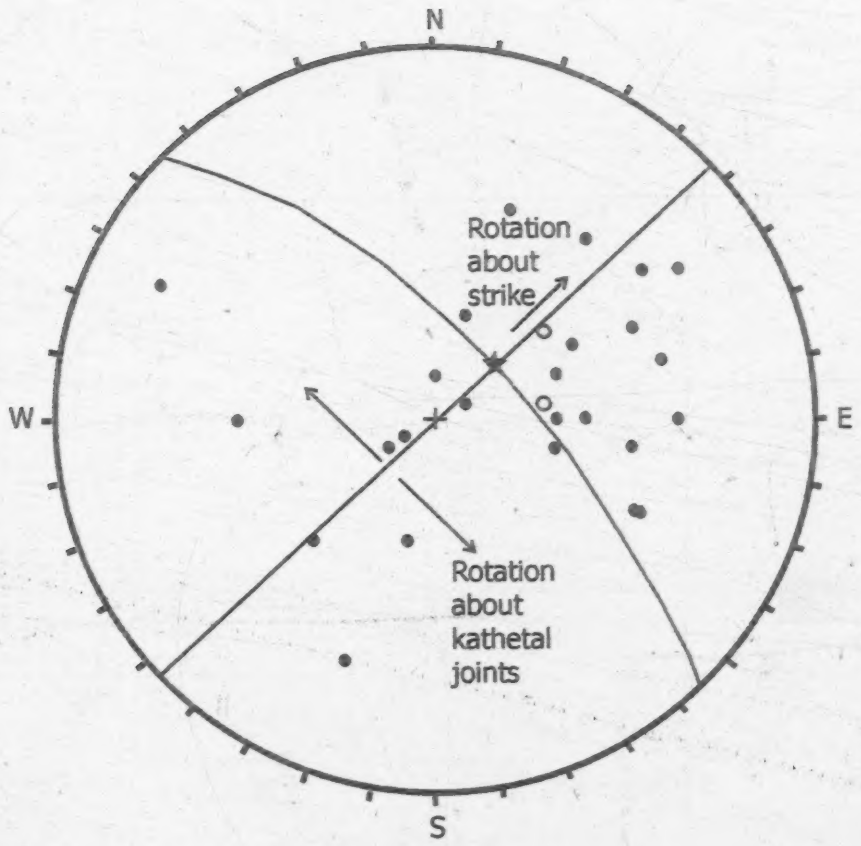

Figure 4.35 – Stereographic projection of measured bedding orientations within the downslope colluvial area of the Rock and Boulder Gardens. Projection of poles to the planes on an equal-angle, lower hemisphere stereogram. The star is a plot of the pole to the average bedding orientation, and the gray poles are plots of poles to two of the regional slopes.

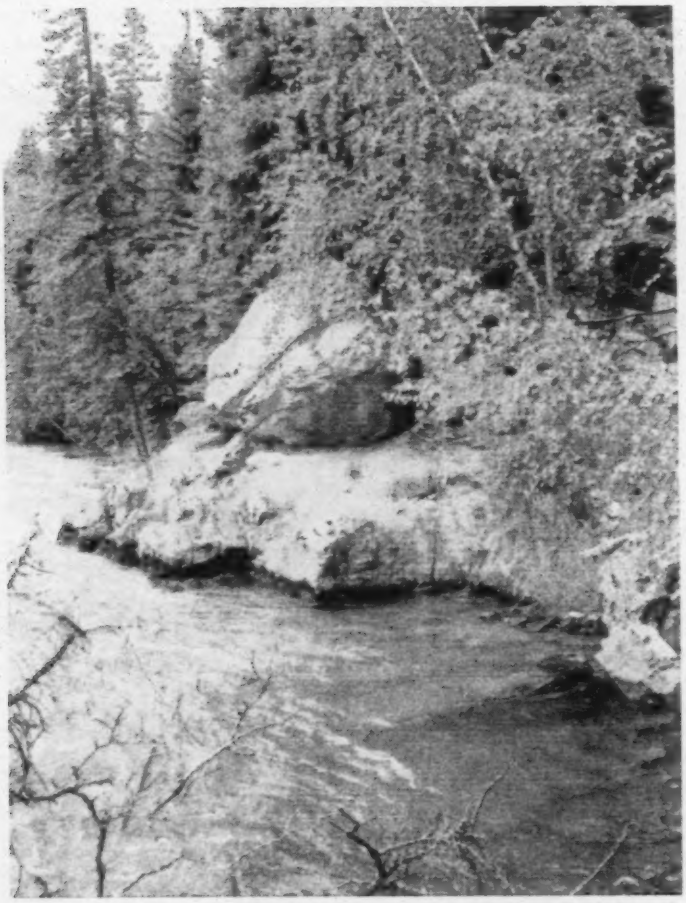

Figure 4.36 – Colluvial material in the Maligne River at the toe of the colluvial area of the Rock and Boulder Gardens. The large boulder is 2m high.

and the distance that these blocks were moved, high water pressures and snow pressures would be required to allow for this type of movement.

In the case of a rock labyrinth, rock blocks have slid out from a scarp along bedding planes, or weak layers within the stratigraphy. Cruden and Hu (1988) concluded that the frictional properties of dolomite result in dolostone having a lower friction angle than calcite on polished surfaces. Within the Palliser Formation there are several beds that have been dolomitized, and this may lead to a lower friction angle for these beds within the formation. As can be seen in Figure 4.32, blocks that are inclined at 26° are not sliding at this location, indicating that the internal angle of friction for this material must be greater than 26°. However, as the sliding surface was nowhere observed at this site, the friction angle along the plane of sliding can not be directly determined.

The steep south scarp of the graben is likely formed by the collapse of a cave system. Karst development is common within the Palliser Formation in this area (Thompson, 1976). The depression that runs along the base of the south scarp and off for a few metres to the east of the graben is likely due to the collapse of a cave system.

The average bedding orientation of 21° toward 218° for the bedding measured in place along the crest of the scarp indicates that the bedding dips less steeply than the expected angle of friction for a pure limestone, and dips at the low end of the range of angles of internal friction for carbonate rocks (Cruden and Hu, 1988). The collapse of the cave system to the south would provide the kinematic freedom for blocks at the south of the graben to begin sliding given sufficient pore water pressure. In addition, the general trend of the slope in this region is oblique to the strike, as the slope is to the west locally, providing the kinematic freedom for some blocks to slide out along bedding in the dip direction (Figure 4.37) and topple over the slope break to the west. Once the first blocks have moved out from their in-place location to the south and the west, blocks behind were then kinematically free to move out from the scarp, creating the kinematic freedom for the upgradient blocks to slide as well.

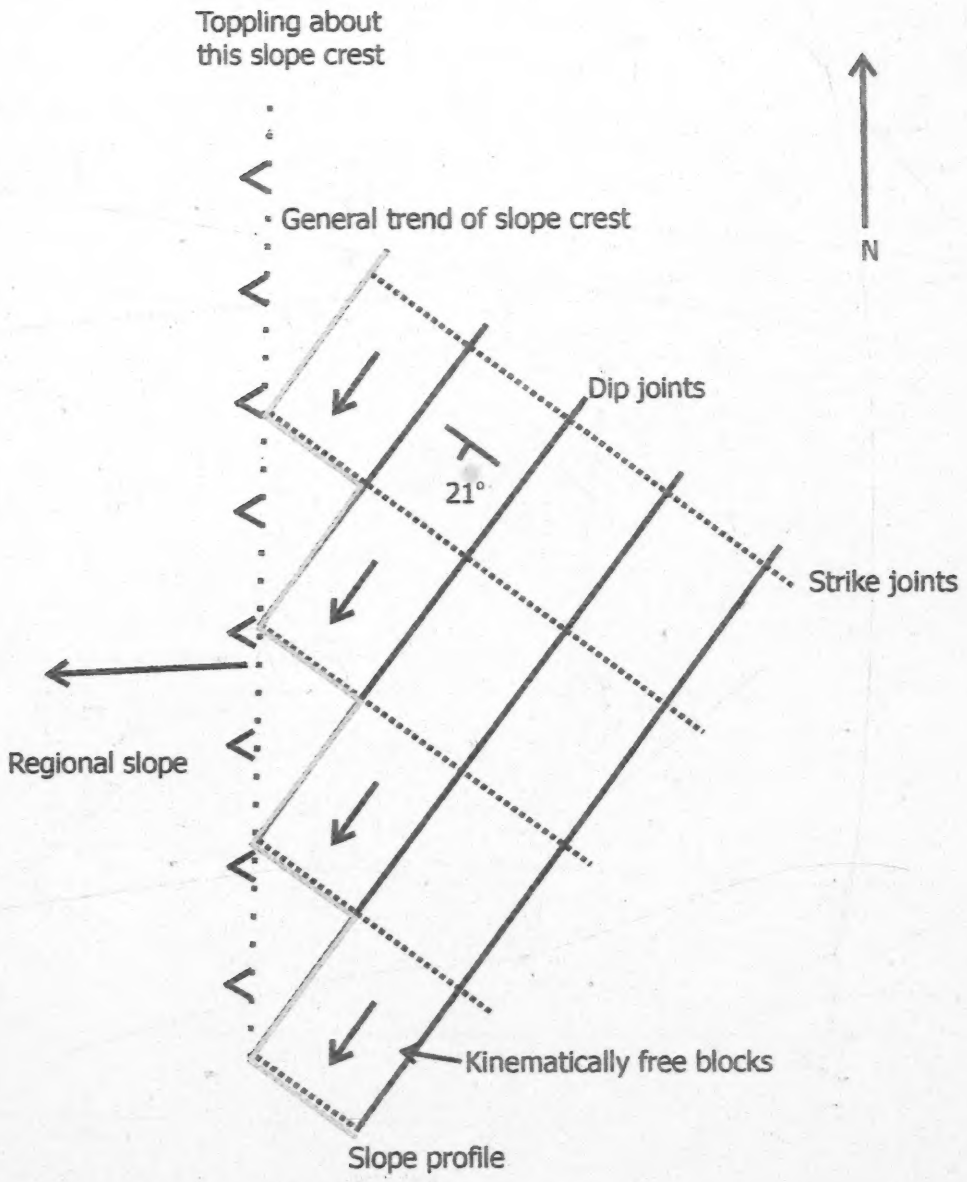

Figure 4.37 – Diagram showing the general trend of the slope break, and the resulting kinematically free blocks.

As the first movements occurred where there was kinematic freedom, it is likely that these blocks subsequently toppled over the slope that was formed during glaciation, and ended up as colluvial materials along the Maligne River, where it emerges onto the Athabasca River flood plain. Subsequent blocks would also have toppled, until a point where the blocks did not have the driving force to slide to the brink of the slope into the Athabasca valley, due to a drop in the driving force. Subsequent to the creation of the graben and the labyrinth, blocks toppled off of the south scarp to infill the depression left in the graben, resulting in the transitional area of the Rock and Boulder Garden.

High pore water pressures would be required to drive the sliding of these blocks on bedding planes that are dipping between 21° and 41°. As shown in Figure 4.22, the site of the Rock and Boulder Gardens lies along the area of the lateral moraines of the Athabasca Glacier where the Maligne Valley is a hanging valley into the Athabasca Valley. As the Maligne Glacier is believed to have retreated before the Athabasca Glacier, abundant meltwater would have been blocked from draining out of the Maligne valley by the Athabasca Glacier (Mountjoy, 1974), resulting in a build up of water in the Maligne valley, and high water pressures along joints and porous beds. In addition, snow would be able to build up in opened joints, and exert a downslope force on the blocks.

The blocks that did not experience sufficient water or snow pressure to slide the entire distance to the break in the slope formed the area of the labyrinth proper. The blocks that make up the labyrinth proper were some of the last blocks to move. There are, however, still a few blocks that have not moved out more than 1 metre from the southeast scarp of the slide. The first of the blocks to slide out of their original positions would have toppled over the break in the slope once the force of gravity exceeded the frictional forces holding the block on the slope. Once water pressures dropped, through the draining of water, the rock slope would not experience the required driving force to move these large blocks to the crest of the west slope, and movement would cease,

leaving the blocks sitting on the sliding surface at a new location, creating the labyrinth.

The area of the downslope colluvium is the result of the toppled blocks that reached the crest of the west slope. Blocks underwent complex topple-sliding and came to rest on this slope, and all the way down into the Maligne River. As karren that are found on the surface of the blocks in this area are developed on the surfaces of the blocks insitu, there has been very little movement of the colluvium after initial deposition. On one block the pitch of the karren indicate rotation, but no other blocks could be found to have undergone movement after the development of erosional karren.

The Maligne River is presently at the toe of the slope, and colluvial materials were found to rest within the Maligne River. Figure 4.20 shows a bend in the Maligne River that occurs where the colluvial material enters into the Maligne River, and a small braided section that occurs immediately downstream of this location.

Movement of the rock within the Rock and Boulder Gardens occurred post-glacially, under periglacial conditions with abundant water and high water pressures. This area is no longer active, with the exception of occasional rock fall from the steep scarp that bounds the south of the graben, and the toppling on the occasional colluvial block on the slope into the Maligne River.

4.6 Conclusions

Several modes of movement on cataclinal slopes are observed in the Colin Range, including toppling, exfoliation and sliding. All of the sites discussed in this chapter are plotted on Figure 4.1, indicating that the modes of movement that occur on cataclinal slopes are controlled by the orientation of the bedding and the slope. Toppling occurs on cataclinal underdip slopes, driven by external forces. When the driving moment of rotation is removed, blocks are left in a rotated orientation, until the disturbing force occurs once again. Exfoliation

occurs on steep dip slopes to steep underdip slopes. The driving mechanism of exfoliation is likely the outward rotation of blocks of rock under the force of water along the bedding planes. Assisted sliding occurs on gentle overdip slopes, as in the case of the Rock and Boulder Gardens. High water pressures were present at the time of movement of the blocks along this slope, and kinematic freedom to move was created by the collapse of a cave system along the south boundary of the feature, and the slope left by the Athabasca Glacier to the west of the feature.

5 Debris Flow Creek

5.1 Introduction

Debris Flow Creek is an informal name for an unnamed creek draining into the Athabasca River at the southern end of the Colin Range. The creek, within the Colin Range north of Maligne River (Figure 5.1), flows intermittently throughout the year. Debris Flow Creek can be approached from the 6th Bridge over the Maligne River, by following the Overlander Trail for 2.75km to the first alluvial gravels within the conifer forest. At this location, leave the trail and follow the alluvial gravels upslope until a graveled area with much less tree cover is encountered. Debris Flow Creek flows at the southern extremity of the gravel area.

Debris Flow Creek was chosen for further study based on the reconnaissance of the Bridgland Repeat Photography Project (Higgs, 2001), as it is an area of current slope movement that can be seen on the repeat photographs. Dougherty (1991) described Debris Flow Creek as follows: "This hike used to be quite straightforward until heavy rain in July 1989 dramatically changed the character of the canyon" (pg 292), giving a time frame for at least one event in the period between photographs. Debris Flow Creek is different from the rest of the slope investigations, as the bedrock geology is much more complex in this area of the Colin Range, leading to different modes of slope movement than those that were explored in Chapters 3 and 4. The alluvial fan of Debris Flow Creek is also much more extensive than the other alluvial fans from the creeks within the Colin Range.

Debris Flow Creek can be divided into 3 parts: the hanging upper valley, the canyon and the alluvial fan (Figure 5.2). The upper valley consists of 4 creeks (Figure 5.1) that join and feed into the canyon, which is cut through the Palliser Formation, similar to Maligne Canyon. Yet the canyon here cuts through the axis of a plunging syncline, with the Palliser Formation forming the resistant

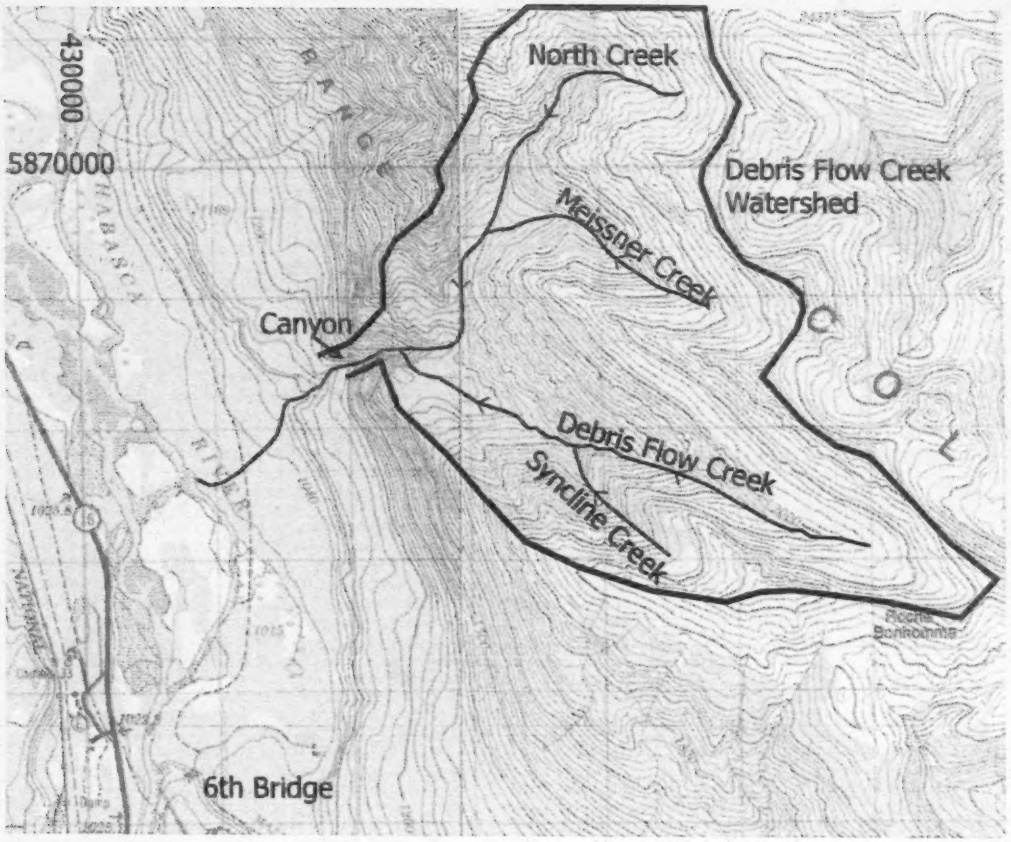

Figure 5.1 – Topographic map showing Debris Flow Creek, and tributaries that feed into the canyon. UTM co-ordinates are given in the northwest corner of the map. Map is at a scale of 1:50000.

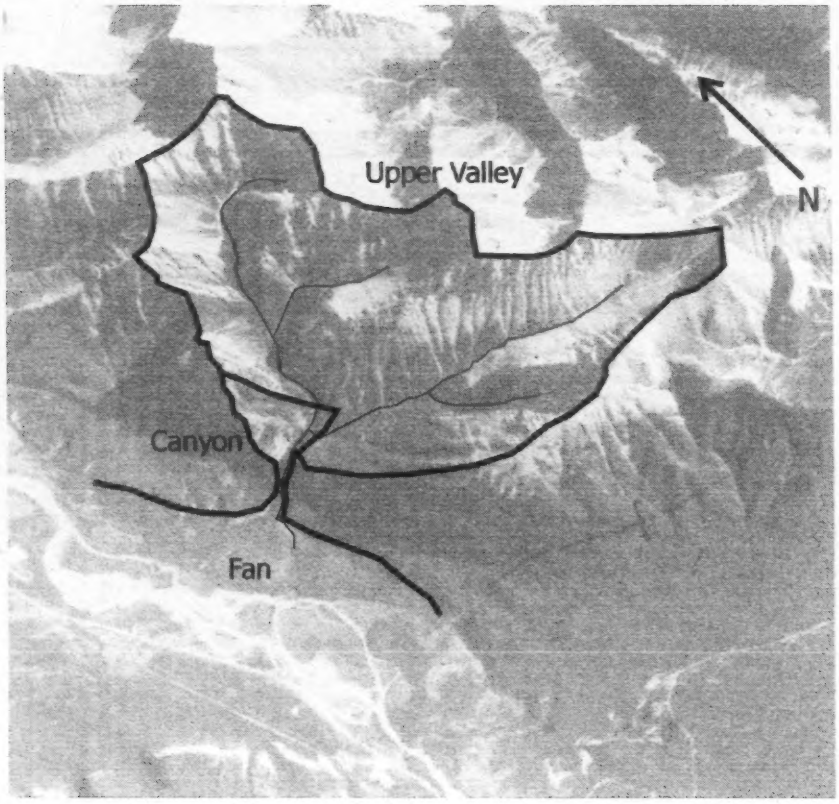

Figure 5.2 – Outline of Debris Flow Creek on airphoto A23015-139, showing the division of the area into the upper valley, the canyon and the fan.

outer edge of the syncline, much different from the Maligne Canyon (Figure 2.2). The alluvial fan at the base of the canyon cuts through the lateral moraine of the late stage Athabasca Glacier (Mountjoy, 1974) and out into the Athabasca Valley.

The bedrock geology is examined in Chapter 5.2 and the structural control of the watershed is explored. A terrain analysis for this area in Chapter 5.3 shows the geomorphology contributes to the slope movements in this watershed. Evidence for past movements from the field is included and changes are documented in order to explore the intermittent slope movements that take place within this portion of the Colin Range. Chapter 5.4 discusses the historical sediments.

Debris Flow Creek is interpreted in Chapters 5.5 and 5.5 as a complex area of intermittent debris flows, with the power to carry blocks up to 3.2m in length. Debris flows are recurrent within this watershed, and pose a potential hazard to any who use this canyon for recreational purposes, especially in times of heavy rain or snow melt, around the month of June.

5.2 Bedrock Geology

The structural geology in the area of Debris Flow Creek is more complex than the regular homoclinal thrust sheet structure of the rest of the Colin Range (Figure 5.3). North Creek originates on the Triassic Sulphur Mountain Formation within the Colin Thrust Sheet, and then crosses onto the Chetamon Thrust Sheet, where the creek cuts up the stratigraphic section, beginning in the Cambrian Lynx Formation, to the Devonian Palliser Formation (Figure 5.3) (Mountjoy and Price, 1976). Debris Flow Creek originates along the boundary of the Banff and Palliser Formations, and flows within the Banff Formation to the Devonian Palliser Formation, where the tributary enters the creek within the canyon. Meissner Creek and Syncline Creek also feed into the canyon at this location. Three minor thrust faults are present within the watershed of Debris Flow Creek (Figure 5.3).

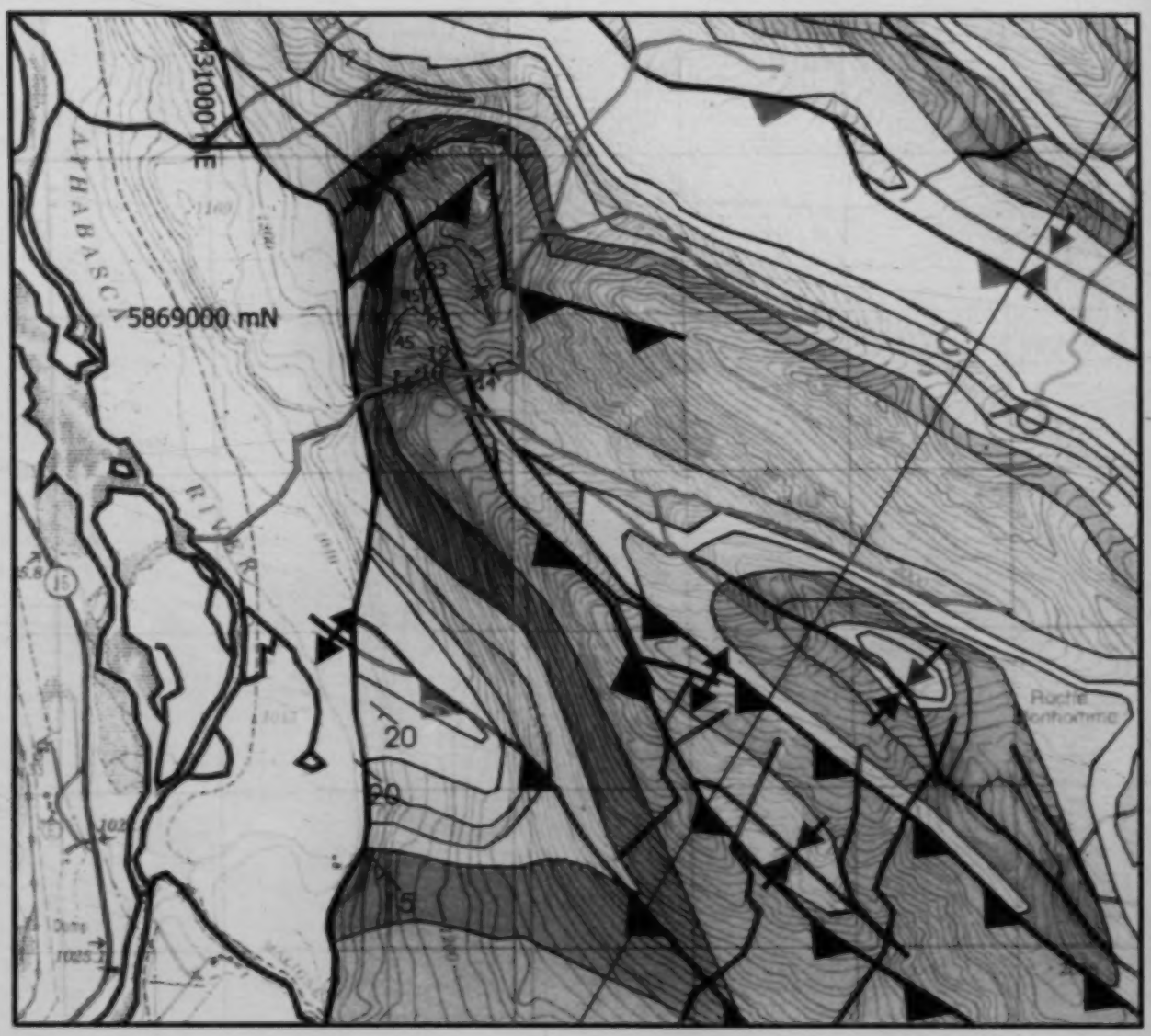

Figure 5.3 – Portion of Figure 2.3 enlarged to show the area of Debris Flow Creek. The outline of the bowl shaped feature on the north side of the creek is shown with some bedding orientations. The locations of Figures 5.10-5.12 are shown on the map. Data from Mountjoy and Price (1976) and Mountjoy and Price (1985).

Mountjoy and Price (1976, 1985) indicated that the Palliser Formation is thicker at this location due repetition by 2 thrust faults (Figures 2.2 and 5.3). In addition, as this is the axis of a syncline, the Palliser Formation is wider, due to the low angle of dip in the hinge of the fold (Figure 5.3). The bedrock is jointed, and the joints in the vicinity of Debris Flow Creek are open.

A bowl is created by the syncline (Figure 5.4) which has a hinge orientation of 12°/169°. An analysis of the orientation of the bedding and the north slope of the canyon using DIPS (Hoek and Diederichs, 1989) indicates that the sliding of wedges is unlikely on rocks with a friction angle of 30°; sliding is possible along the fold axis, with the added driving forces of water pressures. The situation that is set up is that of an orthoclinal slope, as discussed in Chapter 3. While initial movement is in the dip direction, on cataclinal overdip slopes that were created by glaciation, the plunging axis of the syncline creates the situation of an orthoclinal wedge, as discussed in Chapters 3.2.2 and 3.3.2, as the axis of the syncline is plunging in a direction perpendicular to the slope of the north wall of the canyon (Figure 5.4). Chapter 2 shows that the movement on wedges on an orthoclinal slope is kinematically possible, and, therefore, the sliding or toppling of these wedges is possible along the fold axis into the canyon of Debris Flow Creek.

There is evidence for past movements along the synclinal axis north of the canyon, and in the canyon. The fold hinge is bounded to the east by rocks dipping 35° toward 212°; rocks that dip toward the east define the west boundary of the fold. The dips of the east-dipping rocks vary from 23° near the north end up to 75° at the south of this feature. Further south along the west boundary of this feature the dip changes to 45° toward 100° (Figure 5.3). At the top of the canyon, the Palliser Formation bedrock is exposed, dipping 14° toward 227° with open joints (Figure 5.5).

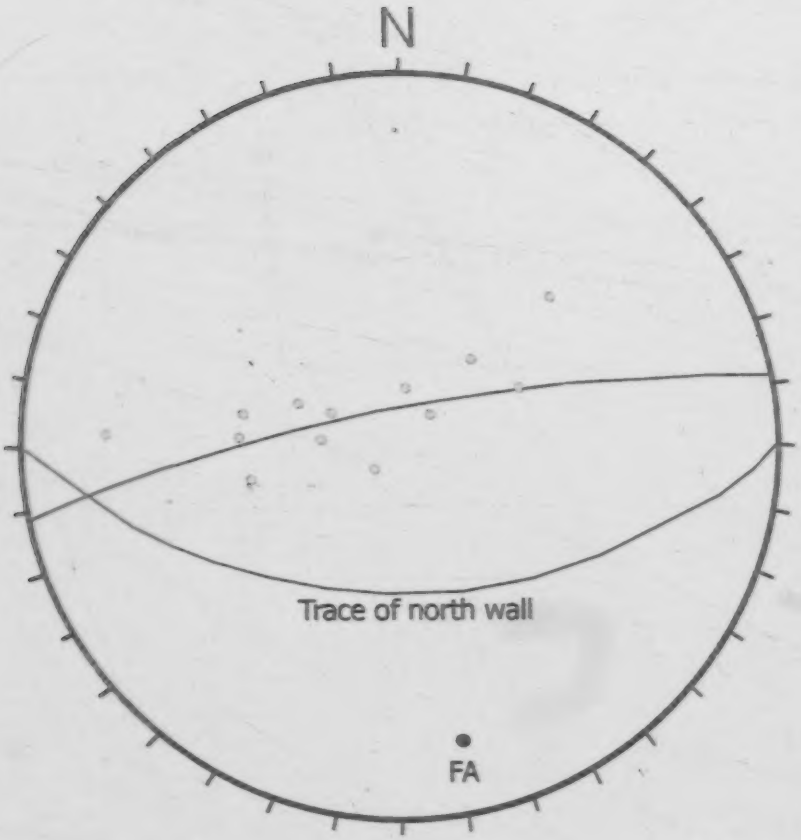

Figure 5.4 – Equal angle, lower hemisphere stereogram of the poles to bedding in the vicinity of the syncline, and the fold axis. The fold axis has an orientation of 12°/169°.

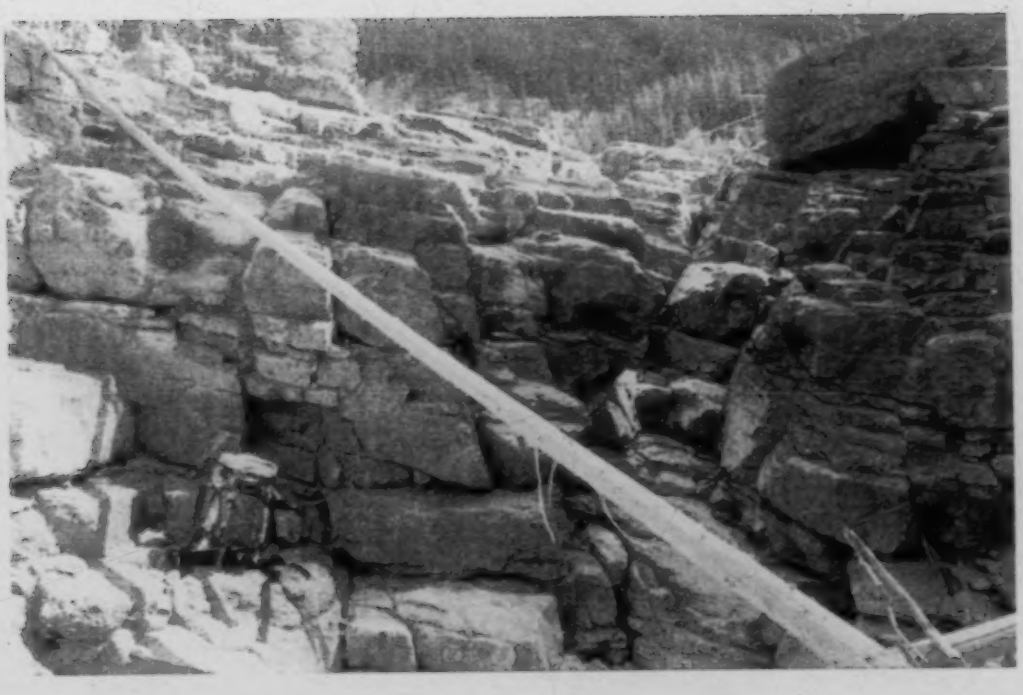

Figure 5.5 – Photograph of the bedrock at the top of the canyon. Note that the beds are gently dipping, with open joints.

5.3 Terrain Analysis

The surficial geology of Debris Flow Creek is more complex than the surficial geology of the rest of the Colin Range (Figure 5.6). An alluvial fan is present where the creek enters the Athabasca River floodplain after it cuts through the lateral moraine of the Athabasca Glacier (Bayrock and Reimchen, 1976). Upstream, the creek cuts through colluvial materials on its north side, while the south side of the creek is confined in bedrock (Figure 5.6). On the south side of the creek, the upper portion of Debris Flow Creek enters into the main creek where fluvial deposits overlie glacial material (Figure 5.7), sitting on top of open jointed bedrock. All of the tributary valleys upstream of the canyon are confined in bedrock valleys, which are subject to avalanching, and are flanked by talus slopes (Figure 5.6). Alluvial gravels, or sediments derived from eroded till, line the beds of the creeks in the upper valleys.

Along the hinge of the syncline (Figure 5.8), large blocks of the Palliser Formation limestone are scattered in differing orientations (Figure 5.9). In-place rock was not observed within the depression. Trees grow along the outside boundary of the depression, yet trees were not observed to be growing in the centre of the depression. The blocks are angular, with little to no rounding. The surfaces of the boulders are covered with well-developed karren (Figure 5.9). This area is shown on Figures 5.6 and 5.8 as $C^{l}b$, and is interpreted to be a relict landslide.

Blocks around the boundary of the depression are larger, with less variation in size. The blocks within the centre of the depression are more thinly bedded than the Palliser Formation at other locations. The blocks on the east side of the depression vary in bedding thickness from a few centimetres up to 20 centimetres. The blocks in the west part of the depression are more thickly bedded, with bedding thicknesses up to 1 m.

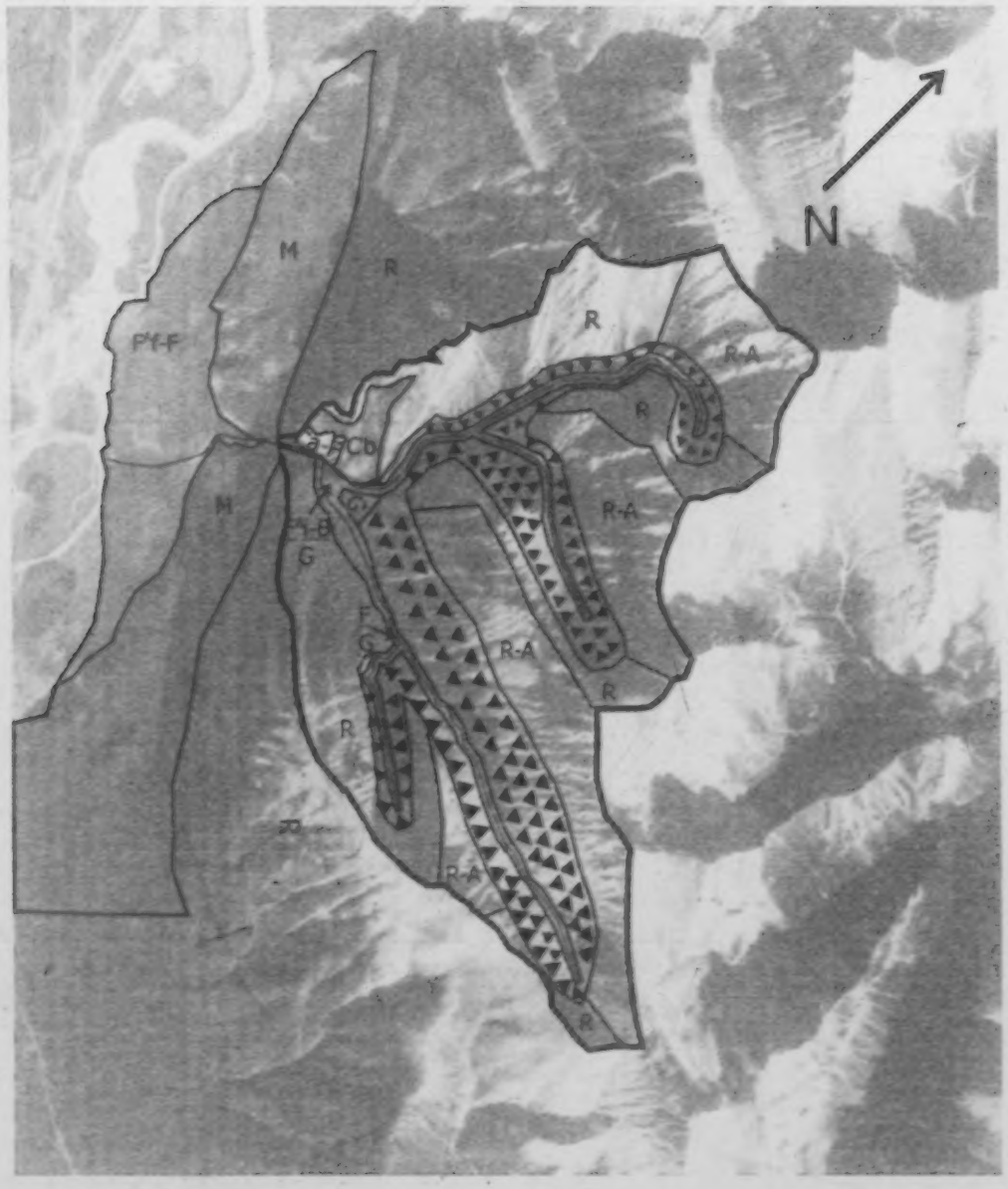

Figure 5.6 – Terrain analysis of Debris Flow Creek on airphoto A23015-139. Terminology follows that of Cruden and Thomson (1987) with triangles indicating talus slopes.

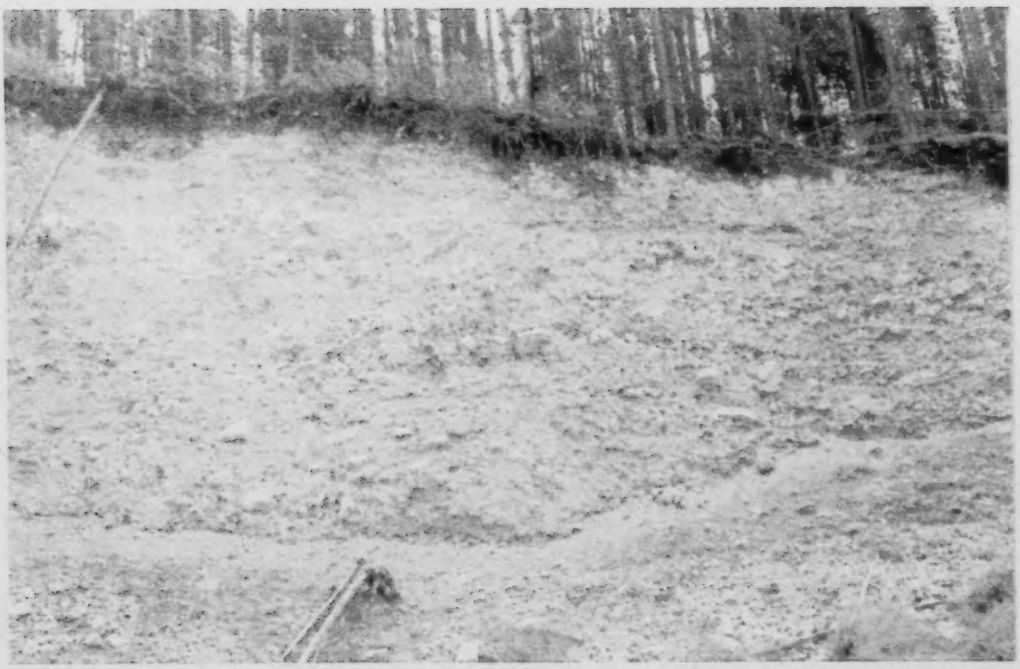

Figure 5.7 – Till deposits within the upper canyon, at the location where the large U-shaped valley meets with the main creek, near the top of the canyon.

Figure 5.8 – Oblique photograph showing the location of the syncline adjacent to Debris Flow Creek. Photograph number 460 by M.P. Bridgland. The locations of Figures 5.9, 5.15 and 5.16 are shown, along with the different terrain units to the north of the creek.

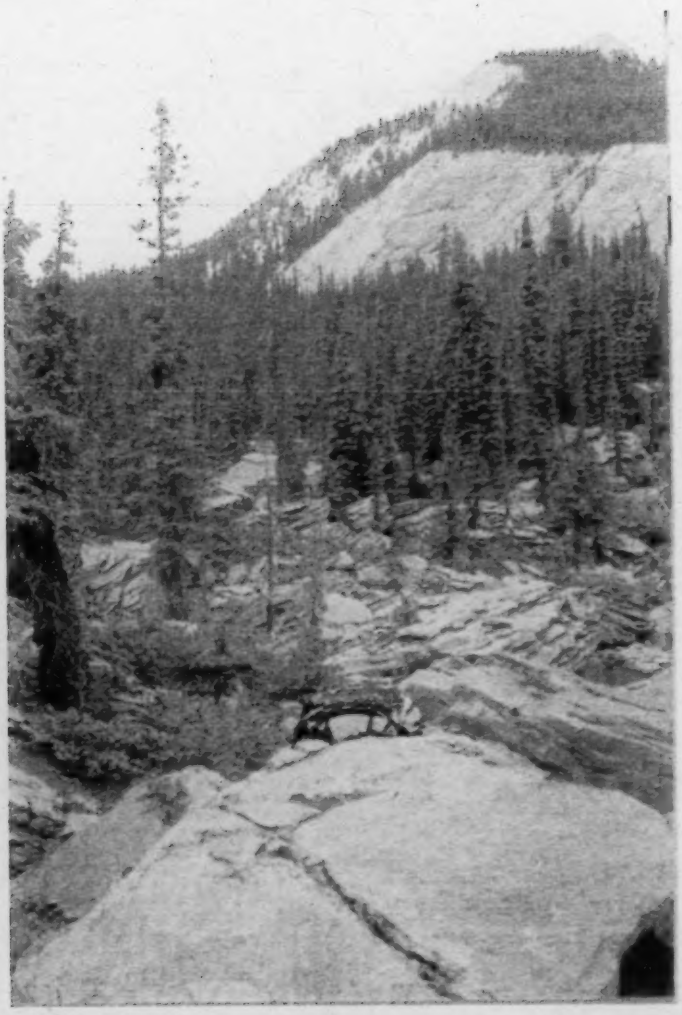

Figure 5.9 – Photograph of an area of large displaced boulders. Location of this photograph is on the east side of the syncline at the base of the cataclinal overdip slope (Figure 2.8). Karren are present on the surface of the boulders, and can be seen on the boulder in the foreground. Pack is used for scale.

The north wall of the canyon is shown on Figure 5.8 as Ca-F. Where in-place bedrock is observed within this region, it is broken, with open, closely spaced joints (Figure 5.10), and is Devonian Palliser Formation rock. The colluvium is composed of Palliser Formation, and the block size ranges from sand sized grains up to 3m by 6m by 10m (Figure 5.11). The colluvium is cemented by calcite on the surface and forms slopes greater than the angle of repose. The slight cementation is from secondary deposition of dissolved calcite from the surrounding carbonates; the solution of the surrounding carbonates is evident by the presence of karren on the surface of the rocks. The colluvium has formed as an apron over bedrock at this location, also contributing to the steep angle of slope of this material, as the bedrock slope controls the angle of slope.

Vegetation is more prevalent in the inactive colluvium than in the actively failing colluvium. Where vegetation is present, conifer trees of a much smaller size grow as isolated trees, and some juniper bushes are present (Figure 5.12). The blocks of colluvial material within the inactive colluvium are much larger than that in the failing colluvium, where fine-grained materials are present. The area Ca-F forms a lobate deposit encroaching on the present creek bed. Where the lobe occurs, fine-grained material dominates the deposit, with the inclusion of blocks up to 1m. On windy and still days, rockfall could be heard occurring within the canyon.

Scattered erratics of Gog Quartzite are found with the colluvial deposits, indicating that the Athabasca Glacier overrode this area at some point (Clague, 1989). Rocks from units from the Mississippian Banff Formation up to the Triassic Sulphur Mountain Formation outcropped along the hinge of the syncline prior to glaciation (Figure 2.4). Figure 5.13 shows the location of cirques within the watershed, and the inferred direction of the flow of ice. The cirques head within the weaker formations; the cirque within Syncline Creek heads within the Turner Valley and Shunda Formations, Debris Flow Creek has a cirque that heads within the Banff Formation, the cirque within Meissner Creek heads in the Mount Hawk Formation, and the cirque in North Creek heads in the Sulphur Mountain

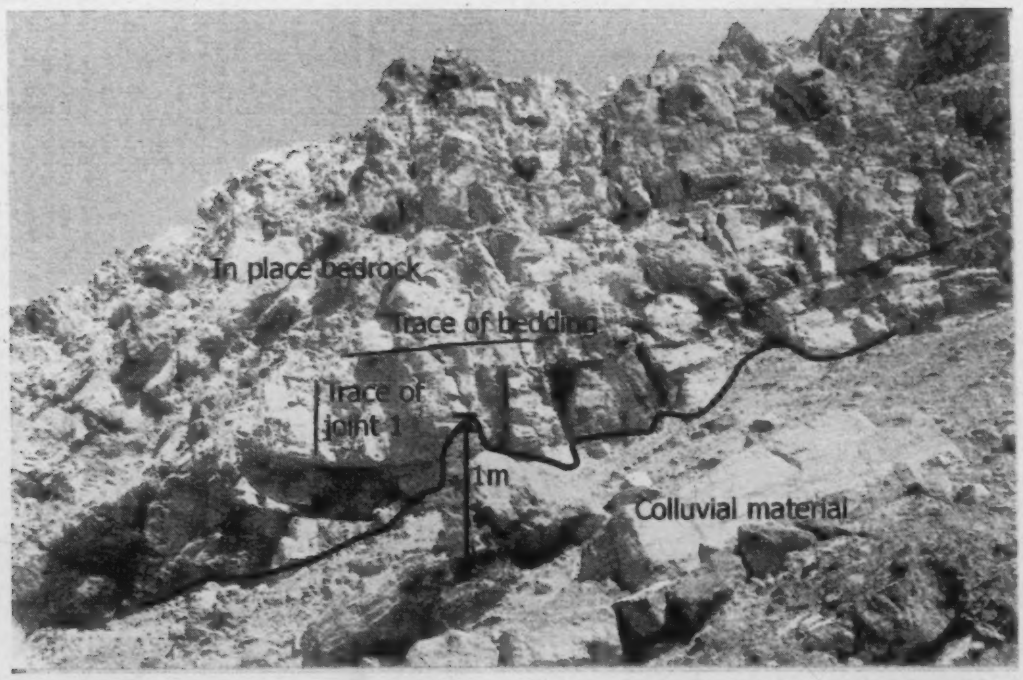

Figure 5.10 – Jointed bedrock of the Palliser Formation within the canyon of Debris Flow Creek. The trace of the bedding and the trace of joint 1 are shown on the photograph. The line in the photograph is the boundary between the colluvial material and the in place bedrock.

Figure 5.11 – Photograph of the north wall of the canyon, showing the colluvium that composes this wall. Notice the angular nature of the material, as well as the distribution of grain sizes. View is from the creek bed looking NE. The goat is for scale.

Figure 5.12 – The north slope of the canyon showing the difference in vegetation between the active and the inactive colluvium. Photograph is taken from the creek bed looking west, near the axis of the syncline.

Figure 5.13 – Enlargement of air photograph A23015-139, showing the location of the heads of the cirques within the watershed of Debris Flow Creek, and the corresponding direction of ice flow. The headwalls of the cirques are orthoclinal slopes, and are indicated by the black lines, with the hatch marks indicating the direction of the slopes.

Formation. All of the cirques face west, and their orientations are controlled by preglacial drainage. Post-glacially, drainage has been reestablished within the glacially enlarged pre-glacial drainages, which were left as hanging valleys into the Athabasca Valley.

As drainage was reestablished postglacially, the creek cut down to the level of the Athabasca River. With glacial retreat, oversteepened slopes were left, which then slid to produce colluvial material (Figure 5.14). The creek cut through colluvium, till and jointed bedrock to form the canyon. As the canyon was cut through the synclinal axis, blocks were kinematically free to slide along the plunging fold axis of the syncline (Figure 5.4), producing more colluvium on the north side of the canyon, and the lack of colluvium on the south side of the canyon. These newly created slopes underwent mass wasting, resulting in the lobate form of the colluvium in the canyon; the finer grained material results from the break-up of the larger blocks involved in the secondary movement. Later water erosion moved the fine-grained fraction of the deposit, and then subsequently re-deposited it down-stream.

The slope-movements that occurred at this location are interpreted to have begun soon after deglaciation of the area, based on the lack of older karren that did not form in the current orientation. In addition, the oversteepened slopes that were left when the glacier retreated would not be stable for long without the support of the ice, resulting in the sliding of the slopes soon after the retreat. The cataclinal overdip slopes have, for the most part, been exhausted.

5.4 Historic Sediments

Several of the larger boulders within the canyon have striations on the surface that are oriented roughly east-west (along the length of the canyon) (Figure 5.15). Water was observed to be flowing along a preferred path within

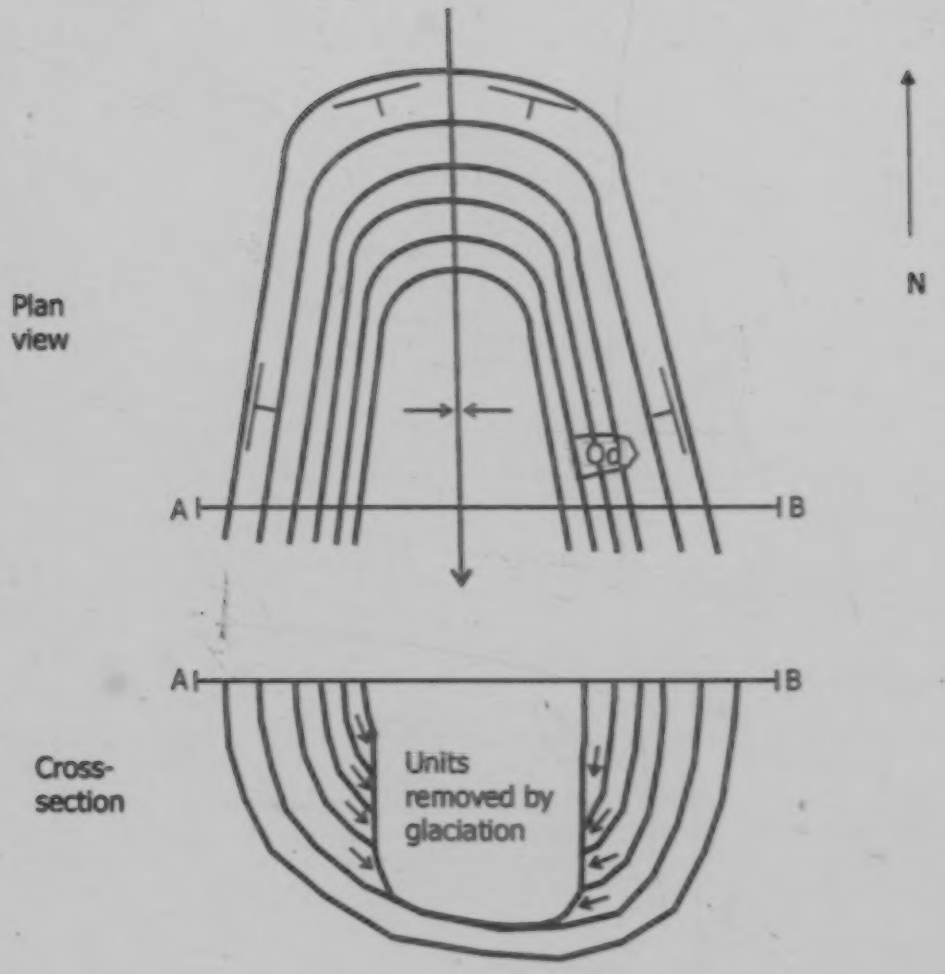

Figure 5.14 – Diagram showing one possible source of the colluvial material present to the north of the canyon. The colluvial material is produced after glacial retreat by the sliding of rock along bedding planes on oversteepened slopes. Only one cataclinal overdip slope remains in this area. Diagram is not to scale, and the cross-section is vertically exaggerated.

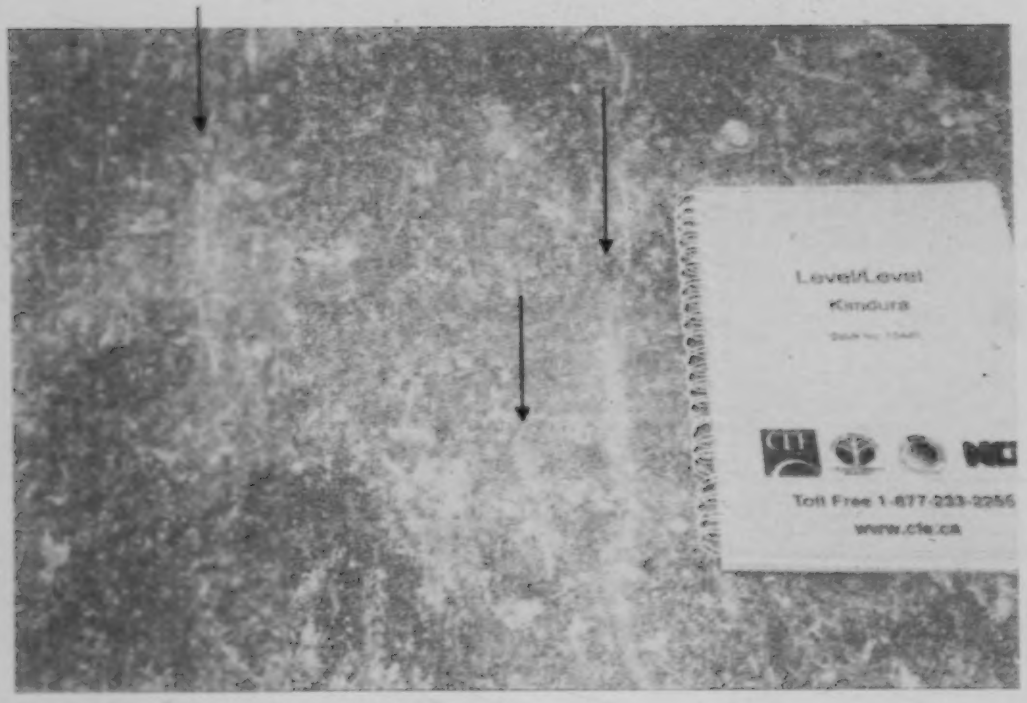

Figure 5.15 – Photograph of striations on a boulder of Palliser Formation limestone within the canyon of Debris Flow Creek. The arrows point out some of the striations, and indicate the direction of flow.

the canyon for 2 days after a snow fall, when temperatures rose, but the canyon was dry throughout the remainder of the study.

Within the upper valley, fluvial sediments are well-sorted, coarse-grained, with little to no fines, consisting of carbonates and quartzites that are sub-rounded to rounded. Vegetation is not common, and where vegetation is present, it is in the form of small conifer trees (Figure 5.16). Tree trunks and branches were observed at several locations, lying strewn on the sediments. On the south side of the creek bed, a 2m high wall of till is exposed, where it has been eroded by fluvial processes (Figure 5.7). Water was not observed to be flowing within this section during the study.

Along Debris Flow Creek, the sediments consist of till overlain by fluvial sediments. These sediments may be from fluvial transport and deposition of material from up valley, or removal of fines from the till, resulting in a boulder pavement in the creek (Figure5.16). Talus is common in this valley, from rock fall and avalanches along the steep slopes flanking the valley.

The third area of Debris Flow Creek is the fan at the base of the creek (Figure 5.17). A creek flows on the fan, originating from springs located among the trees on the south side of the unvegetated area of sediments (Figure 5.18). The creek disappears into the sediments 500-600m downstream of where the springs emerge. The sources of these springs may be either a karst system within the bedrock of the Palliser Formation, or the water that flows along the sediment-bedrock contact, and emerges at this point on the fan, as the bedrock is near surface.

The sediment varies from well-sorted in places, to poorly sorted at other locations across the fan. The majority of this area is composed of sub-rounded to well-rounded grains that range in size from fine-grained sand up to boulders of Palliser Formation rocks.

Vegetation varies greatly over the area of the fan. As seen in Figure 5.17, there are three vegetation zones present within the fan area. The first type of vegetation, Zone 1, is Douglas Fir. Douglas Fir are common along the outer

Figure 5.16 – Photograph of the sediments in the upper valley, taken from the location of Figure 6.15, at the top of the canyon, where the upper valley starts. Notice the rounding, and the well sorted nature of the sediments. Photograph is taken from the narrow top of the canyon, looking upstream to the east.

Figure 5.17 – Photograph of the fan of Debris Flow Creek. Vegetation Zone 1 is dominated by coniferous trees, Zone 2 is mixed coniferous and deciduous trees and Zone 3 is mostly unvegetated, with Poplar trees making up the majority of the vegetation. The location where the creek changes flow direction around the till is shown with a white dot.

Figure 5.18 – Location of the spring system on the alluvial fan, showing the spring and the regularly flowing stream at the base of the till in white. The intermittent stream location is shown in black where the two creeks meet. The inset is a photograph of one of the springs.

edge of the area and on the lateral moraine, but not as common in the area of the coarse-grained sediments. Douglas Fir do not survive in areas that are subject to flooding, as they can not adapt well to changing water levels, indicating that Zone 1 has a stable soil moisture regime, with no periods of flooding. Poplar trees are common among the sediments, mixed with some Douglas Fir in Zone 2. Adjacent to the creek, the roots of some of the poplars are exposed above ground surface (Figure 5.19). Poplar trees are able to adapt to flood waters and sedimentation by growing new roots at the new ground level. When the sediments are then stripped off the surface by erosion, the roots of the tree are exposed, and the tree then dies. The erosion of the sediments also erodes the trunk of the tree, making the diameter of the tree smaller where organic material has been eroded. In Zone 3, vegetation is either non-existent or is dominated by Poplar trees with coniferous trees uncommon, except for those less than 0.5 m tall. Vegetation on the alluvial fan has changed drastically over the time period between 1915 and 1999, as documented by the Bridgland Repeat photographs, discussed further in Chapter 6. In places, trees have toppled over and lie across the bed of the current creek. At location UTM 11U 0431463 5867982 several coniferous trees have fallen over, across an area of excavated sediments. Also at this location, rocks and dead wood were observed piled up against a Douglas Fir tree trunk (Figure 5.20).

To the north of the creek bed, terraces of sediments 2-3m wide and 30-50cm high are present. The surface of the terrace is generally flat, with a slight slope down fan. The south side of the creek is bounded by southeasterly dipping sandstone of the Devonian Sassenach Formation, which is being undercut and sliding along kathetal joints into the creek.

One other feature of interest, seen on Figure 5.17, is where the current creek cuts the base of the lateral moraine left by the Athabasca Glacier (Mountjoy, 1974). At this location, the creek changes flow directions from westerly to southerly and is incised 2m into the fan. The creek flows underneath the northern extension of the till (Figure 5.21), and has cut a

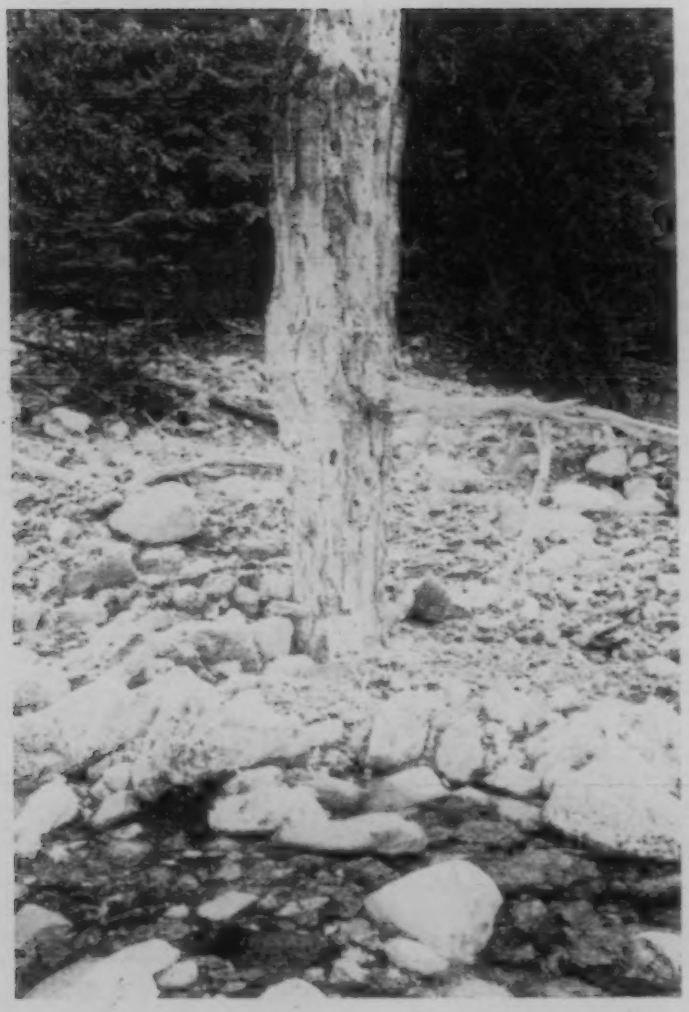

Figure 5.19 – A poplar tree showing roots that are exposed above the surface of the ground. The location of the photograph is in the fan area, downstream from the glacial till deposits.

Figure 5.20 – Several trees that have recently been knocked over, and the accumulation of debris on the upstream side of a tree trunk on the alluvial fan. The presence of needles on the fallen tree indicate that this event is no older than 2-3 years old.

Figure 5.21 – The current creek flowing underneath the edge of the till, a few metres upstream from the 90 degree turn of the creek. The creek has cut roughly 1 m into the unit.

notch roughly 1 m into the till deposit, and tension cracks are forming in the till deposits above this spot (Figure 5.22).

At the apex of the fan, located at UTM 11U 0431900 5868532, the creek divides into 2 channels that are separated by a stand of coniferous trees. The channel that forms on the north side contains little to no vegetation and can be seen on the air photos, while the channel to the south has more vegetation present, and is 2m higher than the north channel. Downstream from the head of the fan, the south channel becomes tree covered until it reemerges at a spring within the tree cover. The two channels merge 10-15m upstream of the creek's 90° turn around the edge of the till.

At the apex, a deposit of boulders was observed 1-2m above the material of the south creek bed. The deposit is 56m in length and trends 260° for the first 24m, and then changes direction at a stand of trees to trend 206° along the remainder of the deposit. The deposit contains organic debris throughout, including dead tree trunks. Several trees were knocked down at the downstream end of the deposit, and the tree trunks that remain are oriented roughly 206°-026° (Figure 5.23).

The majority of the sediments found within this deposit are blocks of Palliser Formation, with some clasts of Gog Group Quartzite. The blocks are angular to sub-angular, and range in size from sand sized particles up to 3.2m long. The larger blocks that are present within the deposit have long axes that are oriented in the same direction as the orientation of the deposit, with flat surfaces that dip in the downstream direction (Figure 5.24).

Vegetation is not common within the area of the deposit, while immature vegetation, 10-15 years old, is present south of the deposit. The vegetation that occurs there is grasses and small deciduous plants (Figure 5.25).

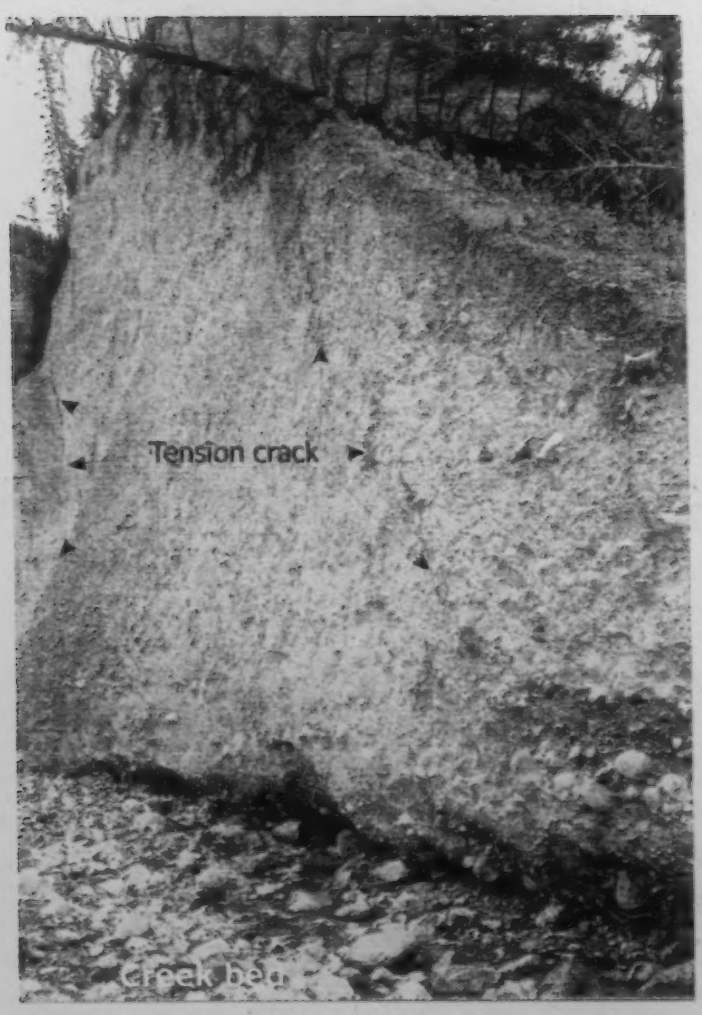

Figure 5.22 – Cracks in the till above where the creek is undercutting the till.

Figure 5.23 – Dead trees in front of a large boulder at the downstream extent of the deposit. The boulder on the left side of the photograph is 175cm long. Photograph is taken in a direction perpendicular to the inferred flow direction.

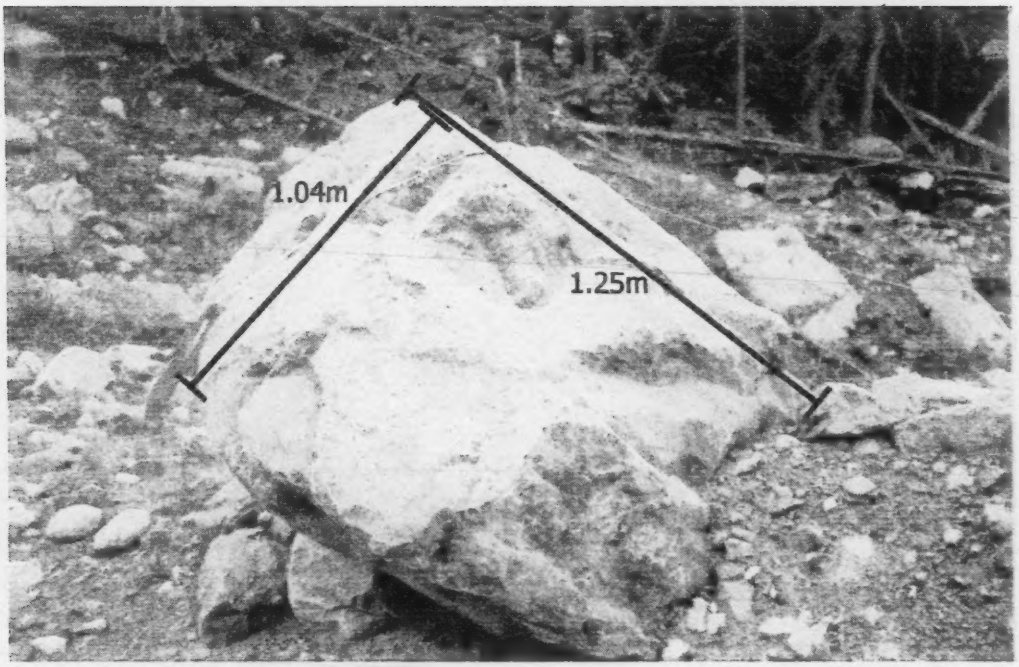

Figure 5.24 – Photograph of the large boulder at the head of the deposit. The boulder is oriented with its long axis in the downstream direction, with the upper surface of the boulder dipping in the downstream direction.

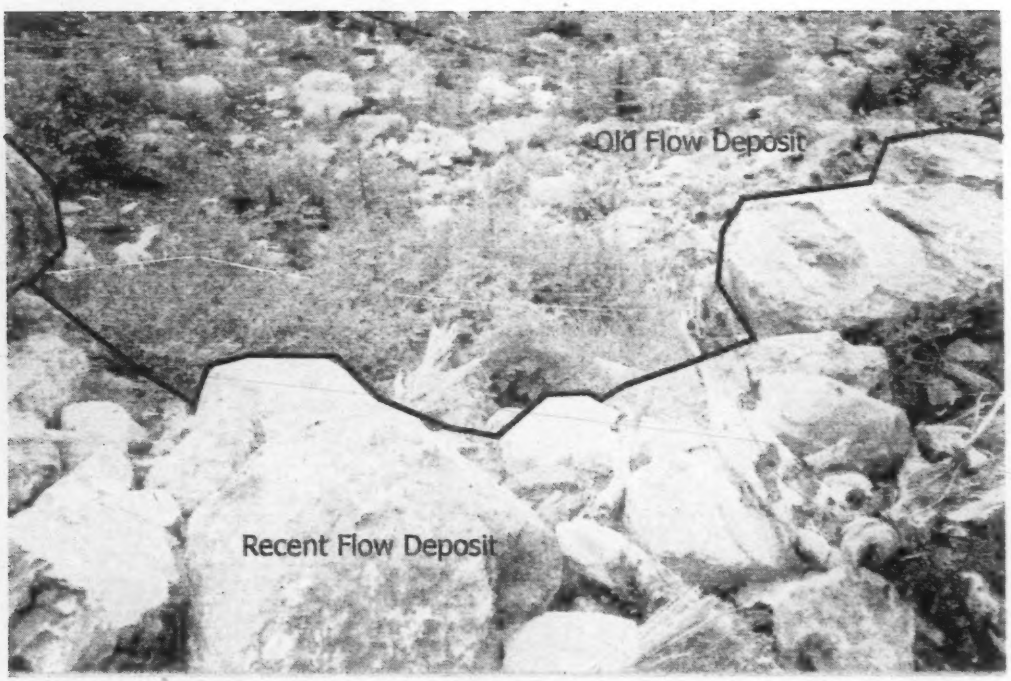

Figure 5.25 – Photograph of vegetation adjacent to the deposit. The thick black line shows the boundary of the deposit. Vegetation is likely 10-15 years old. The tape measure in the photograph is 1.2cm wide.

5.5 Current Debris Movement in Debris Flow Creek

Debris Flow Creek is an area of active stream erosion. Within the upper valley, at periods of snow melt or high rain fall, stream erosion takes place. Periods of high flow, in the creek have transported tree trunks and other debris (Figure 5.16). One hazard from this stream is the erosion of the till and talus within the tributary hanging valley. The sediment charged flow then enters directly into the canyon.

Within the canyon of Debris Flow Creek, water was observed to be flowing at least once during the summer months. Based on the presence of striations on the surface of boulders within the canyon (Figure 5.15), and the presence of rounded sediments within the canyon, water erosion occurs at times of peak flow of the creek. The water flowing through the canyon erodes the colluvial material that forms the north side of the canyon, resulting in unstable colluvial slopes, and further mass wasting of the material on this slope. Melting of snow in the spring and high precipitation lead to flows of water within Debris Flow Creek. As a result, the water level within the colluvial deposits rises, making mass wasting more likely.

Stream erosion is currently occurring on the alluvial fan. This can be interpreted from the exposure of the roots of the poplar trees adjacent to the current creek bed (Figure 5.19). The presence of terraces adjacent to the current stream, and in other locations on the fan, shows this is an active alluvial fan, with both deposition and erosion taking place.

Where the creek cuts through the lateral moraine of the Athabasca Valley glacier water is eroding the till. The till is cemented, as the hoodoos on the north side of the fan and the high, steep slope of the unit show. Erosion is undercutting the till cliff and tension cracks are forming (Figure 5.22). Where the creek passes by the toe of the outcrop of the Devonian Sassenach Formation, the creek is actively eroding the toe of the slope, leading to sliding of

blocks of sandstone on kathetal joints. These blocks of sandstone are then deposited within the current creek bed.

During periods of high flow on the fan, torrential waters erode into the sediments of the fan, as the deep unvegetated channels show. In addition, boulders are piled on the upstream side of tree trunks, along with branches and other debris (Figure 5.20). An obstruction in the flow of the torrential waters, for example a tree, would lead to the eddying of the water, and the subsequent deposition of boulders and debris carried along with the flow of water on the alluvial fan.

The deposit at the head of the fan is a flow deposit, either from an avalanche, a slush avalanche or a debris flow. Based on the size of the boulders that are a part of the deposit, a driving force is needed to transport these boulders from their original location. In addition, the trees lying at the down fan extent of the deposit have been knocked over by a blow, a flow coming out of the canyon of the creek, and running onto the fan. The trees arrested the flow. The lack of vegetation in the vicinity of the deposit suggests that this flow occurred within the last 10-15 years, not allowing time for the regeneration of vegetation at this location.

Observations over the alluvial fan suggest that debris flows occur here intermittently. There are several deposits within the area of the fan that show similar characteristics to the deposit described above, with differing recoveries of vegetation present. The deposits at this location can be attributed to a debris flow as greater than 50% of the particles are greater than sand size (Bates and Jackson, 1984).

5.6 Conclusions

The canyon of Debris Flow Creek is cut through the Devonian Palliser Formation, and cuts the axis of the gently plunging syncline that occurs at this location. The north wall of the canyon cuts through the area of extensive

colluvial deposit, perpendicular to the regional strike of the bedrock. This creates the kinematic freedom for blocks of rock to slide along the synclinal axis as wedges on an orthoclinal slope. The south wall of the canyon is intact bedrock of the Devonian Palliser Formation that forms a steep (roughly 80°) slope into the canyon, and the axis of the syncline is visible in the wall.

The surficial geology in this area is dominated by glacial till, colluvium and fluvial deposits. Glacial till is present throughout the area, in the hanging valley and its tributaries, as well as in the lateral moraine that is present at the base of the bedrock slope, where the creek enters into the Athabasca Valley. Colluvium is present in the form of talus along all of the upper valleys, as well as in the centre of the syncline, where slopes were actively moving post-glacially. Fluvial deposits line the bottom of the upper valleys, and are present on the alluvial fan of the watershed.

Flows occur intermittently within Debris Flow Creek, and may originate in one of three locations, the upper hanging valley, the canyon, or the point where the fan emerges from the till. In addition, a debris flow may originate without a damming mechanism, at times of high rain fall and snow melt Within the hanging glacial valley, there are abundant till and fluvial deposits, along with talus from avalanches and rock fall along the slopes that flank the valley. While water was not observed to be flowing in this valley during the summer of 2002, water flows through this valley during times of high precipitation and snowmelt. Water flow can be obstructed by run-out from avalanches and rock fall, leading to the build-up of pressures behind the obstruction, resulting in the catastrophic flow of materials once the upstream pressures exceed the resistance of the obstruction.

Another possible mechanism for the occurrence of intermittent debris flows at this location is blocking of the creek upstream, within the canyon by mass wasting of the colluvial materials on the north side. Within the watershed, at times of high snowmelt or high precipitation, the creek within the canyon contains flowing water. If this creek becomes blocked within the canyon, water

pressures are able to build up behind the blocked section, causing the water table within the colluvium to rise, increasing the possibility of reactivation of this material. Once pressure upstream of the obstruction has built up, with the addition of both water and sediment, the dam breaks, releasing the very dense flow. This flows downstream at high velocities, until stopped, either on the fan by run out, or else by an obstacle in the path of the flow. This mechanism of formation of debris flows may explain the deposits at the apex of the fan.

Another possible explanation for the erosion that occurs further down stream on the fan, and was evidenced by the recently knocked over trees, is the undercutting of the glacial till. Active erosion into the till on the alluvial fan has resulted in the formation of tension cracks on the face of the till unit. When tensional forces overcome the resisting forces on the face of the till cliff, blocks of till fall into the creek bed, blocking the flow of the creek. Water pressures then build up, until either the obstruction is overcome, or else the channel avulses, creating a new channel. In either circumstance, the damming up of flows would lead to high flow velocities upon overcoming of the obstacle, enabling the water to erode the sediments and the trees in its path.

The north wall of the canyon and the open area on the fan, Zone 3, are hazardous at times of snow melt or intense or prolonged rainfall. Zone 2 on the fan may be hazardous in more exceptional meteorological conditions, as this area is on the historic flood plain of Debris Flow Creek.

6 The Use of Repeat Photography in the Analysis of Landslide Hazards

6.1 Introduction

Surveyors such as M.P. Bridgland and David Thompson conducted much early mapping in the mountainous regions of Canada. They went into places with no maps, and created the early maps of areas that are now widely available for our use. They used several different tools in creating the early maps of these areas, the most important being photographic surveying, as discussed by Bridgland (1924).

M.P. Bridgland was a surveyor for the Dominion Lands Survey, and in 1915 he undertook the task of creating the first topographic map of Jasper National Park, created as a forest reserve in 1907 (Parks Canada, 2000). Bridgland took a total of 735 photographs in his survey in 1915 (Higgs, 2001). In 1998 and 1999 Higgs and Rhemtulla of the University of Alberta repeated all 735 photographs that were taken by Bridgland (Higgs, 2001).

This chapter considers the usefulness of photography from the Bridgland Repeat Photography Project in the assessment of landslide hazards, where a hazard is defined as "a condition with the potential for causing an undesirable consequence" (IUGS Working Group, 1997). This analysis is expanded to other repeat photography projects that may be available, either at the current time or in the future.

The usefulness of these photos is discussed in Chapter 6.2 for types of slope movement that have been documented from the ground, and have been discussed in Chapters 3, 4 and 5, focusing on toppling, exfoliation and debris flow movements. The repeat photographs are available in digital form on the Bridgland Repeat Photography website at bridgland.sunsite.ualberta.ca. Chapter 6.3 discusses the history of photographic surveys in Canada, and the past use of repeat photography in analysis of landform change. Chapter 6.4 discusses the

technical aspects of the photographs. A summary and conclusions on the usefulness of repeat photography projects is presented in Chapter 6.5.

6.2 Recent Slope Movements and the Photos

Modes of movement observed in the area are discussed in Chapters 3, 4 and 5. The modes of movement that are used to determine the usefulness of the photos in this chapter are toppling on orthoclinal, cataclinal and anaclinal slopes, exfoliation and debris flows. Figure 6.1 outlines the slopes that are going to be used to examine the usefulness of the photos.

Figure 6.2 is a set of repeat photos from the Bridgland collection, showing the north part of the area in Figure 6.1. The figure was composed using two photographs from the Bridgland collection, creating a panoramic photograph of the area in both 1999 and 1915. The photographs are examined in detail in the areas where slope movements have been documented.

From the photographs it is clear that the vegetation in the area has changed over the 84-year period between the sets of photographs. As vegetation can be an indication of landslides, the vegetation changes can be used to analyze landslide hazards with repeat photographs, along with other changes on the slopes.

6.2.1 Toppling

Evidence for active toppling is observable in numerous areas of the Colin Range of Jasper National Park, on cataclinal, anaclinal and orthoclinal slopes

The main location of toppling on cataclinal slopes is along the west slope of the Colin Range, where the Athabasca River cuts the range at an angle that is oblique to the geological structure of the area, and is discussed in detail in Chapter 4.2. Figure 6.2 covers the majority of this area that is currently experiencing toppling on cataclinal slopes. For the most part, from the

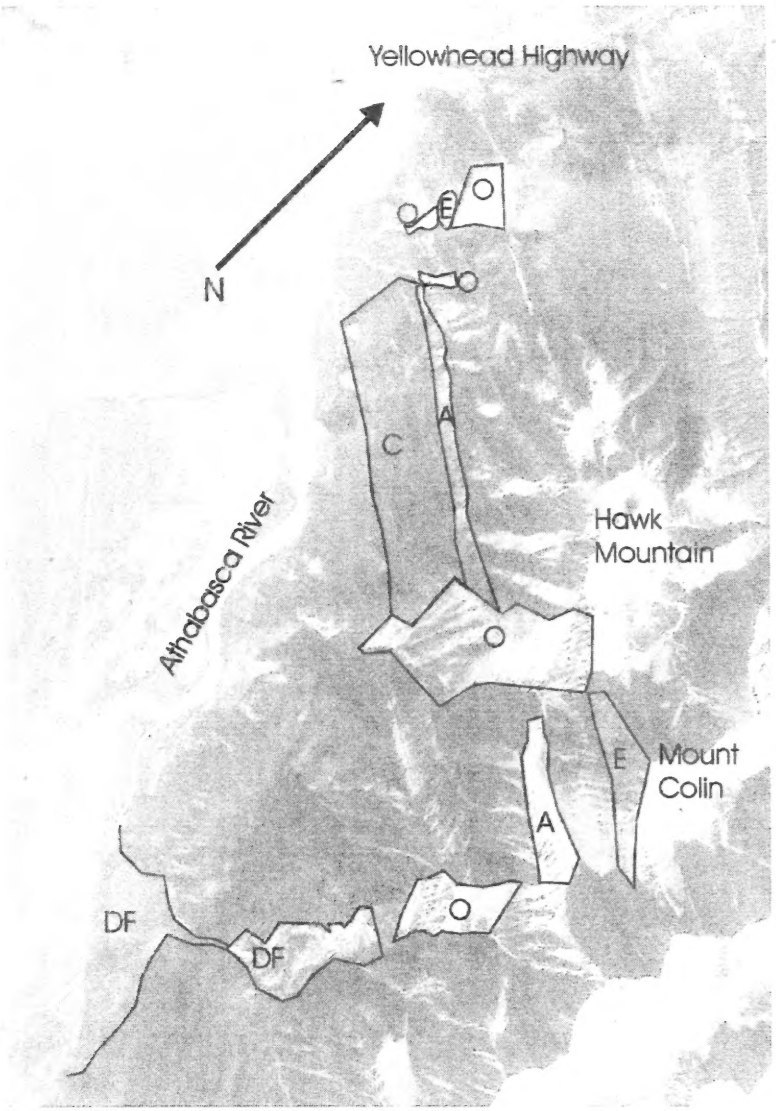

Figure 6.1 – The west slope of the Colin Range, Jasper National Park, showing areas of exfoliation, E; orthoclinal toppling, O; cataclinal toppling, C, anaclinal toppling, A and debris flow deposits, DF, overlain on part of aerial photograph A23025-138, Natural Resources Canada. Original photograph has a scale 1:60 000.

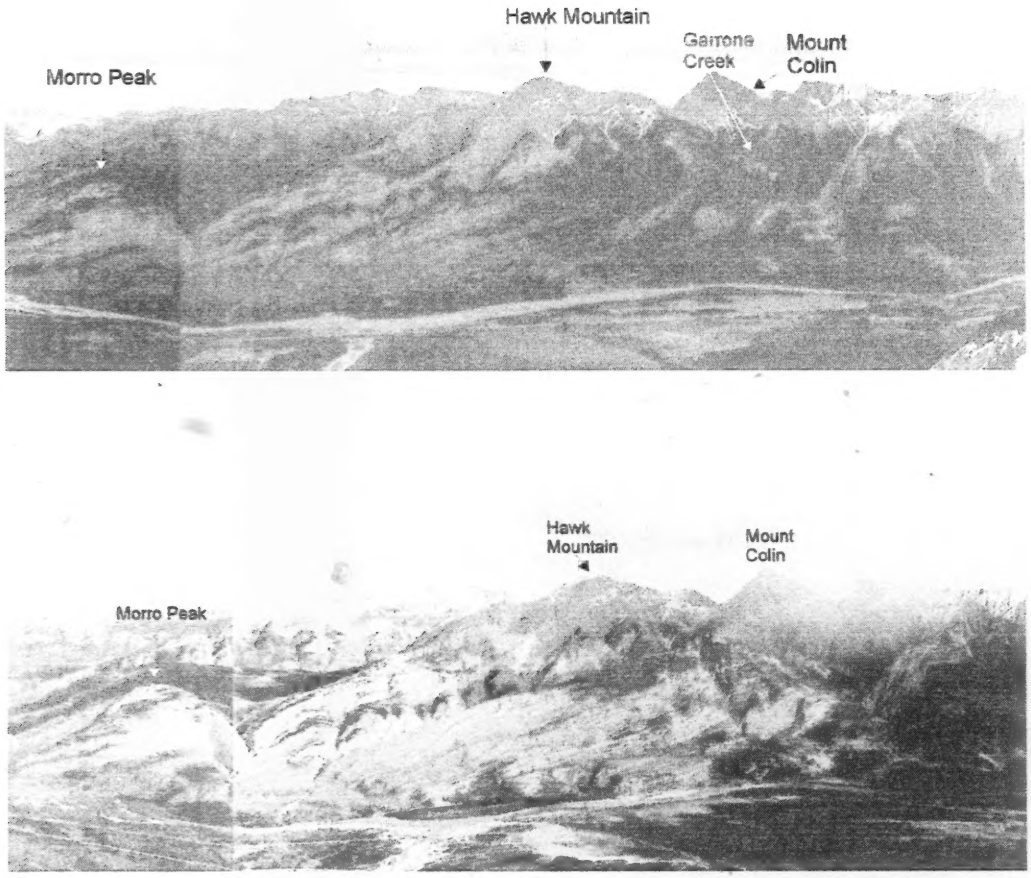

Figure 6.2 – View of the Colin Range from the Palisades repeat photography set from the Bridgland collection. The upper set of photos is the repeat set from 1999, photos 470 and 471, and the bottom photograph is that of Bridgland, 1915, photo numbers 470 and 471 (Higgs, 2001).

observation of these photos, toppling blocks on these slopes can not be seen. However, the 1999 photographs do show areas where there is no vegetation. These are where toppling is occurring on these slopes and where toppled rocks are falling. Yet, these locations are not the only locations on this slope where toppling occurs (Chapter 4.2).

Garrone Creek is an area of active toppling on orthoclinal slopes. The creek can be seen near the centre of the photographs in Figure 6.2. Again, the presence of active toppling can not be readily determined from these photographs, yet this area appears as unvegetated in the 1999 photographs as in the 1915 photographs. A change in the slope due to orthoclinal toppling can not be determined from these photographs.

Toppling on anaclinal slopes occurs on the northeastward facing slopes of the Colin Range, which are not visible on Figure 6.2. From photographs shown in Figure 6.3, changes due to anaclinal toppling can be seen along the creek that runs along the southwest face of Hawk Mountain. Changes were observed using Corel Draw, creating layers for both of the photographs, which were overlapped (Figure 6.3). New layers were added, one where the slope profile was traced on the 1915 photograph, and a fourth layer was created to trace the slope profile on the 1999 photograph. The two slope profiles were then compared, showing a change in the slope profile, indicating that at least one large block moved from the slope, with the most likely mode of movement being toppling. This slope on map 83E/1 is anaclinal. The skyline portion of the slope was used to determine the change in the slope profile, as the contrast with the sky makes it much easier to pick out detailed features.

For individual block topples, repeat photography does not prove useful in determining a hazard. As the topples range in size from 5 mm up to 1.25 m (Chapter 4.2), these topples are not expected to be visible on the photographs. The scale of the photograph is calculated by the ratio of the focal length of the camera to the distance from the lens to the object at the centre of the photograph at the same elevation as the camera. The focal length of the camera

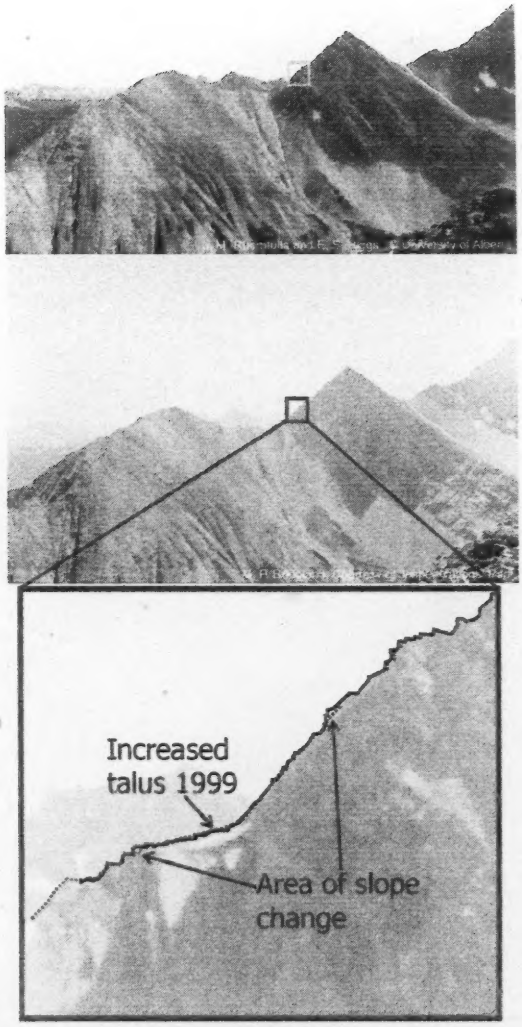

Figure 6.3 – Original and repeat photographs number 336 showing the enlarged area shown at the bottom, with Rhemtulla and Higgs photograph in front of Bridgland's photograph. The dotted line corresponds to the slope profile of the 1999 photograph, and the solid line corresponds to the slope profile in the 1915 photograph. The areas where the slope profile differs are shown in the figure. In addition, there is more talus in the 1999 photograph than in the 1915 photograph.

is 164mm (Bridgland, 1924). The distance to the central object is determined on the 1:50 000 topographic maps. The scale of the photograph in Figure 6.2 is 1:30 488 at the centre of the photograph, so a topple would need to be 300m on the ground in order to show up as 1mm on the photograph. The scale is valid for the central portion of the photograph, yet image displacement occurs away from the centre of the photograph, resulting in a distorted, smaller scale at the edges of the photograph.

6.2.2 Exfoliation

Exfoliation has occurred at two locations, as documented in Chapter 4.3. Both exfoliations occur near the base of steep cataclinal underdip slopes, formed in steeply-dipping, bedded sedimentary rocks. The results of this mode of movement cannot be easily observed on aerial photographs, as the features are on extremely steep slopes. This mode of movement occurs under a ledge along a cataclinal underdip slope, leaving the appearance of an undisturbed slope from above (Figure 6.4), depending on the angle of slope and the angle to the slope from the camera. Exfoliations can be observed on terrestrial photographs with relative ease (Figure 6.5).

Within the exfoliated area, no definite change was noted. With exfoliation, the skyline cannot be used to determine whether or not the slope is changing. The scale at the centre of this photograph is the same as that of Figure 6.2, giving a scale of 1:30 488 without enlargement, again indicating that in order for a change in the slope to be visible in this photograph, 300m of material would need to be moved in order to see a 1 mm change in the photograph.

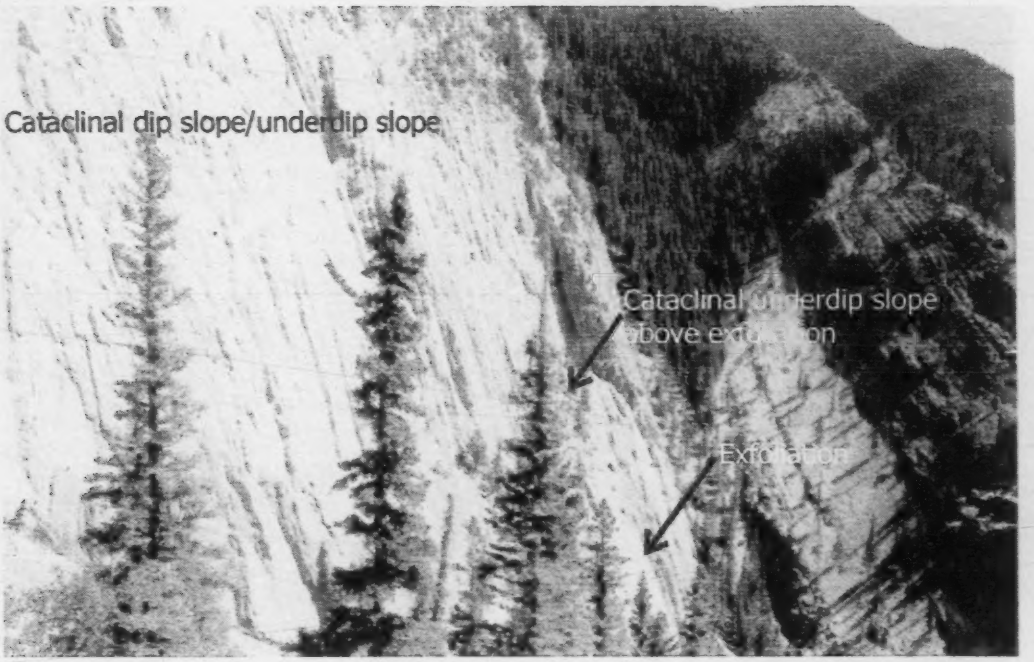

Figure 6.4 – View of exfoliation below a cataclinal underdip slope, showing no sign of the exfoliation from above, limiting the ability of exfoliation to be observed on aerial photographs.

Figure 6.5 – Area of exfoliation on the face of Morro Peak, enlarged from Bridgland photo 470 on the top, and enlargement from photo 467 on the bottom. The photographs have been enlarged 400% to make the exfoliations visible. The individual bedding planes create the flat, planar surfaces above the depressions.

6.2.3 Debris Flows

Intermittent debris flows in colluvial material were documented at the south end of the west slope of the Colin Range, along Debris Flow Creek, as discussed in Chapter 5.

As can be seen in the set of photographs of Figure 6.6, the vegetation in the area of Debris Flow creek has changed over the 84 year time period. This change is especially notable on the alluvial fan of the creek, where coniferous trees have replaced the deciduous trees. Minor changes can be observed in this area between the two photos (Figure 6.7). The first area where slope movement can be inferred is the area on the north side of the creek canyon, where vegetation is not present on either of the photographs (Figure 6.6). This is an area of colluvial deposits which are constantly being reworked by the creek and by further mobilization of the colluvium under gravitational forces (Chapter 5). This area is one of the main contributors to the intermittent debris flows that occur at this location.

Another area where change can be observed on these photographs is the area where the creek cuts through the till deposits, left from the retreat of the Athabasca Glacier (Mountjoy, 1974). The till face on the south side of the alluvial fan has been altered between 1915 and 1999 (Figure 6.7).

6.3 History

The Bridgland Repeat photography is a unique tool, with many potential applications. Changes in land use and in vegetation cover have been discussed using the repeat photography project (Rhemtulla, 1999). The question is whether or not repeat terrestrial photogrametric surveys are useful in the analysis of landslide hazards.

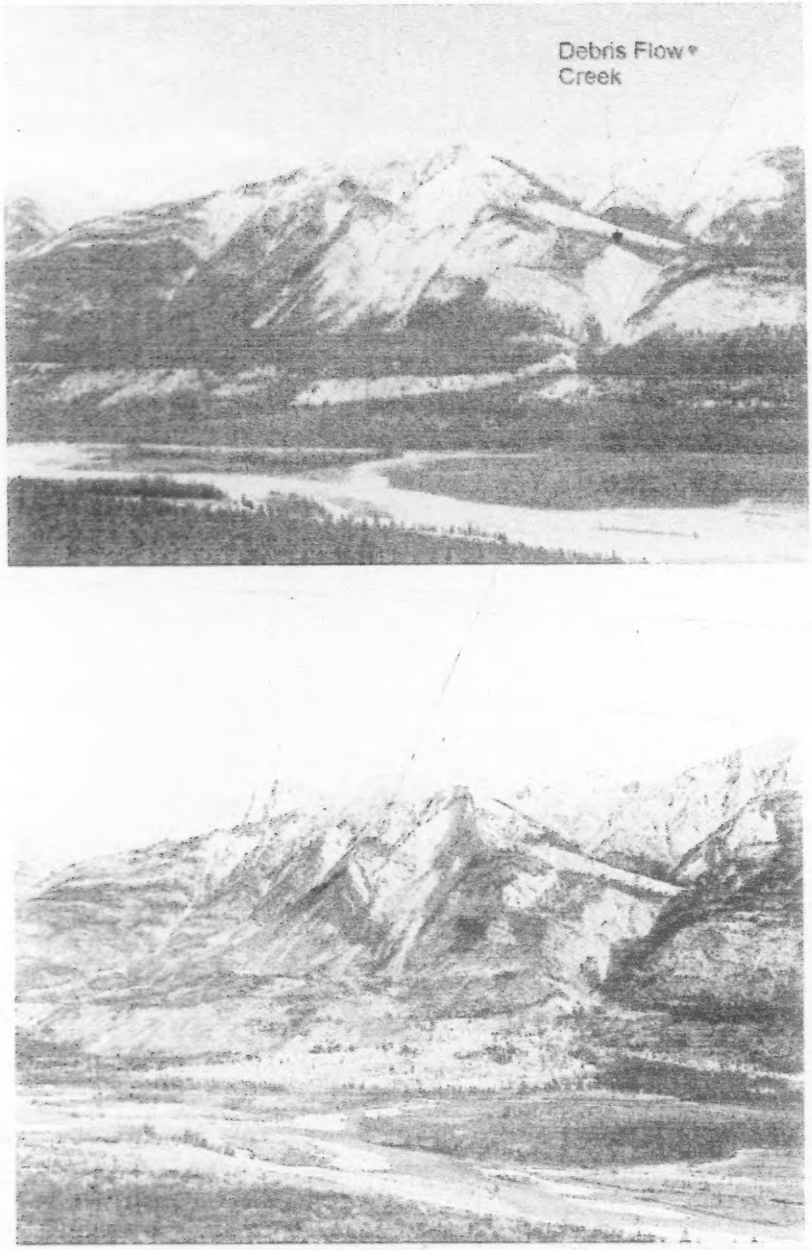

Figure 6.6 – Set of repeat photographs, photos #460, with the top photo from Higgs and Rhemtulla, and the bottom photograph by Bridgland. The photograph shows the area of Debris Flow Creek.

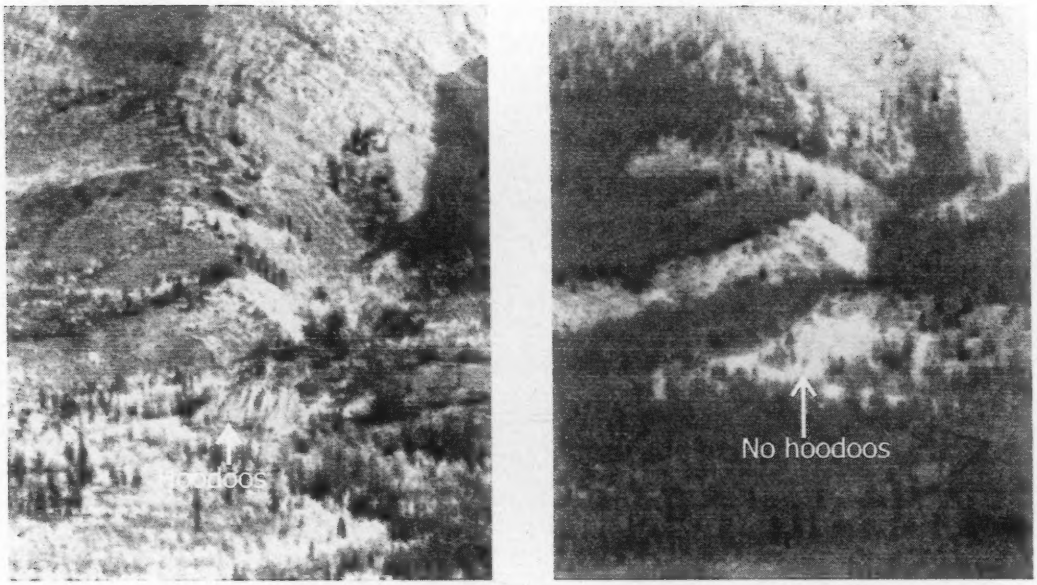

Figure 6.7 – Enlarged 200% repeat set of photograph number 460, with the original photo on the left and the repeat photograph (Higgs and Rhemtulla) on the right side. Vegetation changes are easy to see of the alluvial fan, and the changes in the moraine include the removal of the hoodoos over the 85 year time span between the photographs.

Since the introduction of aerial photography to Canada in the 1920's, these photos have proved useful in the analysis and quantification of landscape changes (Natural Resources Canada, 2002). Prior to the use of aerial photography, topographic maps of areas of high relief were compiled from data acquired using photographic surveys. Phototopography was a common method used by surveyors, and was used for the mapping of the Selkirk Mountains (Wheeler, 1905), and the mapping of Jasper National Park (Higgs, 2001). A list of principal photographic surveys prior to 1924 is included in Table 6.1.

Photography taken by Bridgland of the west shore of Brazeau Lake in 1929 has been used by Cruden (1982) to establish conditions before the 1933 Brazeau Lake slide. McConnell and Brock (1903) used photographs from an early photographic survey to examine the change in the skyline at Turtle Mountain after the Frank Slide in 1903. Luckman et. al. (1999) used early survey photographs in order to examine the retreat of the Athabasca and Dome glaciers in Jasper National Park. The Bridgland Repeat Photography Project webpage (Higgs, 2001b) includes a partial listing of websites including repeat photography on the Resources page.

6.4 Photographic Information

In the case of smaller slope movements, such as toppling and exfoliation, changes may not be readily visible at the natural scale of the photographs. However, as digital collections of repeat photography become more readily available, repeat photography projects are likely to be useful in reconnaissance studies. Areas that remain active are often shown by a lack of vegetation, and can be further examined on the ground, based on areas of interest identified on repeat photos.

One benefit of the Bridgland collection of repeat photographs is the digital database of photographs, with 1000 DPI scans of both the original and the repeat photographs. The tone and contrast of these digital images can be

Year	Locality	Department	Area (square miles)	Surveyor
1886-92	Main Range of the Rocky Mountains adjacent to the Canadian Pacific Railway	Interior - TSC	2500	J.J. McArthur
1893	British Columbia-Alaska boundary	Interior - IBS	5000	Dr. W.F. King
1897	Columbia Valley from Revelstoke to Arrowhead, B.C.	Interior - TSC	600	J.J. McArthur
1896-99	Alberta foothills southwest of Calgary, Alta	Interior - TSC	2000	A.O. Wheeler
1900	Crowsnest Coal area near Crowsnest Pass, B.C.	Interior - TSC	550	A.O. Wheeler
1901-02	Selkirk Mountains adjacent to the Canadian Pacific railway, from Beavermouth to Revelstoke, B.C.	Interior - TSC	1100	A.O. Wheeler
1903-1905	Southern boundary of British Columbia	Interior - IBS	1200	J.J. McArthur
1903-06	Rocky Mountains adjacent to the Canadian Pacific railway, from Mount Castle to Beavermouth, B.C.	Interior - TSC	2200	A.O. Wheeler M.P. Bridgland
1907-13	Yukon-Alaska boundary (141st Meridian)	Interior - IBS	1000	J.D. Craig
1911	Rocky Mountains, Robson District, north of Yellowhead pass	Interior - TSC	1100	A.O. Wheeler
1913	Rocky Mountains, Banff-Windermere road from Vermillion Pass to the junction of Kootenay and Vermillion rivers	Government of B.C.	500	R.D. McCaw
1913-14	Crowsnest forest reserve, southwestern B.C.	Interior - TSC	1500	M.P. Bridgland
1913-14, 20	Thirtystone Mile Lake watershed, Que	Interior - IBS	200	D.H. Nelles
1913-23	British Columbia-Alberta Boundary	Interior - TSC	5100	A.O. Wheeler A.J. Campbell
1914-19	Okanagan Lake district, B.C.	Government of B.C.	3300	R.D. McCaw
1915	Jasper park adjacent to the Canadian National railways	Interior - TSC	900	M.P. Bridgland
1916	Kananaskis, B.C. and Alta	Mines - GSC	1500	D.A. Nichols
1917	Hazelton, B.C.	Mines - GSC	225	F.S. Falconer

1917-20	Bow River and Clearwater forest reserves, Alta	Interior - TSC	2000	M.P. Bridgland L.E. Harris
1918	Coquihalla river, B.C.	Mines - GSC	275	F.S. Falconer
1918-19	Britannia, B.C.	Mines - GSC	90	K.G. Chipman
1918-21	North Thompson river, B.C.	Mines - GSC	800	D.A. Nichols
1919	Harris Creek watershed, B.C.	Government of B.C.	175	R.D. McCaw
1919-20	Lower Similkameen valley, B.C.	Government of B.C.	650	R.D. McCaw G.J. Jackson
1920	Cariboo, B.C.	Mines - GSC	260	D.A. Nichols
1920	Kitsault river, B.C.	Mines - GSC	40	W.H. Miller
1920-22	Upper Nicola Valley, B.C.	Government of B.C.	1100	R.D. McCaw
1921	Pitt Lake basin, B.C.	Interior - TSC	250	M.P. Bridgland L.E. Harris
1921	Okanagan watershed, B.C.	Government of B.C.	400	G.J. Jackson
1922	Babine, B.C.	Mines - GSC	195	W.H. Miller
1922	Similkameen valley, B.C.	Government of B.C.	400	G.J. Jackson
1922-23	South part of Kootenay park and vicinity	Interior - TSC	1150	M.P. Bridgland L.E. Harris
1923	Reconnaissance surveys	Mines - GSC	9000	

Table 6.1 – List of the principal photographic surveys in Canada in chronological order up to 1923, as included in Bridgland (1924). Interior – TSC is the Topographical Survey of Canada, Department of the Interior; Mines – GSC is the Geological Survey, Department of Mines; Interior – IBS is the International Boundary Surveys and the Geodetic Survey, Department of the Interior.

manipulated, and photographs are easily enlarged. Photographs can also be imported into programs like Corel Draw and Adobe PhotoShop, where comparisons of the photographs can be made in great detail. The photographs in 1915 by M.P. Bridgland were taken on 102mm by 127mm glass plates. Grain sizes on the order of 10^{-6} m on the negative (Tupper et.al., 1952) allow for images on the scale of 10^{-5} m to be resolved, allowing for individual bedding planes to be observed when the photograph has been enlarged (Figure 6.5). Some of this detail is lost on the development of the photograph, and the digital images are scanned at a resolution of 1000 DPI, losing much of this detail.

In Figure 6.2, any change that is greater than 48m would appear as greater than 1mm on the photograph, and in the case of Figure 6.6, any change in the centre of the photo that is greater than 20m will appear larger than 1mm on the photographs. One square millimetre on the photograph is composed of 1521 pixels, indicating that this area can be enlarged, and not much detail is lost. With the increase in the sophistication of digital photography, digital databases of repeat photographs will increase in quality, and prove to be able to detect smaller changes. The smallest feature that is resolvable on the glass plate slide negatives is roughly 1m on the ground. Much of this detail is lost in the development of the photograph and the subsequent scanning of the photograph into the digital database.

6.5 Conclusions

One advantage of using oblique terrestrial photography is the range of views that are available. Within the Bridgland collection, there are several stations that contain photographs of the west slope of the Colin Range. The use of differing angles of photographs leads to a more encompassing view of the area that is being studied. In addition, the use of differing viewpoints may illuminate aspects in shadows, or aspects that are obscured by intervening objects.

One other application of the repeat photography projects includes identifying areas that are subject to repeated and intermittent slope movements, as documented with Debris Flow Creek. The area of Debris Flow Creek is one that is visible in both the original and the repeat photographs as an area which is hazardous.

Oblique photographs also prove useful for identifying areas of slope movement that are not visible from aerial photographs, such as exfoliations.

While repeat photography is not yet an exact science, the information that can be gained from oblique terrestrial photographs that were taken before aerial photographs were available can prove to be useful in reconnaissance studies, and in identifying areas of slope movements, or else areas that require further study. The retreat of glaciers is also something that can be studied using repeat photography. Repeat photography is useful in studying dynamic systems where change is on the scale of 50m or greater.

7 Conclusions

7.1 Introduction

The study area lies in the Front Ranges of the Rocky Mountains, within the Canadian Cordillera, in Paleozoic carbonates and clastics. The local climate indicates that the area is prone to seasonal freeze and thaw conditions, with a daily mean temperature of 3.3°C, averaged over the year. The average precipitation in the area is 398.8mm per year, the majority falling as rain in the months of June, July and August.

The surficial geology in the vicinity of the Colin Range is dominated by glacial sediments, with lesser amounts of alluvial and colluvial sediments. Most of the preglacial sediments were removed during the last glaciation of the Athabasca and Maligne Valleys. Of greatest importance to this study are the lateral moraines that were left behind by the Athabasca and Maligne glaciers during the last retreat. Rivers have formed steep-walled valleys and canyons post-glacially, and have created alluvial fans onto the flood plain of the Athabasca River. Glacially oversteepened slopes have moved, and deposited colluvial material throughout the area.

The bedrock consists of sedimentary rocks that range in age from Late Cambrian to Triassic. The rock formations in the study area contain both clastic and carbonate sedimentary rocks, with carbonates dominating the sequence. The regional structure is homoclinal, with strike northwest-southeast and dip to the southwest. Two thrust sheets, the Chetamon Thrust Sheet and the Colin Thrust Sheet, compose the bedrock, with the addition of blocks bounded by small splay faults off the Chetamon and the Pyramid Thrust faults. There is one syncline that gently plunges to the south, between the Maligne River and Garrone Creek (Figure 2.3).

The study area consists of cataclinal underdip slopes, cataclinal dip slopes, orthoclinal slopes and, to a lesser extent, anaclinal slopes. One cataclinal overdip slope was observed; all other cataclinal overdip slopes have now formed dip slopes. Cataclinal and orthoclinal slopes are the most frequently occurring slopes. Cataclinal underdip slopes are composed of alternating dip slopes and gentle cataclinal underdip slopes. Cataclinal slopes can range from gentle slopes of 17° up to steep slopes of 65°. Orthoclinal slopes may be gentle slopes, where formed by glaciation with little post-glacial shaping, other orthoclinal slopes have angles up to 90° where creeks have cut post-glacially, and slope movement is active. Slope types can be divided on aerial photographs using information from geological maps and topographic maps, which provide useful tools for the analysis of slope movement hazards.

7.2 Results

The modes of movement on orthoclinal slopes are considered in Chapter 3. A limit equilibrium analysis of kinematically possible block movements showed both sliding and toppling can take place on an orthoclinal slope. The analysis for sliding motion on an orthoclinal slope indicates that a block on an orthoclinal slope is able to slide if there is sufficient water pressure to drive the sliding of the block. Equation 3.4 shows that blocks with a block ratio between 1.75 and 2.75 (Table 3.1) in vertically bedded strata are able to slide on an orthoclinal slope. In the situation where the bedding is inclined, a block ratio between 3 and 5 is required in order for sliding to occur (Table 3.2). The predicted slope angles for an orthoclinal slope with an inclined bedding orientation range from 76° to 82°; a slope angle between 60° and 72° is predicted in the situation where bedding is vertical or horizontal.

Slope movements by toppling were examined in Chapter 3.3. An analysis showed that on an orthoclinal slope with vertical bedding, a block ratio between 2.0 and 2.5 is required for a block to be able to topple, resulting in a slope with

an angle of 63° to 69°. In the situation where bedding is inclined, a block ratio of 3.0 to 3.7 is required for toppling to occur, and the resulting slope angle would be between 68° and 73°.

Toppling takes place on orthoclinal slopes at lower water pressures than sliding does. Both sliding and toppling require steep slope angles in order to occur on orthoclinal slopes.

Evidence for orthoclinal movement was documented in the field, and compared with the models of toppling and sliding that were presented in Chapter 3.2 and 3.3. Morro Creek and Garrone Creek are two areas where evidence for movement on natural orthoclinal slopes is documented, and a slope along the Yellowhead highway is used to document evidence for movement on an artificial orthoclinal slope. The slope angles on these orthoclinal slopes range from 34° to 90°. A 34° slope occurs in the less resistant rocks of the Rundle Group along Morro Creek, while a 90° slope occurs in the resistant rocks of the Survey Peak Formation adjacent to Garrone Creek. The slope angle of 34° is less than that predicted in Table 3.7, and is formed by modes of movement other than the idealized model. A slope angle of 90° is greater than that predicted in Table 3.7, and is due to the rapid formation of the canyons post-glacially, not allowing time for their equilibration to the stable slope angles. All of the slope movements on orthoclinal slopes are relatively small scale movements, often involving the movement of individual blocks.

Calculations in Chapter 3, using the simple model, indicate that slope movements that occur on orthoclinal slopes are not driven by water pressure alone. The one example of the large block in Morro Creek indicates that toppling does occur perpendicular to bedding in orthoclinal slopes, though the exact mechanism of this motion is not explained in the model, and external forces are involved.

Evidence for three types of movement was observed on cataclinal slopes: toppling, exfoliation and translational sliding, with all three modes of movement plotting on Figure 4.1. The most common mode of movement on cataclinal

underdip slopes and dip slopes is toppling. Evidence for toppling is found on most of the cataclinal slopes, regardless of slope angle. Five examples of toppling observed in the field are discussed in Chapter 4.2.

Two types of topples are discussed, block topples and multiple block topples. Block topples were found to occur in rocks with a block ratio up to 5, and occur in the Palliser Formation, in thick beds within the Banff Formation and in the Rundle Group. Blocks are moved out from the bedding plane, and rotate about an axis defined by the intersection of the strike joints with the bedding plane. Multiple block topples occur in rocks with a block ratio greater than 2, within the thinly bedded shales of the Banff Formation.

Toppling occurs in outcrops along the Overlander Trail, the trail across Morro Creek and the approach to Hawk Mountain. For the most part, the topples that occur in the Colin Range are individual block topples, and are not likely to create a large rock fall.

Exfoliation occurs in steeply dipping rocks of the Palliser Formation on steep cataclinal underdip to dip slopes. Exfoliation produces circular to inverted tear drop shaped concavities in the face of the slope. The depressions are created by the removal of slabs of rock from beds near the base of slopes. These beds daylight either at the top of the slope, or on a shallow underdip slope above the depression. There are three possible mechanisms of movement of the beds that result in exfoliation: buckling of the rock under its own weight, the outward pressure of bedding plane water or the expansion of water upon freezing within the interstitial space between bedding planes. Exfoliation depression shapes are controlled by the orientation of bedding and a kathetal joint set.

Evidence for an ancient translational slide is found the south of the study area, adjacent to Maligne Canyon, within the hanging valley of the Maligne Glacier. This movement occurred on what was formerly a cataclinal overdip slope formed in gently dipping rocks of the Palliser Formation. A relict slide scarp, main body and toe remain, producing a closed depression, or graben, and

deposit of colluvial material at the toe. The only movement that occurs presently at this location is rock fall from the southern slope of the scarp.

Periglacial conditions allowed the translational movement of large blocks of limestone on bedding planes that dip between 14° and 47°. As the Athabasca Glacier retreated at the end of the last ice age, a cataclinal overdip slope was left at the mouth of the Maligne Valley. High water pressures from the retreating Maligne Glacier and the Athabasca Glacier, confined by the lateral moraines of both glaciers, allowed the translation of very large blocks. It is likely that the south scarp of the graben is due to the collapse of a cave system , allowing for block in the south of the feature to slide into the steep walled depression. This led to the blocks on the break of the cataclinal overdip slope toppling into the Athabasca Valley, allowing the blocks bounded upslope to be kinematically free to translate.

A dip slope along the north and east, and a steep joint-controlled scarp to the south define the scarp area, or graben. The graben ends where a jumble of large blocks is randomly oriented in the bottom of the depression. The main body of the slide is a rock labyrinth, defined by the regular orientation of bedding, where the blocks are separated from one another along both dip joints and strike joints. The labyrinth terminates at the slope break, where the orientation of the blocks becomes random due to rotation. Colluvial material is covered with karren that formed in the present location of the blocks, indicating that this is a relict slide.

Debris flows occur within the Colin Range within a drainage formed in a hanging valley at the south end of the Colin Range. The debris flows originate in a U-shaped valley containing till overlain by fluvial deposits. The U-shaped valley enters into a canyon that cuts across the axis of a gently plunging syncline. The south wall of the canyon is confined in bedrock, whereas the north slope of the canyon is composed of broken and jointed bedrock covered with colluvial materials originating within the syncline, produced by sliding along the axis of the syncline post-glacially.

Where the creek enters the Athabasca Valley, leaving the canyon, the creek has cut through the cemented moraine of the Athabasca Glacier. The till is being undercut where the creek flows along the base of the unit, and emerges from the moraine onto its fan. A creek emerges from a spring and flows throughout the summer on the alluvial fan, until it sinks back into the fan. The creek is flanked by terraces, and inactive channels, some of which are incised 1-2m into the fan. Channels have undercut the material on the fan, and in one area, several trees were felled by the undercutting of the banks.

Debris flows may originate in one of three areas within the watershed of Debris Flow Creek, in addition to initiation due to heavy rainfall or snow melt, the upper hanging valley, the canyon or on the fan at the base of the till. Within the hanging glacial valley, there is abundant till and fluvial deposits, along with talus from avalanches and rock fall along the slopes that flank the valley. While water was not observed to be flowing in this valley during the summer of 2003, the creek contains water during times of high precipitation and snowmelt, and can be obstructed by runout from avalanches, leading to the build-up of pressures behind the obstruction, and the catastrophic flow of materials once the upstream pressures exceed the strength of the obstruction. Debris flows can originate within the canyon, when colluvial material and jointed bedrock are intermittently remobilized and slide into the canyon, blocking water flow and leading to the build up of water pressures behind the obstruction and the consequential catastrophic outflow of the materials. The debris flows may also originate on the fan, where the creek undercuts the till unit, and tension cracks are forming. When a large block of till separates and falls into the creek, the creek is obstructed, and water pressures are able to build up. As a result, the creek either avulses, or water pressures are built up to the point where the creek is able to overcome the obstacle and flow down the fan, taking the debris from the creek and the obstacle with it. In Chapter 6, the Bridgland Repeat Photographs have shown that the till unit has collapsed in the past, with the removal of the hoodoos between 1915 and 1999.

Repeat photography of Jasper National Park was used to undertake a reconnaissance study of the area, to identify areas of active slope movements, orthoclinal slopes and to plan the field season. The usefulness of the photographs, along with the difficulties involved in using the photographs is discussed in Chapter 6. Toppling could not be identified on the photos due to the small size of the block topples. The photographs are useful in the identification of areas of exfoliation, once the photographs have been enlarged and examined in detail. Debris Flow Creek was easily identified as an area of interest using the repeat set of photographs, based on the lack of vegetation, and the small changes on the alluvial fan. Repeat photography is a useful tool in medium to large scale slope movement studies, especially when used in conjunction with aerial photography, to get a general picture of the area from many angles, and at differing scales. The scales of the photographs that were used in this study are 1:47 561 (Figure 6.2) and 1:19 817 (Figure 6.6) at the centre of the photographs. At this scale, a slope movement that affects an area 20 to 50m will appear as 1mm on the photographs, and can be seen with the naked eye, and enlarged for greater detail. The area of the Rock and Boulder Gardens shows clearly on repeat photographs that cover the area, and other slides that are at this scale would be easily identifiable on repeat oblique photographs.

7.3 Land Use Implications

The study area is located within Jasper National Park, an UNESCO World Heritage Site. The main land uses within the studied area are recreational, including hiking, mountain biking and rock climbing. The only structure within the vicinity is the Mount Colin Centennial Hut, run by the Alpine Club of Canada, located at the base of Mount Colin near the tree line. Though the hut is adjacent to a colluvial deposit, there is no sign of active slope movement in the immediate vicinity of the hut.

A hazard exists at some locations along the Overlander Trail, on the west slope of Morro Peak. The toppling of blocks occurs on this slope, likely at times of high precipitation and high snow melt. Jasper National Park may wish to post signs indicating a hazard exists in the spring, and the trail should be used with caution. This hazard also occurs on trails that branch off of the Overlander Trail, the trails to the Guides Route on Morro Peak and the trail to the summit of Hawk Mountain and Mount Colin.

Exfoliation is a locally active mode of slope movement, and may pose a hazard within Morro Creek and at the base of Mount Colin. Morro Creek was not heavily used in the summer of 2002, yet usage of the creek is likely to increase, especially as the rappel down the canyon becomes more popular. Mount Colin is an area frequently used by rock climbers. The risk of an adverse effect is more likely at this location, as it is used throughout the year. The climbing guides that discuss the climbs on Mount Colin and the rappel down Morro Creek should mention the hazards that exist at these locations. In addition, the Alpine Club of Canada should make the hazard known to their guests at the Mount Colin Centennial Hut.

Debris flows occur within the southernmost drainage on the west slope of the Colin Range, proposed to be named Debris Flow Creek. The hazard from debris flows increases when water is present within the catchment area, at times of heavy rain and high snowmelt. This area is an approach to alpine climbing routes (Dougherty, 1991). A warning of the potential for debris flows to occur in this area should be included in books and route guides.

The Rock and Boulder Gardens are composed of a relict translational multi-block slide that occurred on a cataclinal overdip slope, which has since been exhausted. This is not an area that poses a hazard at the present time, with the exception of minor rock fall from the steep slopes within the Rock Gardens. Rock climbers that use the area should be aware of the hazard, and wear helmets, as recommended in Davidson (1999).

Overall, the hazard along the west slope of the Colin Range in Jasper National Park is low in ideal conditions, and higher in adverse weather conditions, such as high snowmelt, freeze and thaw conditions and heavy or prolonged precipitation.

7.4 Further work recommendations

A simple model for the types of movements on orthoclinal slopes is included in this thesis, yet the factor of safety calculations undertaken do not explain the movement of the blocks on these orthoclinal slopes. A more detailed examination of the causes for block movement on orthoclinal slopes should be undertaken.

Exfoliation is a process that is documented in the Devonian Palliser Formation in the Colin Range and is not a process that is well understood. Further examination of the processes involved in exfoliation, including the limiting conditions of lithology, bedding dip and slope geometry need to be examined in more detail. Other examples of this phenomenon need to be found and documented.

References

Alberta Environment 1980. Surficial geology, Alberta foothills and Rocky Mountains. Alberta Environment, Edmonton and Alberta Research Council, Edmonton, Alberta.

Alpine Club of Canada 2002. http://www.alpineclubofcanada.ca/. Accessed January 30, 2003.

Baird, D.M. 1972. Jasper National Park: Behind the Mountains and Glaciers. Miscellaneous Report 6, The Geological Survey of Canada, Ottawa.

Bayrock, L.A. and Reimchen, T.H.F. 1976. Terrain Analysis of Jasper National Park. Bayrock and Reimchen Surficial Geology Ltd, Vancouver, 23 leaves.

Benn, D.I. and Evans, D.J.A. 1998. Glaciers and Glaciation. Arnold, London, 323-327.

Bridgland, M.P. 1924. Photographic Surveying. Department of the Interior, Canada – Topographical Survey of Canada, Bulletin No. 56, Ottawa, 47p.

Charlesworth, H.A.K., Weiner, J.L., Akehurst, A.J., Bielenstein, H.U., Evans, C.R., Griffiths, R.E., Remmington, D.B., Stauffer, M.R. and Steiner, J. 1967. Precambrian Geology of the Jasper Region, Alberta. Bulletin 23, Research Council of Alberta, Edmonton, Alberta.

Clague, J.J. 1989. Quaternary geology of the Canadian Cordillera in: R.J. Fulton, (ed) Quaternary geology of Canada and Greenland. Geological Survey of Canada, 15-95

Clague, J.J. and MacDonald, G.M. 1989. Paleoecology and paleoclimatology (Canadian Cordillera); in Chapter 1 of Quaternary Geology of Canada and Greenland, R.J. Fulton (ed.); Geological Survey of Canada, no. 1: 70-74.

Cruden, D.M. 1982. The Brazeau Lake Slide, Jasper National Park, Alberta. Canadian Journal of Earth Sciences, 19: 975-981.

Cruden, D.M. 1985. Rock slope movements in the Canadian Cordillera. Canadian Geotechnical Journal 22: 528-540.

Cruden, D.M. 1989. The limits to common toppling. Canadian Geotechnical Journal 26, 737-742.

Cruden, D.M. and Hu, X.Q. 1988. Basic friction angles of carbonate rocks from Kananaskis Country, Canada. Bulletin of the International Association of Engineering Geology 38, 55-59.

Cruden, D.M. and Hu, X.Q. 1994. Topples on underdip slopes in the Highwood Pass, Alberta, Canada. Quarterly Journal of Engineering Geology 27: 57-68.

Cruden, D.M. and Hu, X.Q. 1996. Hazardous modes of rock slope movements in the Canadian Rockies. Environmental Engineering Geoscience, 2, 507-516.

Cruden, D.M., Hu, X.Q. and Lu, Z. 1993. Rock topples in the highway cut west of Clairvaux Creek, Jasper, Alberta. Canadian Geotechnical Journal 30: 1016-1023.

Cruden, D.M. and Thomson, S. 1987. Exercises in Terrain Analysis. Pica Press, Edmonton, Canada, 7-20.

Cruden, D.M. and Varnes, D.J. 1996. Landslide types and processes in: Turner, A.K. and Schuster, R.L. (eds) Landslides: Investigation and Mitigation. Transport Research Board Special Report 247, 395-425.

deFreitas, M.H. and Watters, R.J. 1973. Some field examples of toppling failure. Geotechnique 23, 495-514.

deWit, R. and McLaren, D.J. 1950. Devonian sections in the Rocky Mountains between Crowsnest Pass and Jasper, Alberta. Geological Survey of Canada, paper 50-23, Ottawa: 26-31.

Dougherty, S. 1991. Selected Alpine Climbs in the Canadian Rockies. Rocky Mountain Books, Calgary. 320p.

Eaton, T.M., 1986. Reconnaissance of Rockslide Hazards in Kananaskis Country. M.Sc. thesis, University of Alberta, Canada, 291p.

Environment Canada 2000. Canadian Climate Normals 1971-2000. Retrieved January 16, 2003 from http://www.msc-smc.ec.gc.ca/climate/climate_normals/index_e.cfm. Jasper Station.

Freden, C. 1996. Changes to the landscape – landslides and gullies in: Chacon, J, Irigaray, C. and Fernandez, T (eds) Landslides. A.A. Balkema, 39-46.

Gadd, B. 1999. Handbook of the Canadian Rockies. Corax Press, Jasper, Alberta: 45-203.

Hancock, P.L. 1964. The relations between folds and late formed joints in South Pembrokeshire. Geological Magazine 101, 174-184.

Higgs, E. 2001. The Bridgland Repeat Photography Project: About: Photographs. bridgland.sunsite.ualberta.ca/html/photo.html.

Higgs, 2001b. The Bridgland Repeat Photography Project: Resources. Bridgland.sunsite.ualberta.ca/html/resources.html.

Hoek, E. and Bray, J. 1974. Rock Slope Engineering. Institute of Mining and Metallurgy, London. 402pp

Hoek, E. and Diederichs, M. 1989. Dips – A program for plotting, analysis and presentation of structural geology data using spherical projection techniques. Rock Engineering Group, University of Toronto, Toronto.

Hu, X.Q. and Cruden, D.M. 1993. Buckling deformation in the Highwood Pass, Alberta, Canada. Canadian Geotechnical Journal 30: 276-286.

IUGS Working Group on Lansdslides, Committee of Risk Assessment. 1997. Quantitative risk assessment for slopes and landslides – the state of the art, in: Cruden, D.M. and Fell, R. (eds) Landslide Risk Assessment. A.A. Balkema, Rotterdam, Netherlands, 3-12.

Kindle,E.M. 1929. The succession of fossil faunas in the eastern part of Jasper Park. American Journal of Science:18, 177-192.

Lang, A.H. 1944. Drinnan to Brule Lake, Athabasca Valley, Alberta (summary account). Paper 44-11, Geological Survey of Canada, Ottawa, Ontario.

Luckman, B.H. 1986. Reconstruction of Little Ice Age events in the Canadian Rocky Mountains. Geographie physique et Quaternaire 40:17-28.

Luckman, B.H., Kavanagh, T.A., Craig, I. and St. Georoge, R.S. 1999. Earliest photograph of Athabasca and Dome Glaciers, Alberta. Geographie Physique et Quaternaire, 53: 401-405.

Luckman, B.H. and Osborn, G.D. 1979. Holocene glacier fluctuations in the middle Canadian Rocky Mountains. Quaternary Research 11: 52-77.

MacKay, B.R. 1929. Brule mines coal area Alberta. Geological Survey of Canada, Summary Report 1928, Part B., 1-29.

McAffee, R.P. and Cruden, D.M. 1996. Landslides at Rock Glacier Site, Highwood Pass, Alberta. Canadian Geotechnical Journal 33, 685-695.

McConnell, R.G. and Brock, R.W. 1903. Report on the Great Landslide at Frank, Alberta, 1903. Geological Survey of Canada

McEvoy, J. 1901. Report on the geology and natural resources of the country traversed by the Yellow Head pass route from Edmonton to Tete Jaune Cache, comprising portions of Alberta and British Columbia. Geological Survey of Canada, Annual Report for 1898, Volume 2, Part D.

Mountjoy, E.M. 1959. Geology Miette, Alberta. Map 40-1959, Geological Survey of Canada. Map at a scale 1:63 360.

Mountjoy, E.M. 1961. Rocky Mountain Front Ranges along the Athabasca Valley, Jasper National Park, Alberta In: Jasper, Edmonton Geological Society, 3rd Annual Field Trip Guidebook: 14-42.

Mountjoy, E.M. 1964. Geology Mount Robson, Alberta British-Columbia. Geological Survey of Canada, Map 47-1963, scale 1:126 720.

Mountjoy, E.M. 1974. The Geological Story of the Lower Athabasca Valley in Jasper National Park. Contract Report 83-2, Jasper National Park, Jasper.

Mountjoy, E.M. 1978. Geology Mount Robson, Alberta-British Columbia. Geological Survey of Canada, Map 1499A, scale 1:250 000.

Mountjoy, E.M. and Price, R.A. 1970. Geologic structure of the Canadian Rocky Mountains between Bow and Athabasca Rivers – a progress report in: Structure of the Canadian Cordillera. Geological Association of Canada, Toronto, Ontario.

Mountjoy, E.M. and Price, R.A. 1976. Geology of Medicine Lake, Alberta; Geological Survey of Canada, Open File 372, scale 1:50 000.

Mountjoy, E.M. and Price, R.A. 1985. Geology of Jasper, Alberta; Geological Survey of Canada, Map 1611A, scale 1:50 000.

Natural Resources Canada, 2002. Aerial photography in Canada – A Brief History. http://airphotos.nrcan.gc.ca/history.html. Retrieved January 15, 2003.

Norrish, N.I. and Wylie, D.C. 1996. Rock Slope Stability Analysis, in: Turner, A.K. and Schuster, R.L. (eds) Landslides: Investigation and Mitigation. Transport Research Board Special Report 247, 395-425.

Parks Canada, 1985. Jasper National Park topographic map. Surveys and Mapping Branch, Mines and Resources Canada. Scale 1:200 000.

Parks Canada. 2000. Jasper National Park – The Railway. http://www.worldweb.com/ParksCanada-Jasper/history/railroad.html. Retreived January 15, 2003.

Powell, J.W. 1875. Exploration of the Colorado River of the West and is tributaries. Government Printing Office, Washington, U.S.A. 291p.

Rhemtulla, J.M. 1999. Eighty years of change: the montane vegetation of Jasper National Park. M.Sc. Thesis, Department of Renewable Resources, University of Alberta, Edmonton.

Robinson, David. 1999. Jasper Rock. Otto Press, Jasper, Alberta. p. 45-56.

Roed, M.A. 1975. Cordilleran and Laurentide multiple glaciation, west central Alberta. Canadian Journal of Earth Sciences; 12: 1493-1515.

Selby, M.J. 1993. Hillslope materials and processes, 2nd Edition. Oxford University Press, Oxford: 330-332.

Simmons, J.V. and Cruden, D.M. 1980. A rock labyrinth in the Front Ranges of the Rockies, Alberta. Canadian Journal of Earth Sciences 17, 1300-1309.

Sokolov, N.I. 1963. Types of displacement in hard fractured rocks on slopes. In, Popov, I.V. and Kotlov, F.V., eds. The Stability of Slopes, Consultants Bureau, New York. 83p.

Taylor, P.W. 1960. Some Pleistocene Lakes of Northern Alberta and adjacent areas. Alberta Society of Petroleum Geologists Journal: 8, 167-178.

Thompson, E. 1976. Cave Exploration in Canada. The Canadian Caver, Edmonton, Alberta, Canada. p. 120-128.

Tupper, J.L., Miller, H.A., Clark, W., and Calhoun, J.M. 1952. Photographic Materials and Techniques in: Manual of Photogrammetry. American Society of Photogrammety, Washington, D.C. p. 271-308.

Wheeler, A.O. 1905. The Selkirk Range. Government Printing Bureau, Ottawa, 459p.

Yorath, C.J. 1995. Geology of Jasper National Park and Surrounding Areas, map, scale 1:357 000 in: Yorath, C.J and Gadd, B. Of Rocks, Mountains and Jasper: A Visitors Guide to the Geology of Jasper National Park. Dunburn Press, Toronto.

Yorath, C.J and Gadd, B. 1995. Of Rocks, Mountains and Jasper: A Visitors Guide to the Geology of Jasper National Park. Dunburn Press, Toronto. 170p.